Surface Dynamics, Glass Transition, and Crystallization of Atactic Polystyrene

by

Yu Chai

A thesis
presented to the University of Waterloo
in fulfillment of the
thesis requirement for the degree of
Doctor of Philosophy
in
Physics

Waterloo, Ontario, Canada, 2016

I hereby declare that I am the sole author of this thesis. This is a true copy of the thesis, including any required final revisions, as accepted by my examiners.

I understand that my thesis may be made electronically available to the public.

Abstract

How polymers behave near the glass transition is one of the deepest questions in condensed matter physics. In the past two decades, the surface dynamics, glass transition, and crystallization of polymer thin films have attracted much attention as they are not only scientific questions but also fundamentals of modern polymer industry. However, there are still many phenomena that are not clear, such as whether the glass transition is a real phase transition; whether there is an enhanced mobile layer near the free surface and how thick it is; whether the glass transition temperature reduction is caused by the free surface; whether some polymers cannot crystallize; *etc.* Here we try to gain insight into these questions. In this thesis, there are six chapters. The first chapter is introduction, in which some basic concepts and a literature review are presented. The second chapter contains the experimental details, in which the experimental techniques and data analysis methods are discussed. Chapter three, four, and five focus on three different research areas; however, these topics are related to each other. In chapter three, we conduct a novel stepped film levelling experiment to study the surface dynamics of polymer films near the glass transition temperature, in which several subtopics are involved, such as molecular weight dependent levelling, levelling under soft confinement, and ultra-thin films levelling. In chapter four, we find the direct evidence of the crystallization of atactic polystyrene, and systematically study the growth and melting kinetics of these crystals. In chapter five, the thermal expansivity of polystyrene thin films is measured using ellipsometry. These results confirm the validity of the recently proposed *simple model*, which connects the exis-

tence of an enhanced mobile layer near the free surface to the glass transition temperature reduction in thin films. The last chapter is concluding remarks and future work, in which a brief summary is included and some possible future studies are proposed.

Acknowledgements

This thesis would not be possible without the help, assistance, and support from many individuals, whom I owe a debt of gratitude to.

Firstly, I would like to thank my supervisor James A. Forrest for his guidance, help, and support in the past several years. As a mentor, friend, and idol of mine, his knowledge and passion for science inspired me to pursue research. I could not have imagined having a better supervisor. Thank you Jamie!

I would also like to thank the rest of my committee: John R. Dutcher, Stefan Idziak, and Fue-Sang Lien for their helpful comments and encouragement during my PhD studies. Their guidance always kept me on the right track. I would like to thank Sindee L. Simon and Mark W. Matsen for being on my defence committee. I would also like to thank Kari Dalnoki-Veress, Thomas Salez, Joshua D. McGraw, Elie Raphaël, Michael Benzaquen for our long-time collaboration. I would also like to express my thanks to Judy McDonnell, Anja Drygala, and Bonnie Findlay for a lot of tedious but necessary administrative work.

I would like to say thanks to my fellow students Chad Daley, Kurt Schreiter, Dongping Qi, Brad Hall, Jeremy Flannery, Shipei Zhu, and Fan-Yen Lin for their friendship and help with my research. I would like to thank Qianshi Wei, Yu-Cheng Su, Haipeng Su, Wei Hong, Lu Li, and Bingqing Yang for their valuable discussions. Unfortunately, I cannot list all my friends here but I appreciate them for their support and friendship. They make my life more colourful.

Finally, I would like to thank my parents Guangjun Chai and Bingbing Zeng, and my girlfriend Qinrong Zhang for their long-term support and care. Their endless love lets me know I am not alone in my life. Thank you my family!

Table of Contents

List of Tables

List of Figures

Chapter 1

Introduction

1.1 Introduction to polymers

1.1.1 What are polymers?

Polymers are big molecules with many repeating units, as shown in Fig. 1.1, that are covalently bonded together. Due to their high molecular weight, polymers are also called macromolecules, a term first coined by Hermann Staudinger in 1920 [1]. Nowadays, polymers are widely used in our daily life. For example, more than 299 million metric tons of plastics were consumed all over the world in 2013 [2], and the volume is still gradually increasing. Although the modern theory of polymer has been developed since the mid-19th century, the history of using natural polymers by human beings is quite long. Ancient

Figure 1.1: Graphic definition of polymers.

people used cottons to make clothes and used leathers to make boots and sofas without knowing the nature of these materials. In the late-19th century, chemists systematically started their research on these materials that had been used for a long time but poorly understood. Moreover, some new materials had been synthesized by that time; however, those materials were typically viscous fluids or plastic powders, which were hard to use. We now know that those materials are polymers, and their properties depend on both the molecular weight and monomer group [3]. As mentioned above, the modern theory of polymers was proposed by Hermann Staudinger in 1920. According to his theory, polymers are big molecules rather than aggregations of small molecules. The concept was not commonly accepted when first proposed; however, as new techniques have been developed, such as TEM, SEM, NMR, etc, this concept was quickly accepted. Since then, all kinds of polymer products have been synthesized, such as Nylon, one of the most successful products in the modern industry. Nowadays, human activities are widely affected by polymers, from cheap plastic bags to expensive drug delivery carriers. The properties of these polymer products can be controlled by changing the chemical structures of monomers to adapt people's demands. Some common polymers, like polyethylene (PE), polystyrene (PS), and

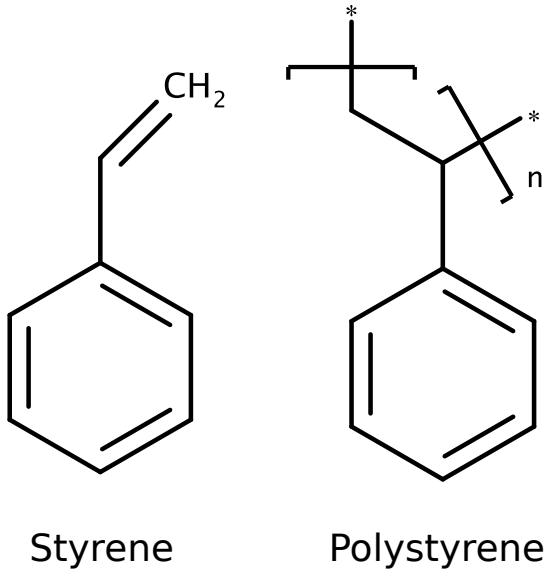

Figure 1.2: Polystyrene and its monomer styrene.

Poly(methyl methacrylate) (PMMA), all have well-defined chemical structures.

1.1.2 Molecular weights and distributions

A unique feature of polymers is the wide range of molecular weights, from several hundreds g/mol to several millions g/mol, which affects the physical properties of polymers dramatically. Taking alkanes as an example, as the number of carbon atoms increases, they change from gas (n = 1 - 4), to liquid (n = 5 - 20), and to solid (n =20 - ∞). Thus, molecular weight plays a crucial role in polymer systems. However, different polymers have different monomers, which have different molecular weights. As a result, the number of monomers in a polymer is more convenient to represent the size of the polymer, which is denoted by N

(degree of polymerization). If a sample is composed of all identical chains with the degree of polymerization of N and molecular weight of the monomer M_0, the molecular weight of the sample can be written as $M = M_0N$. In reality, it is unlikely to find a sample with all chains identical. Consequently, there is always a distribution of molecular weights for polymers. Accordingly, the average molecular weight depends on the method of weighing. The number average and weight average are the most frequently used. The number average molecular weight is denoted by M_n and the weight average molecular weight is represented by M_w. For a sample, which has i components, the weight fraction of the ith component is w_i and the mole fraction is n_i. Thus, the following relations can be given

$$\sum_i n_i = 1 \tag{1.1}$$

$$\sum_i w_i = 1 \tag{1.2}$$

Consequently, the number average molecular weight can be written as

$$\overline{M_n} = \sum_i n_i M_i \tag{1.3}$$

and the weight average molecular weight can be expressed as

$$\overline{M_w} = \sum_i w_i M_i \tag{1.4}$$

The ratio between $\overline{M_w}$ and $\overline{M_n}$ is defined as the polydispersity index (PDI), which demonstrates how broad the molecular weight distribution is

$$PDI = \frac{\overline{M_w}}{\overline{M_n}} \tag{1.5}$$

If the PDI is equal to 1, the sample is monodisperse, which means it is only composed of one molecular weight. In this thesis, all experiments use narrow PDI polymers; however, in industry, broad PDI polymers are more common as many properties of high molecular weight polymers are almost the same at room temperature.

1.1.3 Structures of polymers

Architectures and chain topologies

Polymers are monomers covalently bonded together and there are various possibilities of connecting neighboring monomers. Some typical architectures are linear, star, brush, and branching. Architectures are very important to polymer products because they can affect many physical properties, like density, glass transition temperature, crystallinity, mechanical strength, *etc.* Taking polyethylene as an example, there are several types of polyethylene products in the market, high-density PE (HDPE), medium-density PE (MDPE), and low-density PE (LDPE). LDPE has more branches than MDPE and HDPE, which leads to a lower density and a poorer mechanical strength. In most cases, chain architectures of polymers are determined after they have been made; however, it is still possible to change polymers' architectures by chemical reactions. The most common one is cross-linking, which is a chemical reaction forming covalent or ionic bonds between one chain and the others. Crosslinks act like polymer branches, which can affect polymer density, flexibility, and other physical properties. Moreover, crosslinks can help polymers

form more complicated network structures, such as polymer gels.

Isomerism

Except for chain architectures, isomerism can also lead to different polymer structures with identical molecules. There are three important types of isomerism

- Sequence isomerism
- Stereo isomerism
- Structural isomerism

For sequence isomerism, the specific order of adding new monomers to the backbone is considered. Two typical orders are Head-to-Head and Head-to-Tail. For some certain polymerization methods, one sequence is more favourable than the other.

For stereo isomerism, due to the chiral carbons in the backbone, side groups can be located on different sides. Consequently, polymers with side groups naturally have a specific property: tacticity. There are three extreme cases, all on one side (isotactic), all alternate (syndiotactic), and all random (atactic).

For structural isomerism, when carbon double bonds exist in the backbone, there are two configurations for two neighboring monomers, *cis* and *trans*. For the *cis* configuration, two identical side groups are on one side; for the *trans* configuration, two identical side

groups are on different sides. In this thesis, all polymers used do not have any double bonds in the backbone so the structural isomerism does not need to be considered.

Ideal chains

From the macroscopic perspective, the conformations of polymer chains represent the arrangement of polymers, which can be affected by the conditions of polymers. In other words, the conformations are different under different temperatures, solvents, pressures, *etc.* In reality, many interactions need to be considered, such as covalent bonding between neighboring monomers; monomer-monomer interactions where monomers are far apart along the backbone or belong to different chains; polymer-solvent interactions, *etc.* Of course, the simplest case is that all other interactions are neglected and only the interactions among neighbouring monomers in the polymer chain are considered, which is known as an ideal chain. The concept of the ideal chain is very simple, yet very useful, since in some situations this simplest model is nearly perfect in predicting behaviours of polymers, such as linear polymer melts.

The flexibility of polymers is mainly caused by the rotations of single carbon bonds. The rotations of single carbon bonds lead to different torsion angles ϕ, which are in the range of $-\pi$ to π. In principle, different torsion angles are associated with different energies. Taking polyethylene as an example, there are three minima, $gauche_-$, $trans$, and $gauche_+$. *trans* is the global minimum and the energy difference between *gauche* and *trans* is $\Delta\epsilon$, which is equal to $0.8kT$. Therefore, it is possible that polymers change their conformation

with thermal energy in the absence of any chemical reactions.

If all bond lengths are the same and there is no treatment of bond angles and torsion angles, a polymer chain becomes a freely jointed chain, which is the simplest ideal chain model. In this model, polymer chains can be considered as random walks, in which each backbone bond is treated as a single walk. Given a polymer chain with $n+1$ monomers, r_i represents the vector from the $(i-1)$ th monomer to the ith monomer. Accordingly, the end-to-end vector is defined as

$$\vec{R_n} = \sum_{i=1}^{n} \vec{r_i} \tag{1.6}$$

Because the ensemble average end-to-end distance is zero, the mean-square end-to-end distance is defined and used to quantify the size of a polymer chain.

$$< R^2 >=< R_n^2 >=< \vec{R_n} \cdot \vec{R_n} >=< (\sum_{i=1}^{n} \vec{r_i}) \cdot (\sum_{j=1}^{n} \vec{r_j}) > \tag{1.7}$$

where <> stands for the ensemble average. Since there is no correlation between different bonds, the mean-square end-to-end distance reduces to

$$< R^2 >= nl^2 \tag{1.8}$$

The square radius of gyration, the average square distance from the center of mass of a polymer to its all monomers, is defined as

$$R_g^2 = \frac{1}{n^2} \sum_{i=1}^{n} \sum_{j=1}^{n} (R_i^2 - \vec{R_i} \cdot \vec{R_j}) \tag{1.9}$$

Accordingly, the relation between the mean-square end-to-end distance and mean-square

radius of gyration can be expressed as

$$< R_g^2 >= \frac{< R^2 >}{6} \tag{1.10}$$

For freely jointed chain, the torsion angles can be of any value; however, some polymers are relatively rigid and tend to keep in one direction with some segments, like DNA. Werner Kuhn proposed a theoretical treatment for this problem [3], in which the number of monomers n is replaced by N, and the bond length l is replaced by Kuhn length b. A polymer chain is treated as a chain of Kuhn segments, which are freely jointed. In this case, the mean-square end-to-end distance can be expressed as $< R^2 >= nl^2 = Nb^2$.

Entropic Elasticity

A very important feature of freely jointed chain is that the end-to-end distance follows the normal distribution, which can be utilized to determine the total number of conformations, conformational entropy, and total free energy. According to the random walk statistics, given n walks, and the end-to-end vectors $\vec{R}$, the probability distribution can be written as [3]

$$P(n, \vec{R}) = (\frac{3}{2\pi nl^2})^{3/2} \exp(-\frac{3R^2}{2nl^2}) \tag{1.11}$$

In addition, the probability distribution can also be expressed as the number fraction of conformations with the end-to-end distance between $\vec{R}$ and $\vec{R} + \mathrm{d}\vec{R}$

$$P(n, \vec{R}) = \frac{\Omega(n, \vec{R})}{\int \Omega(n, \vec{R}) \mathrm{d}\vec{R}} \tag{1.12}$$

As a result, $\Omega(n, \vec{R})$ is expressed as

$$\Omega(n, \vec{R}) = P(n, \vec{R}) \int \Omega(n, \vec{R}) \mathrm{d}\vec{R} \tag{1.13}$$

Since $S = k \ln \Omega$, the total conformational entropy can be written as

$$S(n, \vec{R}) = -\frac{3}{2} k \frac{R^2}{nl^2} + S(n, 0) \tag{1.14}$$

where $S(n, 0)$ is the entropy that is independent of the end-to-end distance. The free energy depends on both the enthalpy and entropy, $F = U - TS$, thus the total free energy can be written as

$$F(n, \vec{R}) = \frac{3}{2} kT \frac{R^2}{nl^2} + F(n, 0) \tag{1.15}$$

The free energy depends on R^2, which implies that polymer chains obey Hooke's law and behave like springs with a spring constant of $\frac{3kT}{nl^2}$.

Real chains

The behaviour of ideal chains can be observed in polymer melts or theta solvents, but in other cases, non-bonded monomer-monomer interactions and polymer-solvent interactions need to be taken into account. Thus, in these situations polymers are real chains and do not behave like ideal chains. For real chains, a very important concept is the excluded volume, the volume that is inaccessible for other molecules [3]. It has a general mathematical expression

$$v = -\int f(r) \mathrm{d}^3 r = \int (1 - \exp[-U(r)/(kT)]) \mathrm{d}^3 r \tag{1.16}$$

where f is the Mayer f-function and $U(r)$ is the interaction between monomers. This parameter describes the net effect of all two-body interactions between monomers, and the solvent is treated as a field. For different solvent conditions, the excluded volume is different. In the following discussion, the Kuhn monomer is taken as the smallest unit, which has a Kuhn length b, and a Kuhn width d.

- Athermal solvents: At high temperatures, only the hard-core repulsion contribute to the excluded volume, which is independent of temperature. In this condition, $v \approx b^2 d$.

- Good solvents: In good solvents, monomer-monomer interactions are slightly smaller than monomer-solvent interactions, which leads to a slightly weak attraction. As a result, the excluded volume is affected not only by the hard-core repulsion but also by the attraction. In this condition, $0 < v < b^2 d$.

- Theta solvent: At θ temperature, the attraction is canceled out by the repulsion, which leads to a zero excluded volume, $v = 0$. In this condition, polymers have ideal conformations.

- Poor solvents: In poor solvents, monomers tend to stay closer. As a result, $-b^2 d < v < 0$.

- Non-solvents: The lower extreme of poor solvents is non-solvent, where the excluded volume is $v \approx -b^2 d$.

Assuming a real polymer chain in an athermal or good solvents, the equilibrium size of the chain is determined by the balance of the excluded volume and conformational entropy, where the excluded volume tends to expand the polymer chain, and conformational entropy wants to recover the ideal conformation. As a result, compared with ideal chains, the size of real chains in good solvents is bigger due to swelling. This swelling effect can be calculated based on the free energy

$$F \approx kT(v\frac{N^2}{R^3} + \frac{R^2}{Nb^2}) \tag{1.17}$$

To minimize the free energy, it gives $R_F \approx v^{1/5}b^{2/5}N^{3/5}$, which shows a different scaling law from ideal chains $bN^{1/2}$. This conformation is identical to the self-avoiding random walk in stochastic processes, while an ideal chain follows the pure random walk.

1.1.4 Dynamics of polymers

Rouse dynamics

Rouse dynamics [3, 4], a good model to describe the microscopic dynamics of short chains or for short time scales, assumes a polymer chain is composed of many beads connected by elastic springs. The interactions from solvent or other polymers are treated as hydrodynamic frictions. From Stokes' law, each bead can feel a friction $\vec{f} = \zeta\vec{v}$, where ζ stands for the friction coefficient and v is velocity. Given a Rouse chain with N beads, the total friction coefficient is $\zeta_R = N\zeta$. According to the Einstein relation, the total diffusion

coefficient of a Rouse chain can be expressed as

$$D_R = \frac{kT}{\zeta_R} = \frac{kT}{N\zeta} \tag{1.18}$$

The time it takes to diffuse over a distance of the size of the polymer can be estimated by

$$\tau_R \approx \frac{R^2}{D_R} \approx \frac{\zeta}{kT} N R^2 \tag{1.19}$$

Considering the mean-square end-to-end distance expressed in terms of Kuhn monomers, $< R^2 >= Nb^2$, the relaxation time τ_R can be expressed as

$$\tau_R \approx \frac{\zeta b^2}{kT} N^2 = \tau_0 N^2 \tag{1.20}$$

where $\tau_0 = \frac{\zeta b^2}{kT}$ is the relaxation time of the Kuhn monomer, which is the smallest relaxation time of a polymer chain. A striking feature of Rouse dynamics is that, for any observation time less than τ_0, polymers exhibit elastic response; in contrast, for any observation time bigger than τ_R, polymers behave like simple liquids. This is in good agreement with experiments. Moreover, at the time between τ_0 and τ_R, a viscoelastic response can be observed and it depends on the Rouse mode. For each Rouse mode, a certain number of monomers are involved. For the mode p, which describes the coherent motion with N/p monomers, the relaxation time can be given as

$$\tau_p = \tau_0 (\frac{N}{p})^2 \tag{1.21}$$

Taking the stress relaxation experiment as an example, at time $t = \tau_p$, the number of unrelaxed modes is p. For each unrelaxed mode, it contributes to stress relaxation modulus

G equally with an energy of order kT. At time $t = \tau_p$, the stress relaxation modulus can be expressed as

$$G(\tau_p) \approx \frac{kT}{b^3}\frac{v}{N}p \tag{1.22}$$

where v is the volume fraction. According to Eq. 1.21, the time dependence of mode p can be expressed as

$$p = (\frac{\tau_p}{\tau_0})^{-1/2}N \tag{1.23}$$

Thus, for $\tau_0 < t < \tau_R$,

$$G(t) \approx \frac{kT}{b^3}v(\frac{t}{\tau_0})^{-1/2} \tag{1.24}$$

For $t > \tau_R$, it follows an exponential decay $\exp(-t/\tau_R)$

$$G(t) \approx \frac{kT}{b^3}v(\frac{t}{\tau_0})^{-1/2}\exp(-t/\tau_R) \tag{1.25}$$

According to the relation between the viscosity η and modulus G, the viscosity can be calculated through

$$\eta = \int_0^\infty G(t)dt \approx \frac{\zeta}{b}N \tag{1.26}$$

which indicates that the viscosity is a linear function of the degree of polymerization. This relation is valid until entanglement effects are involved.

Entanglements and Reptation model

According to the Rouse model, viscosity is a linear function of polymer size; however, experimental physicists have found that this is only valid up to a certain molecular weight,

beyond which the viscosity is no longer proportional to N. The deviation from the Rouse dynamics is due to entanglement, which is the topological restriction of polymer chain motion by surrounding polymer chains. In this condition, polymer chains have to slither in the tubes formed by surrounding polymer chains. This is known as the tube model. de Gennes utilized the concept of tubes and proposed a scaling law: reptation model to describe how polymer chains relax within tubes [3, 5]. Fig. 1.3 shows that a polymer chain is confined in a tube, where the tube has a diameter of a. In order to understand how a polymer chain moves in a tube, we assume the tube is composed of many blobs [6] and the size of these blobs is equal to that of the tube. In addition, the polymer segments in the blobs have the random coil conformation, which means in the blobs, the polymer segments are not affected by the tube. Accordingly, the size of each blob can be expressed as

$$a \approx b\sqrt{N_e} \tag{1.27}$$

where N_e is the number of Kuhn monomers in each blob and b is the length of a Kuhn monomer. If the total number of Kuhn monomers in the polymer chain is N, there are N/N_e blobs in the tube. Consequently, the contour length $< L >$ of the tube can be expressed as $a\frac{N}{N_e}$. Finally, the average contour length of the tube can be expressed as

$$< L > \approx a\frac{N}{N_e} \approx \frac{bN}{\sqrt{N_e}} \tag{1.28}$$

According to the Rouse model, the Rouse diffusion coefficient is $D_R = \frac{kT}{N\zeta}$. Consequently, the time for the polymer chain to diffuse out of the tube is simply

$$\tau_{rep} \approx \frac{< L >^2}{D_R} = \frac{\zeta b^2}{kT} N_e^2 (\frac{N}{N_e})^3 = \tau_e (\frac{N}{N_e})^3 \tag{1.29}$$

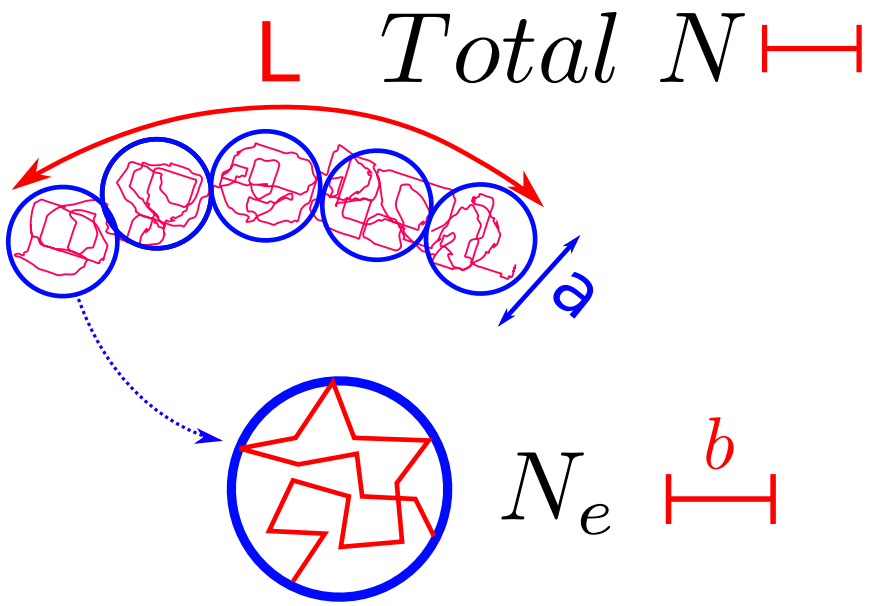

Figure 1.3: Schematic diagram of reptation model.

where τ_e is the Rouse time of a thermal blob with N_e monomers. Given the relaxation time τ_{rep}, the viscosity in the entanglement regime can be expressed as

$$\eta \propto N^3 \propto M^3 \tag{1.30}$$

To summarize, the relation between the viscosity and molecular weight is

$$\eta \sim \begin{cases} M & \text{for } M < M_c \\ M^3 & \text{for } M > M_c \end{cases} \tag{1.31}$$

where M_c is the onset molecular weight of entanglement. In experiments, an exponent of 3.4 was observed, and the deviation from 3 may be due to tube length fluctuations [7] or other relaxation modes [3].

1.1.5 Viscoelastic properties of polymers

For an ideal elastomer, when an external force is applied, the system deforms immediately. On the other hand, for an ideal viscous liquid, the system deforms continuously. Polymers are viscoelastic objects that have both modulus and viscosity. [5]

Taking the creep experiment as an example, for a pure elastic response, the deformation happens right after the external force is applied, which can be described by Hooke's law

$$\epsilon_1 = \sigma / E_1 \tag{1.32}$$

where σ is the stress applied at the beginning, ϵ_1 is the strain induced by the elastic response, and E_1 is the elastic modulus.

For polymers, in addition to the immediate elastic deformation, a retarded anelastic deformation can also be observed since the total deformation is gradually generated by chain segmental motions. The strain (ϵ_2) can be expressed as an elastic deformation with an exponential decay.

Polymers can also respond to external forces through a viscous fluid flow, which can be expressed as

$$\epsilon_3 = (\sigma / \eta_3) t \tag{1.33}$$

where ϵ_3 is the strain induced by the viscous flow, η_3 is the viscosity, and t is the time.

Fig. 1.4 shows the creep experiment, where the x-axis is time t, and the y-axis is the strain ϵ. At t_1, a constant stress σ is applied. At t_2, the stress is released.

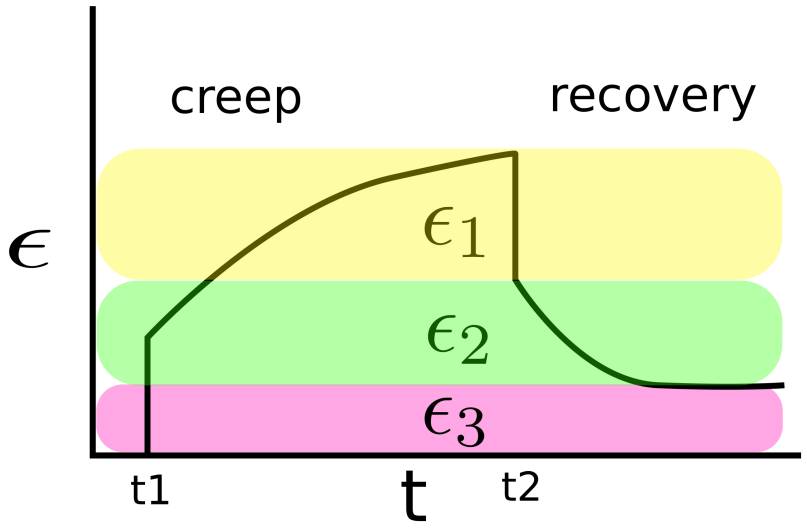

Figure 1.4: Creep curve of a viscoelastic polymer under tension, where ϵ_1 is an elastic deformation, ϵ_2 is a retarded anelastic deformation, and ϵ_3 is the deformation caused by the viscous flow.

The creep curve is composed of three contributions: ϵ_1, ϵ_2, and ϵ_3. The first two are reversible and the last one is irreversible. At different temperatures, the system behaves differently as different mechanisms have different temperature dependences. Below the glass transition temperature, the viscosity is high and the relaxation time is long. Accordingly, ϵ_2 and ϵ_3 are small. As a result, a pure elastic response dominates.

Boltzmann superposition principle

The Boltzmann superposition principle states that the net response of a polymer system to two or more stimuli can be considered as the linear combination of the responses caused by each stimulus individually [5]. Taking a stress relaxation experiment as an example, if a series of step strains $\delta\epsilon_i$ is applied at time t_i, the stress as time t can be expressed as

$$\sigma(t) = \sum_i G(t - t_i)\delta\epsilon_i \tag{1.34}$$

where G is the shear modulus. This expression implies that the final stress depends on the history of the strains, and each individual strain contributes independently to the final stress.

1.2 Amorphous solids and glass transition

1.2.1 What is the glass transition?

Solids can be either amorphous or crystalline. Crystalline solids have well-defined structures, which lead to a sharp transition between solids and melts at the so-called melting point (T_m). In contrast, amorphous solids do not have ordered structures. Therefore, they do not have melting points but rather glass transition temperatures. As mentioned in the previous sections, polymers are complex molecules, and are neither purely elastic nor purely viscous. Similarly, solid polymers are complex solids, and can be either amorphous or crystalline. It is also true that all materials undergoing fast cooling can enter amorphous states, even for ice [8, 9] and metals [10, 11]. The transition temperature from the glassy state to the liquid/rubbery state is defined as the glass transition temperature (T_g). During this transition, many physical properties change significantly, such as density, modulus, refractive index, heat capacity, *etc.* From high temperatures to low temperatures, the viscosity and relaxation time of the system increase dramatically. Therefore, conveniently, the glass transition temperature is defined as that at which the relaxation time of the system is 100 seconds or the viscosity of the system is $10^{12} Pa \cdot s$. When the relaxation time is longer than 100 seconds, the system is considered to be a solid, while when it is shorter, the system is considered to be a liquid.

Fig. 1.5 shows the temperature-dependent volume/entropy, where the highest transition temperature at the discontinuity is the melting point T_m, and the other two lower

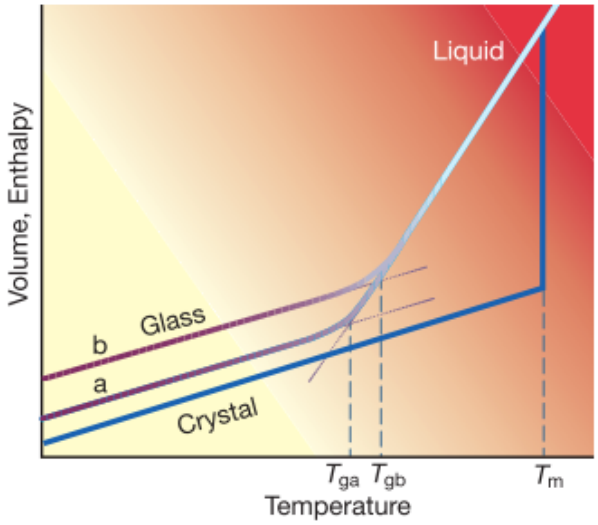

Figure 1.5: Schematic diagram of glass transition. Figure from [12].

transitions are the glass transitions. Two different glass transitions are caused by different cooling rates. A fast cooling rate leads to a higher glass transition temperature, which demonstrates that glass transition is also a kinetic phenomenon. The cooling rate dependence of glass transition temperature is relatively weak. Typically, the glass transition temperature changes by 3 K when the cooling rate changes by an order of magnitude [12]. The figure also shows a significant difference between the liquid/crystal transition and the liquid/glass transition. In general, if a transition involves discontinuous changes in the first derivatives of the free energy, such as volume $V = (\frac{\partial F}{\partial P})_T$ and entropy $S = -(\frac{\partial F}{\partial T})_P$, the transition is a first-order phase transition. Accordingly, the liquid/crystal transition is the first-order phase transition. However, the volume and entropy changes continuously at T_g. In addition, the second derivatives of the free energy, like thermal expansion coef-

ficient $\alpha_p = (\partial \ln v/\partial T)_p$ and isobaric heat capacity $C_p = (\partial h/\partial T)_p$, change abruptly but continuously at T_g. In consequence, the glass transition is not a true phase transition [12] as there is no discontinuous changes in any physical quantities.

Strong glasses and fragile glasses

As temperature decreases, viscosity increases. In general, there are two types of glass formers, strong and fragile. The difference between these two types of glass formers is the temperature dependence of viscosity. Fig. 1.6 shows the viscosity of different glass formers as a function of normalized temperature, in which two types of glass formers are shown (strong and fragile). This plot is also known as an "Angell Plot" as it was originally proposed by Austen Angell [13–15].

For strong glass formers, like silica, the temperature dependent viscosity can be expressed by the Arrhenius equation

$$\eta = A \exp(\frac{E_a}{kT}) \tag{1.35}$$

where A and E_a are temperature independent constants. E_a is also known as the activation energy. In contrast, for fragile glass formers, stronger temperature dependence can be observed, and it has the form

$$\eta = A \exp(\frac{B}{T - T_0}) \tag{1.36}$$

where A and B are temperature independent constants, and T_0 is the Vogel temperature. This equation is called the Vogel-Fulcher-Tammann (VFT) equation. In the field of poly-

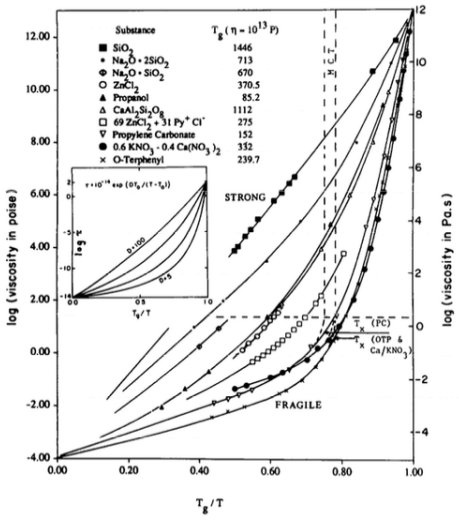

Figure 1.6: Arrhenius plot of different glass formers normalized by their glass transition temperatures. Figure from [14].

mer science, another empirical equation is often used to describe temperature dependent physical properties, known as the Williams-Landel-Ferry (WLF) [16] equation. It has the form

$$\log(a_T) = \frac{-C_1(T - T_r)}{C_2 + (T - T_r)} \tag{1.37}$$

where T_r is the reference temperature, C_1, C_2 are temperature independent constants, and a_T is the shift factor. Taking $a_T = \frac{\eta_T}{\eta_{ref}}$, the WLF equation and the VFT equation are mathematically identical.

In general, the temperature dependent viscosity of glass formers near their glass transition temperatures can be expressed as

$$\eta = A \exp(\frac{E_A}{k(T - T_0)}) \tag{1.38}$$

where $T_0 \sim 0$ for strong glasses and $T_0 >> 0$ for fragile glasses.

1.2.2 Glass transition theories

Free volume theory

Although the nature of glass transition is still unclear, several theories have attempted to explain the experimental observations near the glass transition temperature. Among these, the free volume theory is one of the most acceptable since it is intuitive and powerful. In the free volume theory, first proposed by Fox and Flory [17], volumes in liquids can be considered as *occupied* V_0 or *free* V_f, where the free volume is the volume *holes* between segments. Fox and Flory stated that below the glass transition temperature the free volume is a constant value V_f. Consequently, the total volume below the glass transition temperature can be expressed as

$$V = V_f + V_0 = V_f + A_0 + (\frac{\mathrm{d}V}{\mathrm{d}T})_g T \tag{1.39}$$

where A_0 is the hypothetical volume of the glass at $T = 0K$ and $(\frac{\mathrm{d}V}{\mathrm{d}T})_g$ is the glass expansion coefficient. Above the glass transition temperature, the total volume can be expressed as

$$V = V_g + (\frac{\mathrm{d}V}{\mathrm{d}T})_m (T - T_g) \tag{1.40}$$

where V_g is the total volume at the glass transition and $(\frac{\mathrm{d}V}{\mathrm{d}T})_m$ is the melt expansion coefficient. Then the free volume above the glass transition can be expressed as

$$(V_f)_T = V_f + (T - T_g)[(\frac{\mathrm{d}V}{\mathrm{d}T})_m - (\frac{\mathrm{d}V}{\mathrm{d}T})_g] \tag{1.41}$$

where the difference between the glass expansion coefficient and melt expansion coefficient is the expansion coefficient of the free volume α_f. Using the volume fraction instead of the volume, the free volume above the glass transition temperature can be expressed as

$$f = f_g + \alpha_f(T - T_g) \tag{1.42}$$

Following up on Batschinski's and Macleod's work [18], Doolittle proposed a relation between the liquid viscosity and the free-space (free volume) [19–21], which is expressed as

$$\eta = A\exp(\frac{BV_0}{V_f}) \tag{1.43}$$

where V_0 is the occupied volume, V_f is the free volume, A and B are constants. On top of this, Williams, Landel, and Ferry proposed the WLF equation based on both the free volume theory and the Doolittle equation. Since $f = \frac{V_f}{V_f+V_0} \approx \frac{V_f}{V_0}$, the V_0/V_f term in the Doolittle equation can be replaced by $1/f$. Taking the viscosity at the glass transition as the reference, the Doolittle equation can be further expressed as

$$\ln\frac{\eta}{\eta_{T_g}} = \ln a_T = B(\frac{1}{f} - \frac{1}{f_g}) \tag{1.44}$$

Substituting the free volume expression(1.42) into the equation above, the WLF equation can be derived

$$\ln a_T = \frac{B}{f_g}[\frac{T - T_g}{f_g/\alpha_f + T - T_g}] = -\frac{c_1(T - T_g)}{c_2 + T - T_g} \tag{1.45}$$

where $c_1 = \frac{B}{2.303 f_g}$and $c_2 = \frac{f_g}{\alpha_a}$. Taking $B = 1$, $f_g = 2.5\%$, which means the fraction of free volume is 2.5% below the glass transition temperature. The 2.5% is a general value and can be observed in many polymer systems. In addition to the temperature, the fraction

of free volume is also affected by the pressure. Colucci *et al.* [22] measured the glass transition temperature of poly(carbonate) (PC) in isobaric condition and found out that the glass transition temperature increases as the pressure increases since it squeezes out the free volume. The result confirms the idea of the free volume theory. The free volume theory can predict a lot of phenomena, such as the molecular weight dependence of the glass transition temperature (Flory-Fox curve) [17] and the plasticizer effect on the glass transition temperature [23].

Although the free volume theory has successfully explained many observations near the glass transition temperature, it should be noted that some experimental observations still cannot be explained by the free volume theory. For instance, the free volume theory assumes a constant fraction of free volume below the glass transition temperature, but the aging experiments indicate that the specific volume decreases as the aging time increases. Another example is the isochoric glass transition, where the volume is kept fixed during cooling. If the free volume theory is correct, no isochoric glass transition should be observed. However, both in experiment [22] and simulation [24], the isochoric glass transition can be observed.

Adam Gibbs Model

The free volume model is a kinetic model, in which the glass transition is not a thermodynamic phenomenon. In contrast, Adman and Gibbs proposed a completely different way to consider the glass transition [25]: an entropy theory. Before Adman and Gibbs's

work, Gibbs and DiMarzio [26] proposed a thermodynamic model based on the Flory-Huggins lattice model. In Gibbs and DiMarzio's model, the configurational entropy is calculated and a thermodynamic phase transition temperature (T_2) is defined. At T_2, the configurational entropy is zero. Adam and Gibbs introduced the concept of a *cooperatively rearranging region* (CRR), within which molecules move cooperatively. The size of CRR, highly dependent on temperature, can be determined by the number of configurations in the system. As temperature decreases, the relaxation time of the system increases and the number of configurations available to the system also decreases. The definition of CRR is not very clear in mathematics, but from the physics point of view, CRR is defined as *"the smallest region that can undergo a transition to a new configuration without a requisite simultaneous configurational change on and outside its boundary"* [25]. At the thermal dynamic glass transition T_2, the system requires a larger volume to undergo the configurational change and the size of CRR is comparable with that of the system. In this case, the whole system has only one configuration, which leads to the configurational entropy to be 0 as $S = k \log \Omega$ and $\Omega = 1$.

Taking the isothermal and isobaric ensemble with N CRRs and each CRR with z segments, the probability of CRR changing its configuration is $W(T)$, which is expressed as

$$W(T) = A \exp(\frac{-z\Delta\mu}{kT}) \tag{1.46}$$

where A is a constant and $\Delta\mu$ is the energy barrier. The lower limit $z*$ is the smallest size of CRR that still has a nonzero probability of undergoing the transition. Thus the average

transition probability is expressed as

$$\bar{W}(T) = \sum_{z=z^*}^{\infty} A \exp(\frac{-\Delta\mu z}{kT}) = \bar{A} \exp(\frac{-z^*\Delta\mu}{kT}) \tag{1.47}$$

where $\bar{A}$ is a new constant. This averaging simply states that the contributions to the transition probability from $z > z^*$ are negligible. Taking the configurational entropy of each CRR as s_c, the total configurational entropy S_c can be expressed as $S_c = Ns_c$. For the configurational entropy of each CRR, s_c is defined as

$$s_c = k\ln(W_c^{1/N}) \tag{1.48}$$

where W_c is the average number of configurations in the system. Assuming the system has one mole of segments, the above expression reduces to

$$s_c = k\ln(W_c^{z/N_A}) \tag{1.49}$$

$$S_c = \frac{N_A}{z} k\ln(W_c^{z/N_A}) \tag{1.50}$$

where N_A is the Avogadro's number. This equation indicates that the configuration entropy of CRR increases as the size of CRR increases. Taking the lower limit of CRR as z^*, the critical configurational entropy can be given by

$$s_c^* = k\ln(W_c^{z^*/N_A}) \tag{1.51}$$

$$S_c = \frac{N_A}{z^*} k\ln(W_c^{z^*/N_A}) \tag{1.52}$$

Consequently, $z*$ can be expressed as $N_A s_c^*/S_c$. Substituting the expression z^* into Eq. 1.47, the average transition probability is

$$\bar{W}(T) = \bar{A} \exp(\frac{-\Delta\mu N_A s_c^*}{kTS_c}) = \bar{A} \exp(\frac{-C}{TS_c}) \tag{1.53}$$

where $C = \frac{\Delta\mu N_A s_c^*}{k}$. In addition, since the relaxation time is $\tau(T) \sim 1/\bar{W}(T)$, the temperature shift factor a_T is expressed as

$$\log a_T = \log(\frac{\bar{W}(T_s)}{\bar{W}(T)}) \tag{1.54}$$

Substituting Eq. 1.53 into the above equation, this yields:

$$-\log a_T \sim C[\frac{1}{T_s S_c(T_s)} - \frac{1}{T S_c(T)}] \tag{1.55}$$

In order to determine the temperature dependence of $S_c(T)$, the entropy difference is expressed as:

$$S_c(T) - S_c(T_s) = \Delta C_p \ln T/T_s \tag{1.56}$$

Since $S_c(T_2) = 0$, the above expression becomes:

$$S_c(T_s) = \Delta C_p \ln T_s/T_2 \tag{1.57}$$

Substituting the above equation into Eq. 1.55, the WLF equation is recovered.

$$-\log a_T = \frac{a_1(T - T_s)}{a_2 + T - T_s} \tag{1.58}$$

where

$$a_1 = \log e \frac{C}{\Delta C_p T_s \ln(T_s/T_2)} \tag{1.59}$$

$$a_2 = \frac{T_s \ln(T_s/T_2)}{\ln(T_s/T_2) + [1 + T_s/(T - T_s)\ln(T/T_s)]} \tag{1.60}$$

The major breakthrough of Adam-Gibbs model is that it establishes a link between the dynamics (viscosity/relaxation) and the thermodynamics of supercooled liquids. In

addition, even though CRR is poorly defined, it presents a clear picture of glass transition without complicated mathematical equations. In addition, the real phase transition at T_2 proposed by Adam-Gibbs and Gibbs-DiMarzio is also an interesting topic. In general, T_2 is 55 °C below the glass transition, which is not a very low temperature since T_g for many polymers are above 25 °C. However, T_2 is not approachable, as it requires an infinitely slow cooling rate. As a result, whether or not there is a real phase transition is still an open question.

Cooperative string mode

Recently, Salez *et al.* [27] developed a new theoretical model of glass formation based on the idea of molecular crowding. In the theory, the motion in the system near the glass transition temperature is cooperatively string-like. Considering a system with N particles, the effective radius of these particles is r, and average intermolecular distance λ, the volume fraction can be expressed as $\phi \sim (r/\lambda)^3$. In order to relax, particles need to pass through the *gate* between two adjacent particles, where the *gate* has an average size of $L \sim \lambda - 2r$. When the density of the system is low, the size of the *gate* is big and particles can pass through the gate without involving the movement of other particles (solitary escape). In this case, the system is liquid-like. However, as the density of the system decreases, solitary escape is not possible and relaxation requires a cooperative motion. In this case, the onset average intermolecular distance λ is defined as λ_c. In the extreme case, $\lambda = 2r$, no particles can escape from their surrounding cages. In this case, relaxation is not possible even in

a cooperative motion and the average nearest neighbour distance λ is defined as λ_V. In a real system, the glass transition is in between λ_c and λ_V. When $\lambda_V < \lambda < \lambda_c$, the cooperative motion is required to compensate the too small gate (the average missing space $\delta = \lambda_c - \lambda$). Because the average length between particles is L, the cooperative motion involving N particles can provide a total length $\Delta = (N-1)L$. A particle can pass through the gate only if $\Delta > \delta$. This leads to a threshold $N = N^*$ when $\Delta = \delta$. The expression of N^* is:

$$N^*(\phi) \sim \frac{\lambda_c - \lambda_V}{\lambda - \lambda_V} \sim \frac{(\frac{\phi_V}{\phi_c})^{1/3} - 1}{(\frac{\phi_V}{\phi})^{1/3} - 1} \tag{1.61}$$

As the cooperative motion requires all particles to move in phase, the coherent probability ϵ is introduced. Accordingly, the total probability density of a cooperative relaxation process involving N particles can be given by:

$$P_N(\phi) \sim \frac{1}{\tau_c \lambda^3}(1-\epsilon)\epsilon^{N-1}\Theta(N - N^*) \tag{1.62}$$

where τ_c is the liquid-like relaxation time, Θ is a Heaviside function. Integrating P_N for all $N > N^*$, the total probability density becomes:

$$P(\phi) \sim P_c \epsilon^{N^*-1} \tag{1.63}$$

where $P_c = \frac{1}{\tau_c \lambda^3}$. Defining the molecular relaxation time $\epsilon_0 = \epsilon \tau_c$, the relation between τ and τ_0 can be given by:

$$\frac{\tau}{\tau_0} \sim (\frac{\tau_c}{\tau_0})^{N^*} \tag{1.64}$$

Considering the Arrhenius law, the onset relaxation time can be written as:

$$\tau_c = \tau_0 e^{\Delta\mu/kT_c} \tag{1.65}$$

where $\Delta\mu$ is the energy barrier to pass the gate. Substituting Eq. 1.64 into the above expression, the Adam-Gibbs equation can be recovered.

$$\tau = \tau_0 e^{\Delta\mu N^*/kT} \tag{1.66}$$

In order to determine the temperature dependent dynamics near the glass transition, the density dependent description is mapped to the temperature dependent description through the thermal expansion coefficient $\alpha = -\frac{1}{\phi}\frac{d\phi}{dT}$. This leads to a temperature dependent volume fraction $\phi(T) = \phi_V[1 + \alpha(T_V - T)]$, where T_V is defined as the Vogel temperature and ϕ_V is the volume fraction at T_V. Combining this direct mapping and Eq. 1.61, 1.64, the VFT equation can be recovered.

$$\tau(T) = \tau_0 \exp(\frac{A}{T - T_V}) \tag{1.67}$$

where $A = (T_V - T_c)ln(\epsilon)$. The recovery of both the Adam-Gibbs and VFT equations indicates the correctness of this simple cooperative string model. Moreover, the model requires only a few assumptions and only utilizes the concept of density crowding. All these advantages make this model powerful and intuitive, especially for experimental scientists. A more striking feature of the cooperative string model is that it can even predict the glass transition reduction phenomenon observed in polymer thin films [28–30]. Assuming there is a length scale ξ of the cooperative region, it can be expressed as

$$\xi \sim \lambda_V(\frac{T_c - T_V}{T - T_V}) \tag{1.68}$$

The length scale is a constant at a certain temperature in the bulk; however, near the surface, due to the absence of caging, fewer particles need to be involved to relax. This

leads to a truncated N^*. By introducing an asymptotic function f, the truncated N^* at a distance z from the surface and at temperature T can be expressed as:

$$N_s^*(z,T) \sim N^* f(\frac{z}{\xi}) \tag{1.69}$$

where $f(0) \sim 0$ and $f(z >> 1) \sim 1$. Accordingly, the relaxation at location z and at temperature T can be expressed as:

$$\frac{\tau_s(z,T)}{\tau_0} \sim (\frac{\tau}{\tau_0})^{f(z/\xi)} \tag{1.70}$$

If a local relaxation time $\tau_s > \tau_g^{bulk}$, it should exhibit a glass expansivity; in contrast, if $\tau_s < \tau_g^{bulk}$, it should exhibit a liquid expansivity. In general, the glass transition is defined as the mid-point of the thermal expansivity curve ($\alpha = 1/2(\alpha_m + \alpha_g)$). As a result, the transition should occur when half of the film is glassy and the other half is liquid. Mathematically, it should be $\tau_s(h/2,T) = \tau_g^{bulk}$. Finally, the film thickness dependent $T_g(h)$ should satisfy the following expression

$$2\xi(T_g) f^{-1}(\frac{T_g - T_V}{T_g^{bulk} - T_V}) = h \tag{1.71}$$

1.3 Crystallization of polymers

From the previous sections, we know that polymers are large molecules and they can form amorphous solids when the temperature decreases. However, the amorphous phase is not

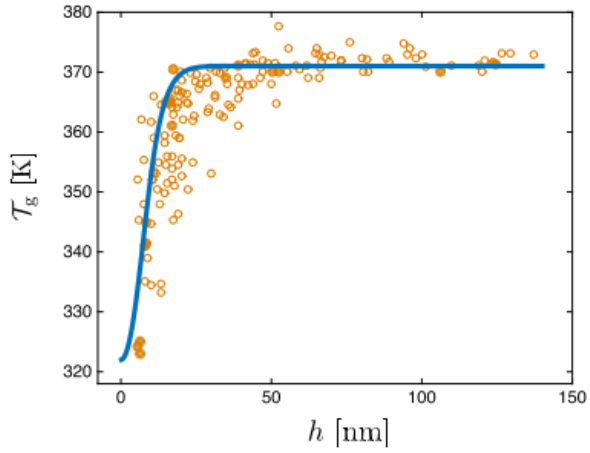

Figure 1.7: Comparison between the experimental $T_g(h)$ and the theoretical values generated based on cooperative string model, where the solid line stands for the theoretical calculation. Figure from [27].

necessary the ground state of polymers as the free energy in the crystalline phase may be lower than that in the amorphous phase. Thus, some polymers under proper conditions can crystallize.

In order to understand the origin of polymer crystallization behaviour, we take oligomers as a starting point [5]. Oligomers have relatively low molecular weights and relatively rigid structures. Therefore, oligomers prefer to form stack layers, which means they align in one direction to form layers that are stacked together to form crystals. As the molecular weight increases, is this description still valid? In principle, stacked layers composed of fully extended polymer chains could form, which is called the ideal crystalline state. In the ideal crystalline state, the system is in the equilibrium state with the lowest energy.

However, polymers have higher molecular weight compared with oligomers, which leads to a lot of entanglements among polymer chains. If polymers crystallize from their melts, a long time is needed for polymer chains to disentangle, relocate, align, and form stacked layers. Instead, polymers tend to form some crystalline domains locally, which does not need a full rearrangement. Between the crystalline domains, there are amorphous domains. Because the system is composed of both amorphous and crystalline domains, crystallizable polymers are called semicrystalline polymers. Consequently, the crystallization behaviour of polymers depends not only on thermodynamics but also on kinetics. This unique feature makes the crystallization of polymers more complicated than that of small molecules.

1.3.1 Thermodynamics of polymer crystallization

Thermodynamics is the fundamental of polymer crystallization, as a system always tends to stay in a lower energy state. Fig. 1.8 shows the temperature dependent free energy. At high temperatures, the liquid state has a lower free energy than the crystalline state does; while at low temperatures, the liquid state has a higher free energy than the crystalline state does. The equilibrium melting point is defined as that at which both the liquid and crystalline states have the same free energy. Since the system prefers to keep itself in the lowest energy state, when $T < T_m^\infty$, polymers tend to form crystals. At T_m^∞, both liquids and crystals can coexist as they have the same free energy. Consequently, the free energy

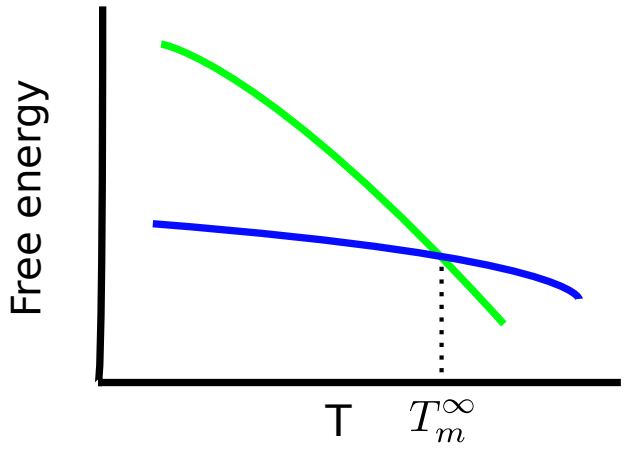

Figure 1.8: Free energy as a function of temperature, where the blue curve stands for the crystalline state and the green one represents the liquid state. The equilibrium melting point is denoted by T_m^∞.

during the melting/crystallization at T_m^∞ is zero

$$\Delta G = \Delta H - T_m^\infty \Delta S = 0 \tag{1.72}$$

Thus, the equilibrium melting temperature can be written as

$$T_m^\infty = \frac{\Delta H}{\Delta S} \tag{1.73}$$

which implies that the equilibrium melting point does not only depend on enthalpy but also entropy. According to Ehrenfest's definition, crystallization and melting are first-order phase transitions. As there is an abrupt change in the first derivatives of the free energy, such as volume V or entropy S in Fig. 1.9. Polymers tend to crystallize at temperatures lower than the melting point. The difference between the crystallization temperature and

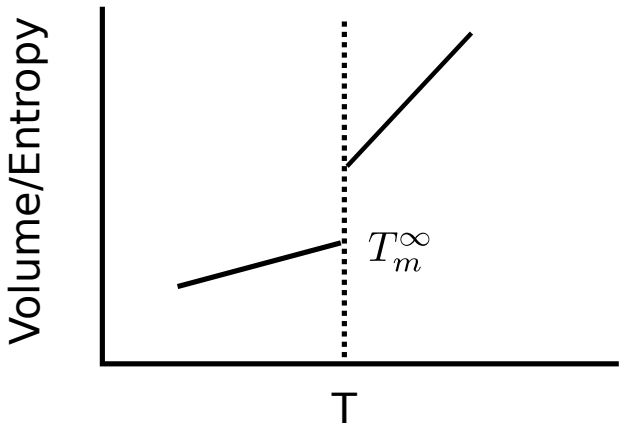

Figure 1.9: Volume/entropy as a function of temperature, where the abrupt change in volume/entropy is the equilibrium melting point.

.

the melting temperature is called the supercooling. In general, the supercooling can be as large as 20 to 30 K for polymers because the first stage of crystallization requires a large driving force (ΔG).

1.3.2 Crystal structures

In history, there are several semicrystalline models. In this section, some famous models are introduced, in which their successes and limitations are also discussed.

The fringed micelle model

The fringed micelle model is the oldest model of semicrystalline polymers and it was first proposed by Hermann, Gerngross and Abitz and then developed by Flory [31, 32]. In the fringed micelle model, a polymer chain can pass though several crystalline domains, between which the polymer segments are amorphous. This description is able to explain the coexistence of both the crystalline and amorphous domains. However, there are some observations that the fringed micelle model cannot explain. One example is the Maltese cross pattern in spherulites observed with crossed polarizers. Spherulites are commonly observed in semicrystalline systems. The observation of the Maltese cross pattern in spherulites indicates a strong alignment preference of polymer chains. However, in the fringed micelle model, polymer chains randomly form crystalline domains and have no alignment preference. As a result, people started to abandon the fringed micelle model and to seek a better model.

Folded chain model

As the development of polymerization techniques, polymers with high crystallinity can be synthesized. In 1955, Jaccodine [34] presented the observation of polyethylene single crystals. Two years later, Keller, Fisher and Till [35, 36] independently studied polymer single crystals with TEM and electron diffraction. They found these single crystals had smooth surfaces and their heights were about 10 nm. Keller then stated that polymers

Figure 1.10: Fringed micelle model of semicrystalline polymers, where two domains are shown. Figure from [33].

chains were perpendicular to the crystal planes and the height of these crystals was much smaller than the length. To account for these observations, he utilized the concept of folded chains, first proposed by Storcks in 1938 [37]. In the folded chain model, polymer chains are folded and aligned regularly. Consequently, a lamellar structure is formed. Fig. 1.11 shows a typical TEM image of polyethylene single crystals, from which thin lamellae with well-defined shapes can be observed.

Random re-entry vs. adjacent re-entry

The folded chain model states that polymer chains are folded; however, how frequent is the fold? In history, two groups of researchers had different points of view on this question and there was an intense debate between these two opinions on the Faraday Discussions of the Chemical Society in 1979 [38–47]. In the adjacent re-entry model, a polymer chain passes through a site and immediately re-enters the neighbouring site. As a result, most neighbouring polymer segments in a lamella belong to one single polymer chain. This structure leads to relatively smooth surface of lamellar crystals. The adjacent re-entry model can be verified by many experiments, like SANS and AFM experiments on single crystals formed from dilute solutions [49].

The random re-entry model is also called *Switchboard* model and was first proposed by Flory [31]. Flory found that the crystallization speed was fast, thus there was not enough time for polymer chains to relax and to form regular chain folds. Consequently, in the random re-entry model, a polymer chain passes through a lamella and does not

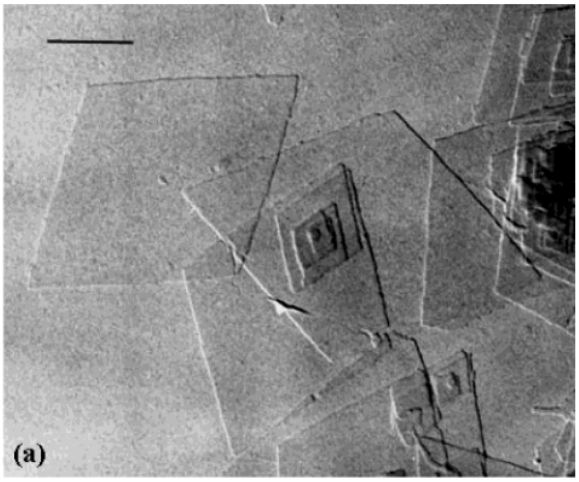

Figure 1.11: TEM image of single crystals of polyethylene. Figure from [48].

need to re-enter the next site. Instead, a polymer chain randomly passes through different lamellae. In this description, the neighbouring segments in a lamella do not necessarily belong to the same polymer chain and there are a lot of amorphous loops and tie molecules between different lamellae. In the small angle neutron scattering studies of polyethylene crystallization from melts [50], the radius of gyration of polyethylene in the crystalline state is similar to that in the melt state. This observation supports the random re-entry model rather than the adjacent re-entry model, as the polymer chain conformation of adjacent re-entry model is significantly different from the ideal random coil conformation.

However, there is a problem of the random re-entry model that it predicts an unreal density near the amorphous/crystalline interface or in the amorphous domain [51]. In reality, polymer crystallization from melts should include enough adjacent re-entry chains

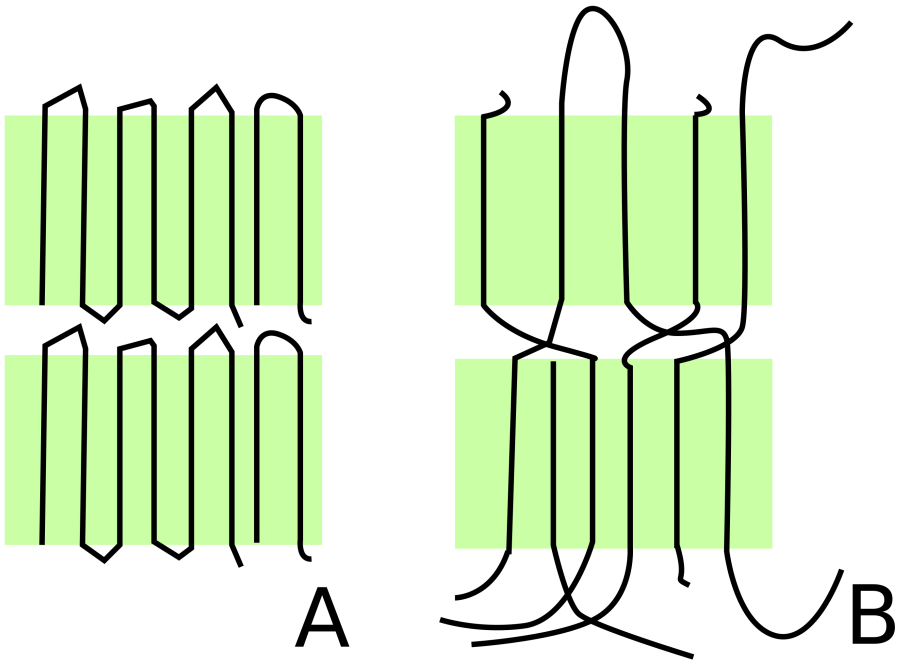

Figure 1.12: Schematic diagram of (A) adjacent re-entry model and (b) random re-entry model.

(to get rid of the unreal density problem) and also some random re-entry chains (to keep the correct conformation).

1.3.3 Crystallization and melting

Lamellar thickness and Gibbs Thomson equation

From the previous section, we know that polymers prefer to form lamellar structure, but what is the lamellar thickness and how does the lamellar thickness affect the melting point? Fig. 1.13 shows the melting point and lamellar thickness of syndiotactic polypropylene (sPP) and sP(PcOx) with different crystallization temperatures, where sP(PcOx) is syndiotactic Poly(propene-co-octene) copolymer and x stands for the weight percentage of octene-units. From the figure, it can be seen that the melting temperature, lamellar thickness, and crystallization temperature have strong correlations.

In fact, the relation between the melting point and the lamellar thickness can be explained by thermodynamics. Assuming a lamella is a cuboid with the length a, the width b, the height l, the surface energy σ_e of the top and bottom surfaces, the surface energy σ of other sides, and the free energy per unit mass on melting Δg, the total free energy for a finite sized crystal $\Delta G(T)$ can be expressed as

$$\Delta G(T) = 2al\sigma + 2bl\sigma + 2ab\sigma_e - abl\Delta g(T) \tag{1.74}$$

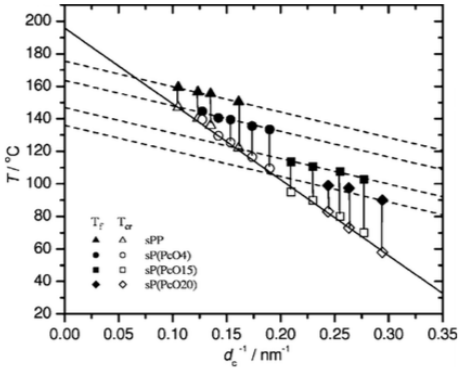

Figure 1.13: Relations between the inverse thickness, the crystallization temperature, and the melting point of sPP and sP(PcOx), where x is the weight percentage of octene-units, open symbols correspond to the crystallization temperatures, and solid symbols are the melting temperatures. Figure from [52].

In general, the $\sigma_e \gg \sigma$, $a \gg l$, and $b \gg l$, thus the above equation can be written as

$$\Delta G(T) = 2ab\sigma_e - abl\Delta g(T) \tag{1.75}$$

At the melting point, the free energy difference between the crystalline and liquid states is 0. Thus, $\Delta G = 0$ and the above expression reduces to

$$\Delta g(T_m) = \frac{2\sigma_e}{l} \tag{1.76}$$

If the melting point of an infinitely large crystal is T_m^∞, $\Delta g(T_m^\infty)$ can be expressed as

$$\Delta g(T_m^\infty) = \Delta h(T_m^\infty) - T_m^\infty \Delta s(T_m^\infty) \tag{1.77}$$

Since $g(T_m^\infty) = 0$, thus the above equation becomes

$$\Delta s(T_m^\infty) = \frac{\Delta h(T_m^\infty)}{T_m^\infty} \tag{1.78}$$

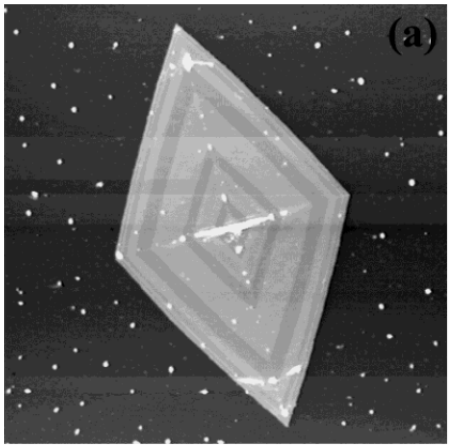

Figure 1.14: AFM topography of polyethylene single crystal formed from a dilute solution at a sequence of temperatures. Figure from [53].

Assuming there is no significant change of the entropy and enthalpy between T_m and T_m^∞, $\Delta g(T_m)$ is given by

$$\Delta g(T_m) = \Delta h(T_m) - T_m \Delta s(T_m) \tag{1.79}$$

Replacing the entropy by Eq. 1.78, the above equation can be expressed as

$$\Delta g(T_m) = \Delta h(T_m) - T_m \frac{\Delta h(T_m)}{T_m^\infty} \tag{1.80}$$

Finally, one can have an expression of T_m

$$T_m = T_m^\infty - \frac{2\sigma_e T_m^\infty}{l\Delta h} \tag{1.81}$$

This equation is called the Gibbs-Thomson equation, which states that the melting point depression is due to the finite size effect. Tian *et al.* did some beautiful work to demonstrate the relation between the lamellar thickness and crystallization temperature [53, 54].

In the experiment, the crystal was grown from a dilute solution and the temperature of the solution changed periodically. Fig. 1.14 shows the AFM topography of a single polyethylene crystal formed from the dilute solution, in which different colours stand for different thicknesses. It is clear that there is a periodic thickness of the single crystal, which is caused by the temperature change during the crystallization process. In general, if one has a plot of the melting temperature vs. the lamellar thickness, the equilibrium melting temperature can be calculated based on the Gibbs-Thomson equation.

Nucleation theory

The nucleation of crystals is the first stage of polymer crystallization. According to the nucleation theory, there are three types of nucleation: primary nucleation, secondary nucleation, and tertiary nucleation. Primary nucleation is the process of forming small nuclei from supercooled liquids, in which the local density fluctuation is the driving force. If the nuclei are cubic, there are 6 new faces formed. Secondary nucleation is the nucleation event on the smooth surface of nuclei, in which only 4 new faces are formed. Tertiary nucleation is the nucleation event at the edge of nuclei, in which only 2 new faces are formed. Fig. 1.15 demonstrates the three types of nucleation. In addition, primary nucleation also has two types, homogeneous nucleation and heterogeneous nucleation. Homogeneous nucleation means there is no foreign particle and the nucleation event is spontaneously induced by thermal fluctuations. In contrast, heterogeneous nucleation is induced by foreign particles, such as impurities and nucleation agents.

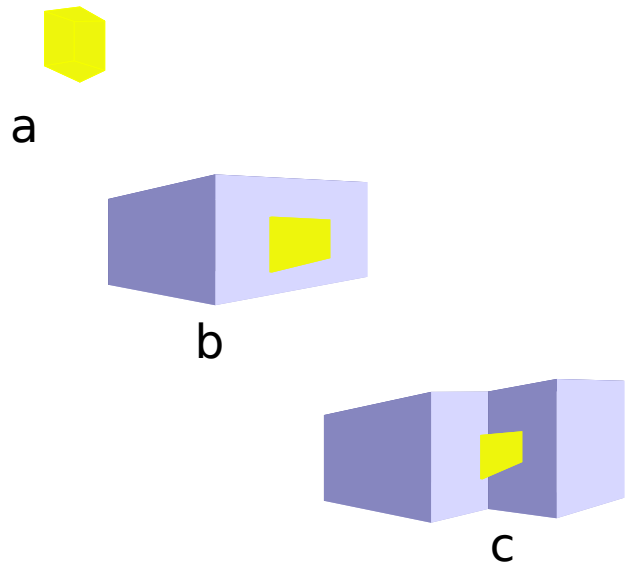

Figure 1.15: Different types of nucleation: (a) primary nucleation, (b) secondary nucleation, and (c) tertiary nucleation.

In this section, homogeneous primary nucleation is discussed. Due to the local density fluctuation, small aggregates can form embryos. In some situations, the size of the embryo is too small and the free energy loss due to crystallization cannot compensate the surface energy gain from the new surfaces formed. As a result, the embryos tend to melt. In contrast, if the local density fluctuation is big enough and the free energy loss due to crystallization is big, it is possible for those embryos to survive. In the following derivation, we focus on the classical nucleation theory and the topological connectivity of the polymer is neglected. As a result, the shape of the embryos is restricted to be spherical [55]. Accordingly, the total free energy of an embryo can be expressed as

$$\Delta G = -\frac{4}{3}\pi r^3 \Delta g + \sigma_e 4\pi r^2 \tag{1.82}$$

where r is the radius of the embryo, Δg is the free energy per unit mass on melting, σ_e is the surface energy.

Fig. 1.16 shows the free energy as a function of the radius of the embryo. When $r < r^*$, the free energy increases as r increases. At the critical radius r^*, the embryo has the largest free energy ΔG^*, after which the free energy decreases as r decreases. This states that if the local density fluctuation is big enough and the newly formed embryo has a radius $r > r^*$, the embryo can survive and keep growing. The critical radius r^* and critical free energy ΔG^* can be calculated by differentiating the free energy with respect to r [56]. This gives the critical nucleation radius r^*

$$r^* = \frac{2\sigma_e}{\Delta g} \tag{1.83}$$

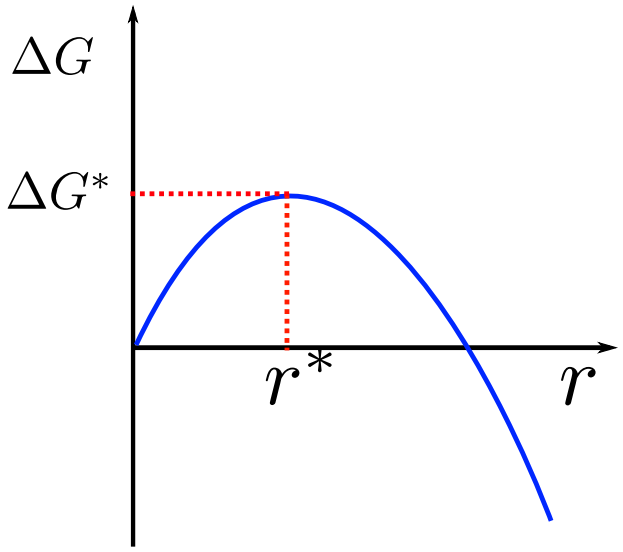

Figure 1.16: Free energy of an embryo as a function of radius r, where r^* is the critical radius and ΔG^* is the critical free energy.

and the critical nucleation energy ΔG^*

$$\Delta G^* = \frac{16\pi\sigma_e^3}{3\Delta g^2} \tag{1.84}$$

Assuming the entropy (ΔS) and the enthalpy (Δh) are not sensitive to the temperature near the crystallization temperature, Δg can be expressed as

$$\Delta g = \Delta h \frac{T_m - T_c}{T_m} = \Delta h \frac{\Delta T}{T_m} \tag{1.85}$$

where T_m is the melting temperature, T_c is the crystallization temperature, and ΔT is called the supercooling: the difference between T_m and T_c. Substituting the above equation into the expressions of r^* and ΔG^*, the relation between the critical nucleation radius/energy

and the supercooling to can be expressed as

$$\begin{aligned} r^* &\propto \Delta T^{-1} \\ \Delta G^* &\propto \Delta T^{-2} \end{aligned} \tag{1.86}$$

Turnbull and Fisher [57] developed the nucleation theory and proposed an expression of the nucleation rate

$$I = I_0 \exp(-\frac{\Delta E + \Delta G^*}{kT}) \tag{1.87}$$

where I_0 is a pre-exponent factor, ΔE is the activation energy, and ΔG^* is the critical nucleation energy. For polymers, $\Delta E/kT$ term satisfies the VFT equation. This equation indicates that there are two factors affecting the nucleation process, ΔE and ΔG^*. When T is close to the melting point T_c, the small supercooling ΔT leads to a big energy barrier. In contrast, when T is close to the glass transition temperature T_g, the diffusion process dominates. Consequently, the nucleation process should have a maximum speed between T_g and T_c. Fig. 1.17 shows the nucleation rate as a function of temperature of different polymers. As it shows, the nucleation rate always displays a bell-shaped curve, *i.e.*, the lower rate at both high and lower temperatures.

Nucleation is the first stage of crystallization. It is typically hard to measure and analyze because there is a fast growth process followed. Massa and Dalnoki-Veress [59] designed a beautiful experiment to test whether nucleation is a bulk process or a surface process. Given many micrometer sized droplets, the nucleation time τ_{nuc} can be precisely measured. The results show that $\tau_{nuc}V$ gives a master curve for all different droplet sizes, revealing that nucleation is a bulk process.

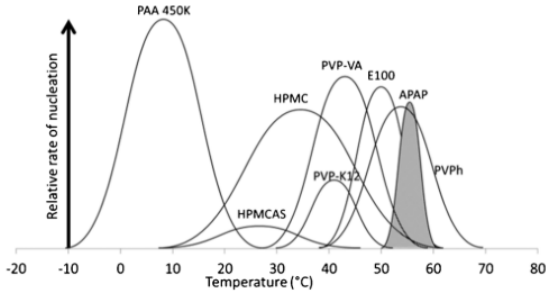

Figure 1.17: Nucleation rate as a function of temperature of different polymers. Figure from [58].

1.3.4 Crystal growth

The next stage after nucleation is crystal growth. As mentioned in the previous sections, semicrystalline polymers tend to form the lamellar structure. Thus, the growth of lamellae determines the final morphology of crystals. In fact, crystal growth is the process that crystallizable materials attach themselves to existing nuclei or small crystals.

Typically, crystal growth is controlled by two mechanisms: diffusion-controlled and interface-controlled. In diffusion-controlled cases, such as in dilute solutions, the growth rate is limited by how fast crystallizable materials can diffuse to the surface of crystals. This effect can be described by Fick's first law

$$J = -D\frac{\partial C}{\partial x} \tag{1.88}$$

where J is the flux of crystallizable materials, D is the diffusion coefficient, C is the

concentration, and s is the distance. Then the diffusion rate can be given by

$$\frac{\mathrm{d}n}{\mathrm{d}t} = 4\pi r^2 J \tag{1.89}$$

Consequently, the crystal growth rate can be given by

$$\frac{\mathrm{d}r}{\mathrm{d}t} = \frac{\mathrm{d}nv/(4\pi r^2)}{dt} \tag{1.90}$$

where v is the molar volume. Integrating the above equation, the relation between the radius of crystals and time can be given by

$$r \propto t^{1/2} \tag{1.91}$$

This states that the linear growth rate under diffusion-control is not constant but depends on $t^{-1/2}$. Fig. 1.18 shows that the crystallization front of Poly(Lactic Acid) exposed to acetone vapor as a function of the square root of exposure time. Clearly, there is a linear relation between the crystallization front and the square root of exposure time. The results demonstrate a diffusion-controlled growth.

When crystals grow from their melts, it usually shows an interface-controlled process. In this case, the crystallization process mainly depends on how crystallizable materials attach to the surface of existing nuclei/crystals because there are enough crystallizable materials near existing nuclei/crystals. As a result, a time independent growth rate is observed. Lauritzen and Hoffman(LH) [61, 62] first proposed the secondary nucleation theory to describe how crystallizable materials attach to the surface of existing crystals and to form lamellae. Although there are some limitations of the LH theory, it has been

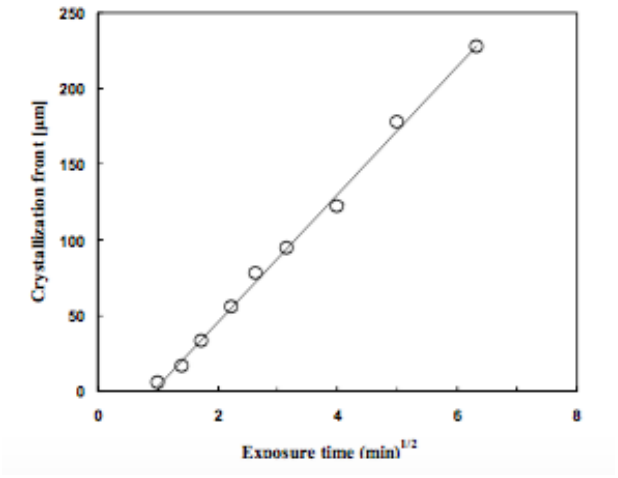

Figure 1.18: Crystallization front as a function of the square root of the exposure time of Poly(Lactic Acid) sample exposed to acetone vapor. Figure from [60].

widely accepted. In the LH theory, a polymer chain unit first deposits onto a crystal surface and crystallizes onto the lattice. After that, the next unit in the same polymer chain continues this process until one stem is formed. Following that, the polymer chain turns over to form the next stem [63].

The LH theory is capable to describe how the growth rate depends on temperature. In the LH theory, there are three growth regimes I,II,and III. In different regimes, the growth rate exhibits different temperature dependencies.

At low ΔT_s, regime I in the LH theory, the surface nucleation rate i is smaller than the lateral growth rate g. As a result, there is enough time for polymer chains to form an

entire layer before a new nucleus forms. Then the growth rate in regime I is expressed as

$$G_I = ib_0L \tag{1.92}$$

where b_0 is the thickness of the new layer formed on the crystal, L is the length of the surface. In this case, the crystal surface is very smooth. If temperature decreases, the supercooling ΔT increases. Consequently, the nucleation time is comparable to the time required to cover the entire surface. As a result, it is possible to form multiple nuclei before the surface is completely covered.

In regime II, the total linear growth rate can be given by

$$G_{II} = b_0(ig)^{1/2} \tag{1.93}$$

which is independent of L. In this regime, the surface is not as smooth as that in regime I, and it shows the molecular roughness. The derivation of the above expression was first proposed by Sanchez and DiMarzio [64, 65] and developed by Lauritzen and Hoffman [66, 67]. In fact, Frank [68] derived the above expression from a differential equation with moving boundary conditions. With the equation, a rounded lateral profile of polyethylene single crystal can be predicted and it was experimentally observed and verified [69–71].

At lower temperatures, regime III is reached, where the nucleation rate i is bigger than the lateral growth rate g. Consequently, the nucleation and the lateral growth can happen at the same time and the surface becomes even rougher. In this condition, the lateral spacing L' between two surface nuclei becomes smaller and the lateral growth does not

play an important role. As a result, the total linear growth rate can be expressed in terms of b_0, i and L'

$$G_{III} = ib_0L' \tag{1.94}$$

In general, the lateral spacing L' is about 1 to 3 stem widths [72].

Considering the primary nucleation rate discussed in the previous section, the expression is still valid in the surface nucleation process. In fact, at high temperatures, the activation energy is almost constant. As a result, the nucleation barrier dominates. Fig. 1.19 shows the growth rate of polyethylene crystals at high temperatures, where three regimes are shown.

In general, the LH theory treats crystal growth as a secondary nucleation process. This implies that the growth rate and the nucleation rate of polymers should have the same temperature dependence. Fig. 1.20 shows the linear growth rate of spherulites with different molecular weights at different temperatures, in which a bell-shaped curve can be observed for all molecular weights.

The above figure also demonstrates the molecular weight dependence of the linear growth rate because the molecular weight affects the mobility of polymers. Low molecular weight polymers have relatively high mobilities, which lead to large growth rates. In 1952, Price [75] observed that low molecular weight polychlorotrifluoroethylene had a larger growth rate than high molecular weight. Magil and Li [76] proposed a relation between

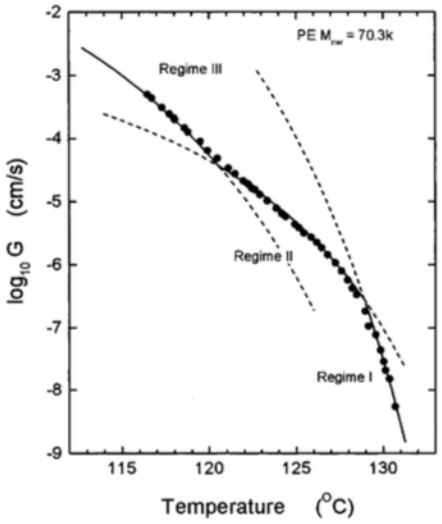

Figure 1.19: Growth rate G as a function of temperature of polyethylene. Solid lines stand for the calculated growth rates based on the LH theory, and dashed lines are the extrapolations from $G(T)$ calculations. Figure from [73].

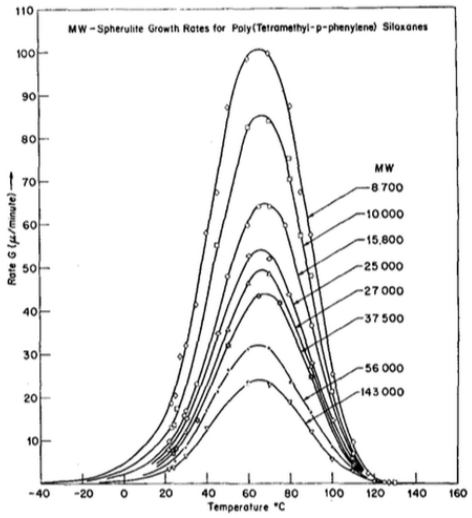

Figure 1.20: Spherulite growth rates with different molecular weights at different temperatures. Figure from [74].

the molecular weight and the growth rate

$$logG \propto M^{\alpha} \tag{1.95}$$

where α is between -1.2 and -0.5. Later, Cheng and Wunderlich proposed another equation. The linear growth rate at a constant supercooling ΔT can be expressed as

$$\log G = A \log[ln(n)] + B \tag{1.96}$$

where n is the molecular length, A and B depend on the supercooling ΔT.

Avrami plot

For semicrystalline polymers, the time dependent crystallinity can be controlled by several factors, such as the nucleation process (homogeneous or heterogeneous), diffusion-controlled growth or interface-controlled growth, dimensions, *etc.* The Avrami plot shows how the crystallization process goes. This equation was first derived by Kolmogorov in 1937, while Johnson and Mehl also derived this equation independently. However, the work done by Avrami [77–79] made the equation popular and widely accepted. The general form of the Avrami equation is

$$1 - Y = \exp(-Kt^n) \tag{1.97}$$

where Y is the relative crystallinity, K and n are constants. The striking feature of the Avrami equation is that the exponent n can tell what the condition is during the crystallization process. Here is a brief summary of the exponent n in different conditions. Table 1.1 demonstrates some typical n values and the growth behaviours. Taking $n = 4$ as an example, it states that the crystallization is based on homogeneous nucleation and followed by a three-dimensional growth. It is true that the above descriptions for different n are in ideal situations. In reality, crystallization can be more complicated and it may lead to different n values. Thus, how to use the Avrami equation and how to explain the fits extracted from the Avrami equation require more analyses. In addition, due to the collision of crystal growth fronts, it shows a decrease of n as time increases. As a result, a deviation from the Avrami plot in the late stage is usually observed. Fig. 1.21 shows the Avrami

Table 1.1: Value of n in the Avrami equation and growth conditions

Growth habit	Homogeneous nucleation				Heterogeneous nucleation
	Linear growth		Diffusion-controlled		Linear growth
	Steady state	$t = 0$	Steady state	$t = 0$	
Sheaf-like	6	5	7/2	5/2	5, 6
3D	4	3	5/2	3/2	3, 4
2D	3	2	2	1	2, 3
1D	2	1	3/2	1/2	1, 2

plot of Poly(ethylene terephthalate) isothermal crystallization at different temperatures. Clearly, good fits can be seen in the early stage, but deviations occur at the late stage.

1.4 Surface dynamics of polymers near their glass transition temperatures

1.4.1 From the glass transition temperature reduction to the surface dynamics

Surface dynamics of polymers can be much different from the bulk dynamics. In the past two decades, a lot of effort has been put to understand the surface dynamics of glassy polymers. In fact, these studies were initiated by the experimental observation that the glass transition temperature of polymer thin films was different from that in the bulk when

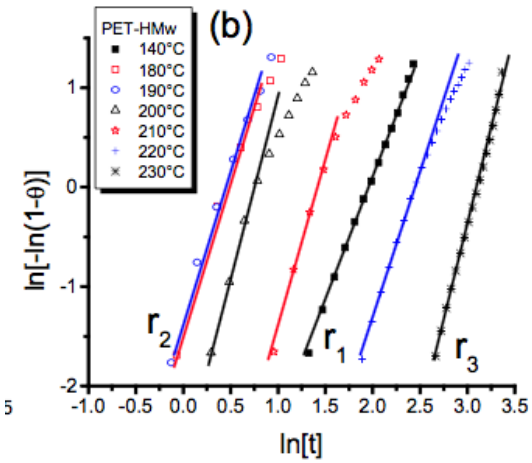

Figure 1.21: Avrami plot of Poly(ethylene terephthalate) isothermal crystallization at different temperatures. Figure from [80].

the film thickness was less than 100 nm. This study was conducted by Keddie, Jones and Cory in 1994 [30], in which they found a film thickness dependent T_g in polymer thin films. In the study, they observed that the T_g reduction was molecular weight independent and there was no chain confinement effect. Instead, they suggested that a liquid-like layer with a lower T_g near the surface of glassy films was the cause of the T_g reduction. In order to quantify the T_g reduction, they also provided an empirical equation

$$T_g(d) = T_g(\infty)[1 - (\frac{A}{d})^{\delta}] \tag{1.98}$$

where d is the film thickness, $T_g(\infty)$ is the bulk glass transition temperature, and A is the characteristic length. To fit data, $A = 3.2nm$ and $\delta = 1.8$ were used. In fact, Jackson and McKenna [81] observed a similar T_g reduction of organic liquids confined in small

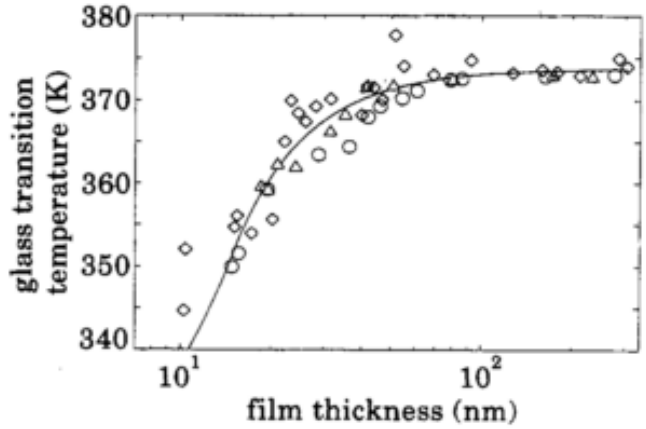

Figure 1.22: Glass transition temperature of polystyrene as a function of film thickness, where the solid line stands for the Eq. 1.98. Figure from [30].

pores. In their study, two glass forming organic liquids (ortho-terphenyl and benzyl alcohol) were confined in small pores and measured by DSC. The results showed a clear pore size dependent T_g of both organic liquids. Although authors gave some possible explanations based on entropy and free volumes, more evidence shows that the origin of the glass transition reduction is due to the free surface effect.

A striking observation found two years later by Forrest *et al.* [28] made the free surface effect hypothesis more reasonable. Compared with Kiddie *et al.*'s study, the new study removed substrates and measured the glass transition temperature of free standing polystyrene films. The observation of a much larger T_g reduction in free standing films compared with supported films indicates that the T_g reduction is highly related to the free surface. If two free surfaces present, the T_g reduction is more pronounced than that with

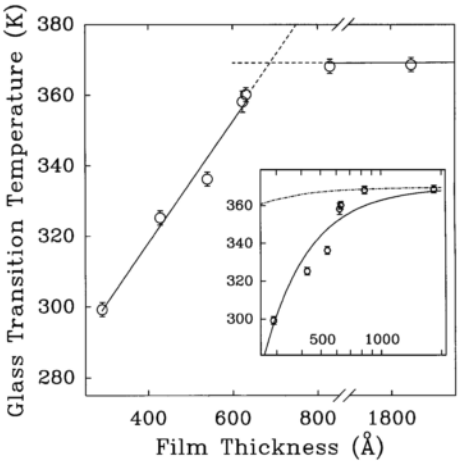

Figure 1.23: Glass transition temperature as a function of film thickness for free standing polystyrene films. Figure from [28].

one free surface.

Can the T_g reduction be ascribed to the existence of a free surface? Sharp and Forrest [82] beautifully demonstrated the relation between the free surface and the T_g reduction. In their study, thin films with the thickness h were made by combining of two half films $h/2$, where one was supported by a Si substrate and the other one was supported by a NaCl crystal substrate coated with Al. With this method, possible artificial effects caused by the evaporation of metal onto polymers can be ruled out. They observed a bulk glass transition temperature when the sample surface was capped by a metal layer. This observation directly reveals the relation between the free surface and T_g reduction.

Similarly Bäumchen *et al.* [83] did another experiment to test whether the T_g reduction is caused by the free surface. In their study, free standing polystyrene films were made

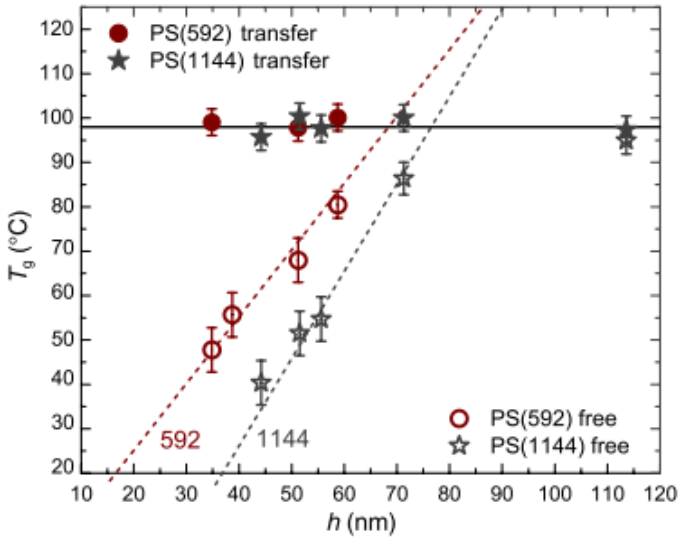

Figure 1.24: Glass transition temperatures of free standing polystyrene films and the same films directly transferred onto Si substrates. Figure from [83].

and their glass transition temperatures were measured by an ellipsometer. After that, the same films were transferred to Si substrates and measured by the ellipsometer again. Consequently, one sample can provide two glass transition temperatures, one for the free standing film and the other one for the supported film. Fig. 1.24 shows the glass transition temperatures in two systems. It is not hard to see that in free standing films, large T_g reductions are observed. In contrast, for the supported films, there is no T_g reduction.

The liquid-like layer plays a significant role in the glass transition temperature of polymer thin films, but how thick is the liquid-like layer? What is the local glass transition temperature of this liquid-like layer? In 2000, de Gennes [84] stated "*future experiments should aim not at the determination of a single T_g, but at a distribution of T_gs.*" Ac-

cordingly, Ellison and Torkelson [85] used dye-labeled thin films to probe the local glass transition temperature in polystyrene thin films. In their study, polymer thin films were composed of multilayers, in which a 14 nm dye-labeled thin layer was either sandwiched by two normal thick layers or placed at the air/polymer surface or polymer/substrate interface. In general, dye molecules in the excited state can dissipate their energy by the fluorescence and other non-radiative decay, such as through vibrational modes. The rate of non-radiative decay is sensitive to the temperature as well as the local density. In addition, due to the competing effect between both mechanisms, stronger the non-radiative decay is, weaker the fluorescence intensity is. Consequently, the fluorescence intensity acts as an indicator of the local density, which can be used to determine the local glass transition temperature. Fig. 1.25 shows the local glass transition shift compared with the bulk as a function of the thickness of the dye-labeled layer. It is clear that even a thick layer underneath the surface still exhibits a very low glass transition temperature. It also indicates that the surface glass transition temperature is independent of the total film thickness.

The next question is whether the glass transition temperature reduction is a general phenomenon. In other words, whether for all polymers, a thickness dependent glass transition can be observed. After the thickness dependent glass transition study on polystyrene, Keddie, Jones, and Cory measured the thickness dependent glass transition temperature of poly(methyl methacrylate)(PMMA) films on different substrates [29]. In their study, a similar thickness dependent T_g of PMMA films on Au substrates compared with that of polystyrene films on Si substrates was observed; however, for PMMA films on Si substrates,

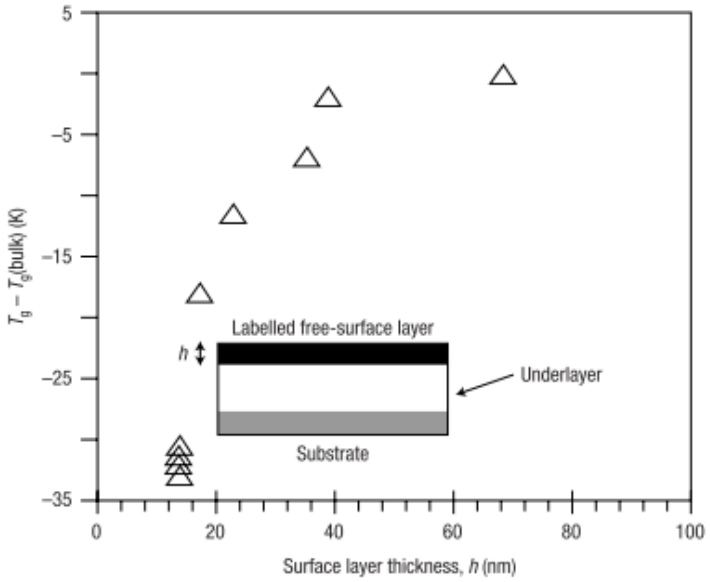

Figure 1.25: Glass transition temperature shift of a dye-labeled polystyrene thin film placed on the top of a thick polystyrene film (270 nm), where the thickness of the dye-labeled polystyrene thin film is h. Figure from [85].

T_g increased as the film thickness decreased. The observation indicates that the apparent T_g depends on not only the free surface but also the substrate-polymer interactions. For polystyrene on Si substrates, the interactions between polymers and substrates are relatively weak; as a result, T_g is only affected by the free surface. In contrast, the strong attractive interactions between PMMA films and Si substrates result in T_g increasing as the film thickness decreases [86]. This result equivalently demonstrates that neglecting the substrate interactions, the glass transition temperature is highly related to the free surface.

Considering the definition of the glass transition temperature, a lower T_g means the presence of enhanced dynamics in thin films. Near the bulk T_g, a temperature decrease by 3 K leads to a relaxation time increase by 10 times [87]. Accordingly, a T_g reduction of 10 K should result in a mobility change by 1000 times. Such a huge change should be captured by experiments. As expected, there is a great deal of evidence showing the existence of enhanced surface mobility near the bulk T_g.

1.4.2 Surface dynamics of polymer thin films

From the previous sections, the conclusion that the free surface is the cause of the T_g reduction in polymer thin films has been established. Thus, the study on the surface dynamics of polymer thin films can help us better understand the nature of the T_g reduction. Of course, the topic of the surface dynamics of polymer thin films near T_g itself is also interesting [88]. The surface dynamics of polymer thin films can be measured in many ways,

such as light scattering [89, 90], dielectric spectroscopy [91, 92], AFM [93], positronium annihilation [94, 95], *etc.* In this section, we review some recent experiments on the surface dynamics of polymer thin films, especially at temperatures near T_g.

Dewetting in ultra thin films

In the early 1990s, Reiter did a series of studies on the dewetting of polymer thin films at temperatures above [96, 97] and below [98] the bulk T_g. In general, dewetting is the rupture of thin films on substrates and eventually forming different droplets. This process is driven by the free energy. As a result, dewetting is a spontaneous process and the speed of dewetting highly depends on the physical properties of thin films, such as surface tension and viscosity. Consequently, the study of the dewetting process of polymer thin films provides the chance to obtain the properties of the probed polymers. In the study from Ref. [97], Reiter observed that for the film thickness h thinner than the end-to-end distance R_{EE} of the polymers on glass substrates, the dewetting process was much different from that with $h > R_{EE}$. In this study, T_v was defined as the temperature at which the diameter of dewetting holes can reach 500 nm in one hour. Fig. 1.26 shows the relation between T_v and the initial film thickness, where the bulk values are based on the bulk dewetting model [99] with the bulk viscosity of polystyrene [100]. Clearly, the thickness dependent T_v implies that the dewetting speed is not constant but thickness dependent. The result is striking as the viscosity in thin films with $h < R_{EE}$ is much smaller than that in the bulk at the same temperature. In the paper, they claimed that these observations

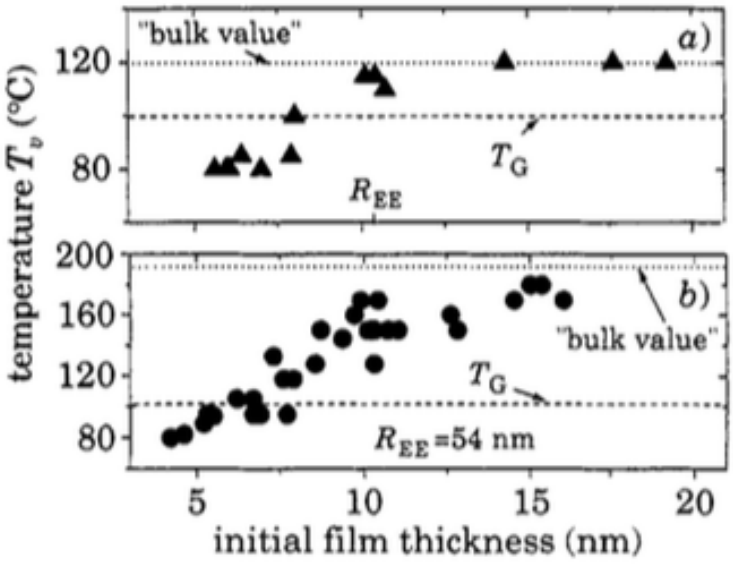

Figure 1.26: Temperature where the dewetting hole can reach 500 *nm* in one hour as a function of film thickness: (a) polystyrene with a molecular weight of 28 kg/mol, (b) polystyrene with a molecular weight of 660 kg/mol. Figure from [97].

should be attributed to the decrease of the density. Of course, whether or not a lower density could lead to a huge change in polymer dynamics in thin films is unclear; however, it is clear that the mobility of polymer thin films at the nanoscale is significantly different from that in the bulk.

In general, dewetting experiments are always conducted in supported systems; however, free standing films can also break and form holes due to the instability. As mentioned above, dewetting is the rupture of films. Thus, there are two steps: hole forming and hole growth. The growth of holes is sensitive to the properties of films. As a result, the study

on the rupture of polymer thin films at the nanoscale may lead to some new observations because much stronger T_g reductions are observed in free standing films compared with supported films. Debrégeas *et al.* [101] did the first experiment on the viscous bursting of polymer thin films. They found that the radius of holes grew exponentially with time and the radius can be expressed as

$$R(t) = R_0 e^{t/\tau} \tag{1.99}$$

where τ is the characteristic growth time. Similar to Debrégeas's work, Dalnoki-Veress *et al.* [102] did another experiment on the hole formation and growth in thin freely standing polystyrene films at temperatures slightly above the bulk T_g. They found that the characteristic growth time τ decreased as the film thickness h decreased. They explained that this was due to the shear thinning effect, which is a bulk phenomenon that the viscosity decreases as the shear rate increases. In general, the viscosity can be written as

$$\eta = \frac{\sigma}{\dot{\gamma}} = \frac{\tau\gamma}{h} \tag{1.100}$$

where h is the thickness of films, τ is the characteristic growth time, and γ is the surface tension. From the above expression, it is clear that the viscosity at the edge of the hole is different from the zero shear viscosity as the shear rate is not negligible. Fig. 1.27 shows the normalized hole radius as a function of time with different initial film thicknesses, where different growth rates and τ values are shown. The results reveal a nonlinear viscoelastic behaviour of polymer thin films at the nanoscale and also indicate that the dynamics of polymers at the nanoscale is extremely sensitive to the experimental conditions. Even a

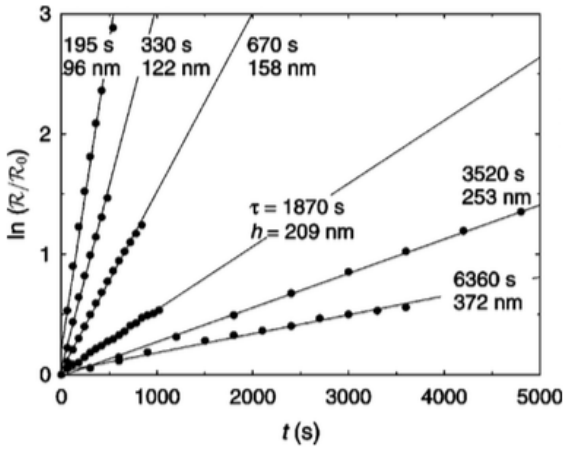

Figure 1.27: Normalized hole radius as a function of time with different initial film thicknesses, where h is the initial film thickness and τ is the characteristic growth time. Figure from [102].

small film thickness change affects the shear rate dramatically and results in a significant decrease of the viscosity. This suggests that in the future, one should be extremely careful about the experimental conditions, otherwise artificial results can be achieved even though they seem to be scientifically correct.

Studies on the free surface

From the previous sections, it is not hard to conclude that the dynamics of polymer thin films is different from that in the bulk. Dewetting experiments provide insight into how thin films behave at the nanoscale; however, the dynamics of polymer thin films is contributed by both the free surface and the materials underneath. Thus, one should expect a way to

probe the dynamics of just the free surface. Atomic force microscopy (AFM) is a powerful tool to probe the local properties of samples. Thus, AFM based measurement near the T_g may lead to some new insights [103–108].

However, these measurements are not consistent. Some experiments show the existence of enhanced mobility as well as a lower local T_g near the free surface, but the others don't. In the shear modulation force microscopy study of polystyrene films carried by Ge *et al.* [104], no T_g reduction was found even in a 17 nm thin film. Similar results can be found in the adhesion study on poly(tert-butyl acrylate) [103], where no noticeable enhancement in the surface was observed. In contrast, the indentation study on polystyrene samples conducted by Bliznyuk *et al.* [106] exhibited a film thickness dependent glass transition temperature. The controversies indicate that the mechanical analysis on the free surface with AFM probes is complicated and the effect of experimental conditions has not been fully understood. Taking the frequency as an example, it has been widely accepted that T_g is kinetic dependent, *i.e.*, the cooling/heating rate and the probing rate can affect T_g values. This implies that the controversial results might be caused by different probing rates. Fakhraai and Forrest [109] studied the cooling rate dependent T_g of polystyrene thin films and found there was no significant reduction with a high cooling rate (130 K/min). Fig. 1.28 shows the relaxation time in the form of the cooling rate as a function of temperature with different film thicknesses. It is obvious that the relaxation time of 90 nm films follows the VTF curve; however, it shows the Arrhenius behaviour for thin films at low temperatures. On top of this, all lines intersect at the same temperature of 378.5

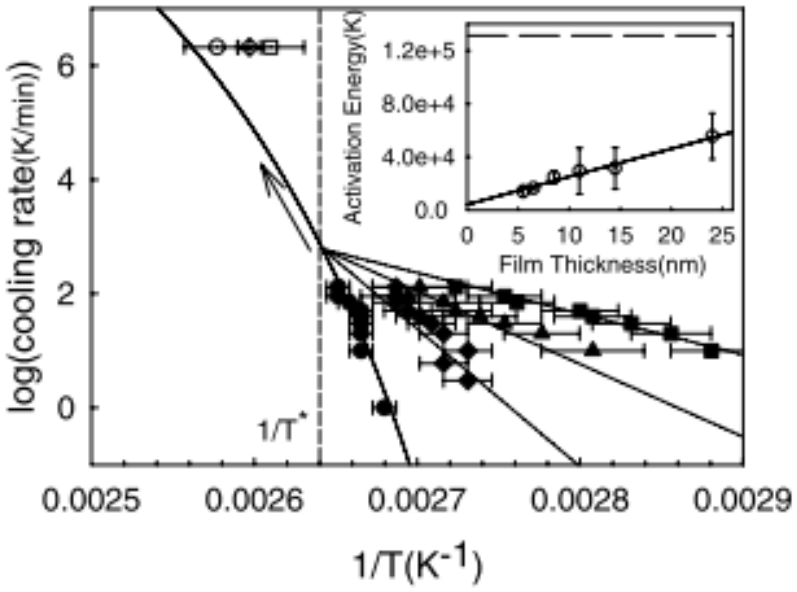

Figure 1.28: Cooling rate as a function of temperature for different film thicknesses, where the cooling rate is obtained from the relaxation time τ. Figure from [109].

$\pm$ 1.4 K, which corresponds to a cooling rate between 168 and 2068 K/min. This suggests that any experiments with a cooling rate larger than 2068 K/min should exhibit a bulk T_g or bulk dynamics.

According to the cooling rate dependent studies, one possible reason for controversial results in different AFM based experiments is the non-consistent probing frequency. For the tapping mode AFM, the working frequency is about a few hundred kHz, which leads to a probing time window of 0.00001 second. It means with a probing frequency of 100 kHz, if the relaxation time of the system is longer than 0.00001 second, glassy dynamics should be observed.

In order to overcome the problem discussed above, studies on the surface dynamics of polymer thin films should use a smaller cooling rate or a longer experimental time . One good candidate is to introduce some small perturbations at the surface of polymers and study the relaxation process of these perturbations. Perturbations may come from either polymers themselves, like nano-indentations, or external sources, like nanoparticles. The advantage of this type of experiment is the long relaxation time due to the relatively large perturbations. As a result, it is possible to keep track of the entire evolution. In addition, a long experimental time leads to a small effective cooling rate as the typical experimental time is in the range of hours and days. Consequently, the cooling rate caused artifacts can be ruled out. The first nanoparticle embedding experiment was conducted by Teichroeb and Forrest [110]. In their study, 10 nm and 20 nm gold nanoparticles were gently spin-coated onto polystyrene thin films with the film thickness of 180 nm. When $T > T_g$, the embedding process should be expected as the polymers want to wet gold nanoparticles and then swallow them in order to minimize the free energy. However if there is no liquid-like layer in the glassy polymer films, the embedding process should not be observed as the cooperative motions are frozen at $T < T_g$. Fig. 1.29 shows the apparent height of nanoparticles as a function of annealing time at different temperatures. It is not hard to see that there are two different processes: above T_g, the nanoparticles fully embed into films; in contrast, below T_g, nanoparticles penetrate into a certain distance about 3.5 nm to 3.8 nm. This demonstrates that even below T_g, the embedding process can still happen. It equally implies that there is a liquid-like layer below the bulk T_g in thin films

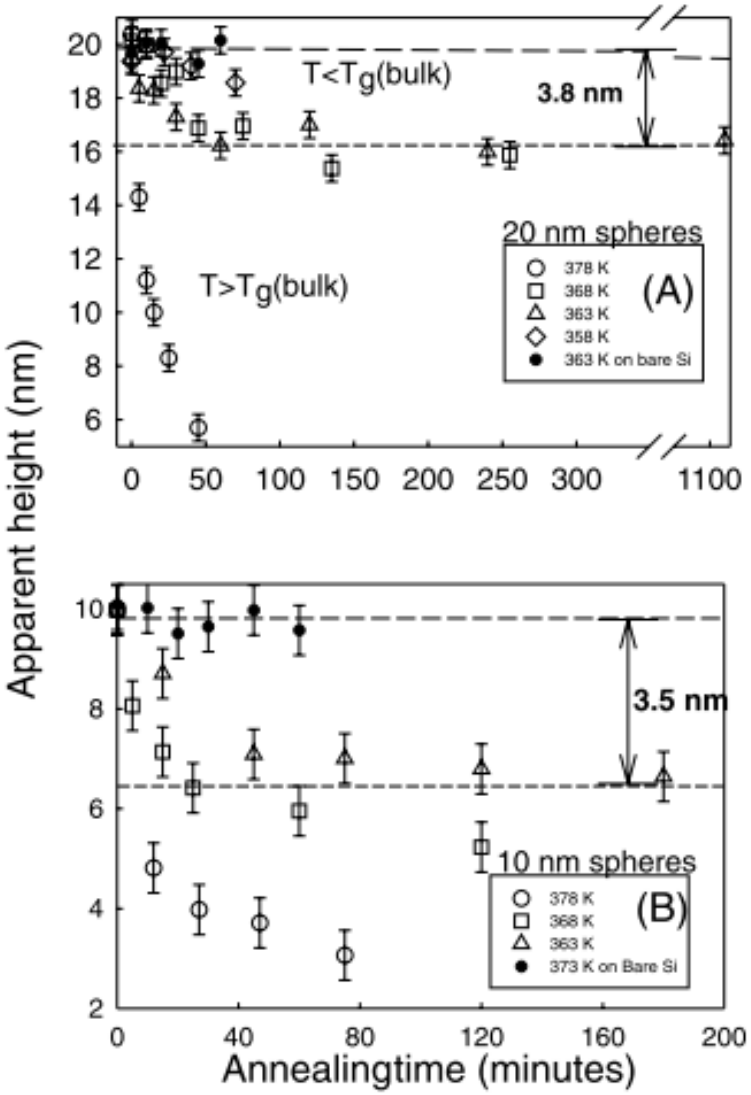

Figure 1.29: Apparent height of nanoparticles as a function of time at different temperatures in polystyrene films. Figure from [110].

with a size of a few nanometers. Sharp *et al.* [111] developed a STF model to account for the embedding process. In this model, the driving force of the embedding process can be written as

$$F(t) = 2\pi R(t)\sin(\psi)\gamma_{polymer} \tag{1.101}$$

where $R(t)$ is the radius of the contact area, ϕ is the contact angle, and $\gamma_{polymer}$ is the surface tension. Applying the above driving force, the apparent height of the nanoparticles can be written as:

$$h(T,t) = 2R - [\frac{3(1-\nu)}{8R^{1/2}}\int_0^t J(T,t-\epsilon)\frac{\mathrm{d}F}{\mathrm{d}\epsilon}d\epsilon]^{2/3} \tag{1.102}$$

where ν is the Poisson's ratio, $J(T,t)$ is the creep compliance and ϵ is the variable of integration (from 0 to t). With this expression and experimental data, the local rheological temperature ($R = T : \tau(R) = \tau_{bulk}(T)$) can be obtained. In this study, the surface rheological temperature is about 374 K when the real experimental temperature is 363 K, indicating that there is indeed a liquid-like layer even when the bulk is in the glassy state. In addition, Hutcheson and McKenna [112, 113] proposed another model to account for the embedding process on the free surface. In their model, the driving force has three parts, γ_{sphere}, $\gamma_{polymer}$, $\gamma_{sphere-polymer}$. This driving force is much larger than that in the model proposed by Sharp *et al.* They concluded that *there is little or no depression in the glass temperature or existence of a liquid layer at the polystyrene surface* [113]. It is clear that the deviation is caused by the different expressions of the driving force. However, how to precisely model the driving force at the interface between the nanoparticles and polymers

near the glass transition temperature is hard due to the complicated viscoelastic behaviour of polymers.

Without considering the model, a simple relaxation study on the nanoparticle embedding process was conducted by Qi *et al.* [114]. In this study, the embedding involved two processes, the surface process and the bulk process. At high temperatures, only the bulk process existed. As a result, a single decay was observed. At low temperatures, the bulk process was so slow that it was impossible to be observed. While near T_g, both the surface and bulk embedding processes co-existed. In order to directly compare these two processes, time dependent nanoparticle height profiles were fitted with two single exponential functions, where the bulk process had a longer relaxation time, and the surface process had a shorter relaxation time. It is clear from Fig. 1.30 that the bulk relaxation follows the bulk VFT curve and the surface relaxation exhibits an Arrhenius type of behaviour. On top of this, Qi *et al.* [115] also conducted a comprehensive study on the molecular weight dependent nanoparticle embedding in polystyrene films near the bulk T_g, in which low molecular weight polymers demonstrated a different behaviour from high molecular weight polymers. They claimed that the difference in dynamics might be caused by the viscous flow near the free surface. Because low molecular weight polymers can flow in the liquid-like layer; in contrast, high molecular weight polymers cannot. A similar study on tris(naphthyl)benzene (TNB) was conducted by Daley *et al.* [116]. In the study, in addition to the bulk embedding process, a material build-up process was observed at temperatures below the bulk T_g, which was considered as the result of the surface flow. Fitting the

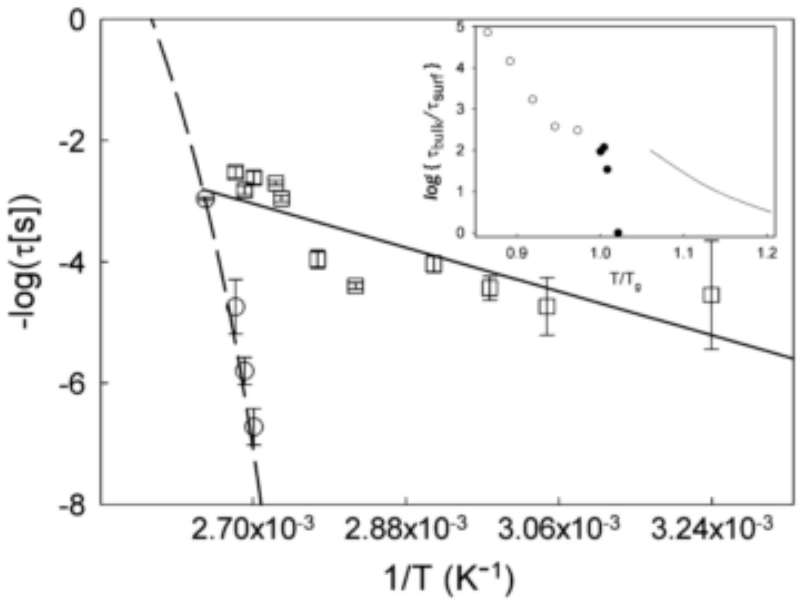

Figure 1.30: Temperature dependent bulk and surface embedding processes in polystyrene films, where the dashed line stands for the shifted bulk VFT curve, open circles are the bulk relaxation, and open squares are the surface relaxation. Figure from [114].

experimental profiles, the relaxation time of both the embedding process and the build-up process were extracted. They found that the embedding process followed the bulk VTF behaviour; while the build-up process exhibited the Arrhenius behaviour.

Nanoindentation recovery

As mentioned previously, perturbations can be classified into two groups: induced by the system itself or induced by external sources. Nanoparticle embedding experiments should be considered as the second one. These experiments are very powerful in studying the surface dynamics of polymer thin films near T_g. However, the interaction between the external perturbations and the system is complicated and hard to model. Thus, an experiment involving perturbations from the system itself would be easier for modeling and analysis. Rapaléo *et al.* [93] developed a beautiful technique to study the surface dynamics of polymer thin films near the bulk T_g of PMMA. In their study, PMMA thin films were irradiated by Au ions, which resulted in thin films with a lot of artificial holes as well as tails beside the holes. Owing to the excessive free energy of these holes, polymers tended to fill these holes. Thus, if there is a liquid-like layer below T_g, a hole recovery process should be observed. Compared with nanoparticle embedding experiments, there was no external force to the surface during the relaxation process. As a result, the relaxation process only dependeds on the local property of polymers. Fig. 1.31 shows the holes and the tails relax at different temperatures, where the bulk VFT curve is also shown. It is clear that there is a shift from the bulk VFT curve. The relaxation follows the shifted bulk VFT curve when

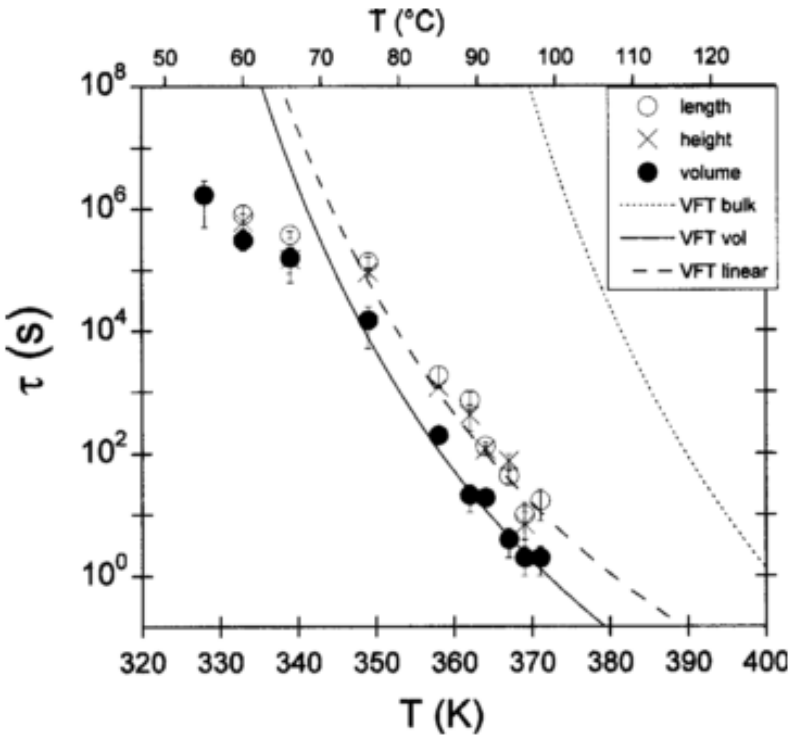

Figure 1.31: Relaxation times of the volume, length and height of the nanodeformations at different temperatures. Figure from [93].

$T > 350$ K and then follows the Arrhenius behaviour. Taking $\tau = 100$ s as the definition of the glass transition, the local T_g is about 30 K lower than the bulk value. Clearly, we can say that compared with the bulk, the surface dynamics is enhanced. This experiment provides a new idea of how to measure the surface dynamics without introducing external sources. However, the impact of high energy ions can dramatically change the surface properties of thin films (*melting, bond breaking, and particle ejection* [93]). As a result, this *not gentle* treatment might lead to unreal surface dynamics. Thus, new experimental designs should not only consider how to make perturbations on the surface of polymers but also consider how to do this gently.

Fakhraai and Forrest [117] designed a novel experiment to produce many artificial holes without introducing high energy ion beams. In their study, nanoholes on polystyrene surfaces were induced by removing partially embedded nanoparticles with mercury. In this way, the possible problems mentioned previously could be avoided. In order to probe the surface dynamics of glassy polystyrene, polymers were annealed at different temperatures for different periods of time. Fitting the time dependent depth profiles of the nanoholes, the relaxation times of these nanoholes were extracted. As expected, the results still support the existence of a liquid-like layer in glassy polymers as the relaxation time deviates from the bulk VFT curve below T_g. At almost the same time, Qi *et al.* [118] studied the surface dynamics of glassy isotactic poly (methyl methacrylate) (*i*-PMMA) films on different substrates. In this study, the embedding process was found even at 42 K below the bulk T_g. In order to quantify the effect of substrates, both Al and Si substrates were used.

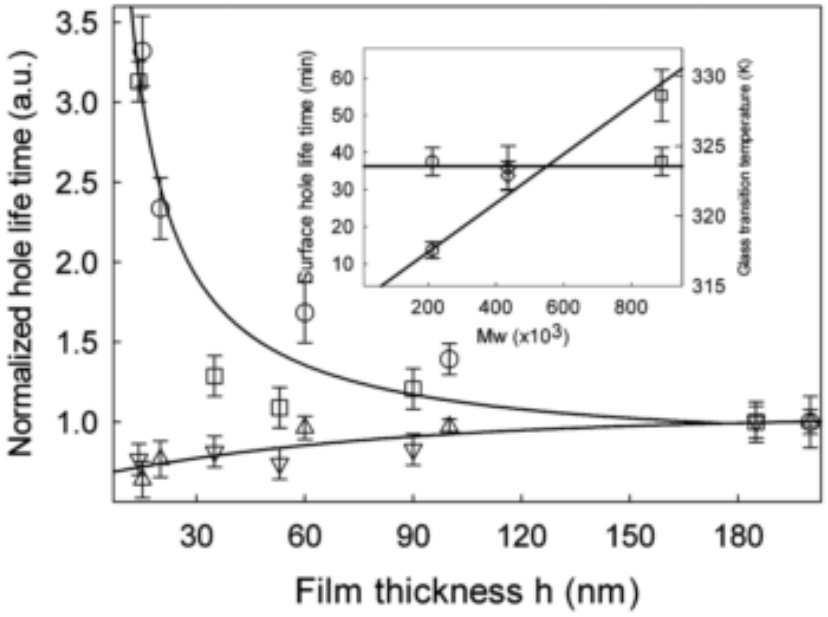

Figure 1.32: Normalized relaxation time of nanoholes as a function of the film thickness of *i*-PMMA films on two different kinds of substrates, Al (triangles) and Si (circles and squares). Figure from [118].

They found different thickness dependences of the relaxation time on different substrates: an increased relaxation time as the film thickness decreased on Si substrates and a decreased relaxation time as the film thickness decreased on Al substrates. Surprisingly, the substrate effect can extend up to 180 nm.

Surface capillary waves and relaxation of artificial gratings

Nanohole-recovery experiments provide the chance to probe the surface dynamics of glassy polymers within a reasonable time window. However, the relaxation process is very fast at temperatures above T_g. As a result, nanohole-recovery experiments can only be conducted within a limited temperature range, from well below T_g up to slightly higher than T_g. Thus, in order to extend the experimental temperature window, new designs are required. Similar to nanohole-recovery experiment, another way to study the surface dynamics of polymers is to study the relaxation of artificial nanogratings or nanosteps, because the size of nanogratings or nanosteps can be controlled precisely. Accordingly, the relaxation experiment far above T_g is doable. Kerle *et al.* [119] made rough polystyrene surfaces with CaF_2 moulds and measured the surface tension driven decay of these corrugations. In their study, only a partial relaxation was observed below T_g and a full relaxation was observed at and above T_g. Thus, they claimed that there was no liquid-like layer in glassy polymers as it would result in a full relaxation rather than a partial relaxation. However, it should be noted that the partial relaxation rather than the full relaxation might be caused by insufficient annealing time because the relaxation of these corrugations is wavelength dependent. Short wavelengths require less time to relax than long wavelengths.

In contrast, Zhang and Yu [120] measured the relaxation of a sinusoidal surface grating made by low molecular weight polystyrene. In their study, the grating can fully relax as the height of the grating reduced dramatically. This indicates that it is a full relaxation

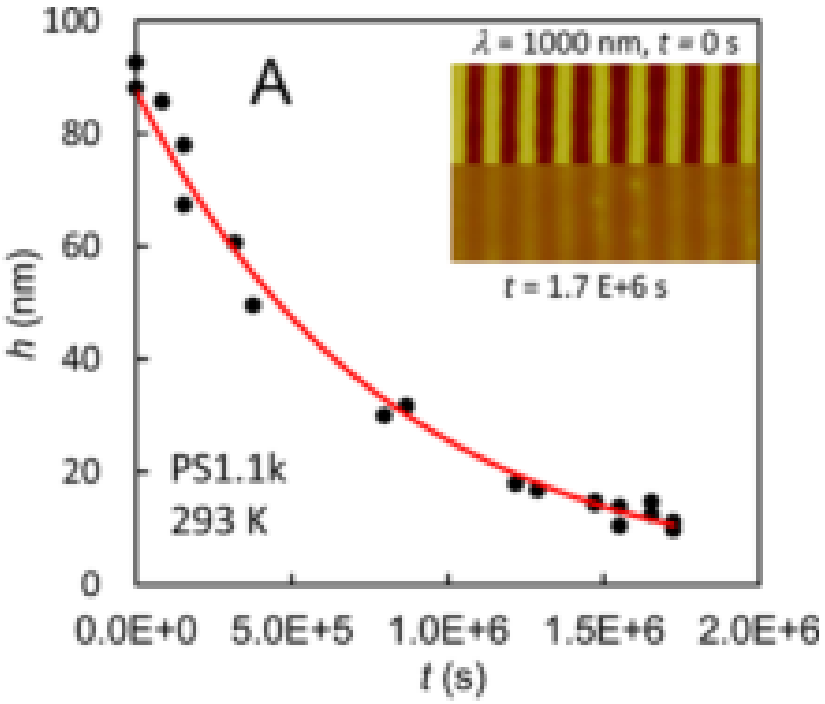

Figure 1.33: Height of the grating as a function of annealing time below the bulk glass transition temperature of low molecular weight polystyrene. Figure from [120].

process rather than a partial relaxation process below T_g. Fig. 1.33 shows the relaxation of the grating below T_g, where the height change is more than 80 %. In addition, they found that the bulk diffusion coefficient followed the bulk VFT curve above T_g; however, below T_g, the surface diffusion coefficient deviated from the bulk VFT curve. This also indicates the existence of enhanced surface dynamics in glassy polymers. A similar behaviour can also be found in the organic glass formers, such as *o*-terphenyl [121], indomethacin [122]. Consequently, we can conclude that the existence of enhanced surface dynamics in

glassy amorphous materials is a general feature, although there are some system-to-system variations.

Moreover, the study on thermally induced capillary wave at the surface of polymers can also provide the information of the surface dynamics of polymers. The surface capillary wave above the glass transition temperature can be measured with x-ray photon correlation spectroscopy [90, 123–125]. However, below or near T_g, the method is not applicable as the decay time of the correlation function is so long that samples can be damaged under x-ray exposure. Consequently, Yang *et al.* [126, 127] used power spectral density spectroscopy to study the thermally induced surface roughness of polymer films. In the study, they found a surface mobile layer, which exhibited Arrhenius dynamics. In addition, they claimed that the thickness of this layer was less than 2.3 nm.

To summarize, there is a lot of experimental evidence showing the existence of a liquid-like layer in glassy amorphous materials and the viscosity of the layer is much lower than that in the bulk. The existence of the liquid-like layer allows artificial perturbations to relax below the bulk T_g, when the bulk is almost immobile. However, how thick the liquid-like layer is and how molecules move in the liquid-like layer are still unclear. One of the main objectives of this thesis is trying to answer these two questions.

1.4.3 Studies on solid polymers

Polymer physics is a fantastic subject as it involves many fundamental topics, which are useful in industrial processing and manufacturing. In this thesis, we focus on solid polymers, especially the transition from melts to solids. In general, solid polymers can be classified into two groups: amorphous and crystalline. Thus, our studies on polymers have two major parts, amorphous solids and crystalline solids. In the first part, we try to understand whether the observed T_g reduction is caused by the liquid-like layer at the free surface. To achieve this, we utilize the stepped film levelling technique to study the surface dynamics of polymer films near T_g in different conditions. On top of this, in order to directly connect enhanced surface mobility to the T_g reduction, the simple model proposed by Forrest and Dalnoki-Veress [128] is verified by the thermal expansivity study on polymer thin films. Crystalline polymers are useful and important to polymer devices as there are significant differences in physical properties between crystalline and amorphous polymers. Atactic polystyrene is known to be non-crystallizable; however, syndiotactic and isotactic polystyrene can crystallize. Nevertheless, it is also true that there are some stereoregular components in atactic polystyrene due to random statistics. Thus, it is possible that atactic polystyrene is able to crystallize in some conditions. Consequently, in the second part, we try to grow crystals from atactic polystyrene melts and systematically study the growth and melting behaviours of these crystals. Lastly, we are not able to answer all these questions but just want to contribute our knowledge to this field and try to offer some new ideas.

Chapter 2

Experimental techniques

2.1 Sample preparation

2.1.1 Materials

Most of the studies in this thesis are based on atactic polystyrene (aPS). For the surface dynamics study, aPS with molecular weights 3.0 kg/mol, 11.9 kg/mol and 22.2 kg/mol were purchased from Polymer Source Inc. For the crystallization study, aPS with molecular weights of 500 g/mol, 600 g/mol, and 890 g/mol were purchased from either Polymer Source Inc. or Polysciences Inc. The glass transition temperatures of these polymers are shown in Fig. 2.1.

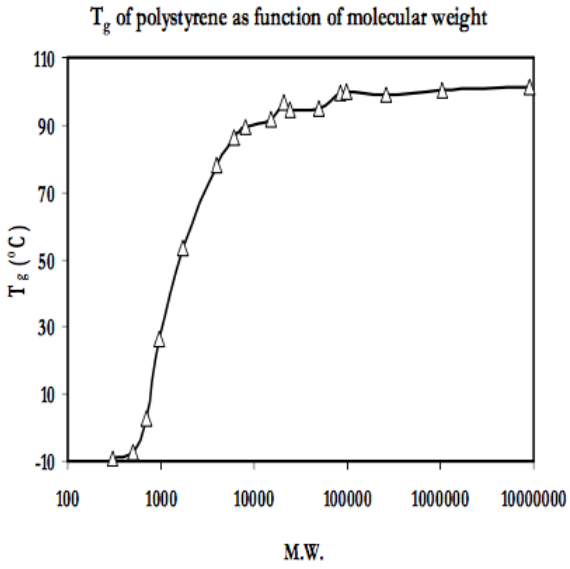

Figure 2.1: Molecular weight dependent glass transition temperature. Figure from [129].

2.1.2 Thin film preparation

Preparation of substrate supported films

Thin polymer films were prepared by spin coating pre-made toluene solutions onto substrates. The thickness of polymer films can be controlled by either the concentration of solutions or the speed of the spin coater [130]. In this thesis, the thicknesses of samples were in the range of 5 nm up to 200 nm. After spin coating, samples were annealed above their bulk glass transition temperatures in a homemade oven flushed with dry nitrogen. For crystallization samples, the annealing temperatures were above their melting points.

Preparation of stepped films

Stepped films were made using the following protocol:

1 Make two supported films with desired thicknesses on two different substrates, Si and Mica, where h_2 is the film thickness on mica (*film-1*), and h_1 is the film thickness on Si (*film-2*).

2 Anneal samples above their bulk glass transition temperatures for at least 12 hours in a homemade oven flushed with dry nitrogen.

3 Draw several lines on *film-1* (Fig. 2.2) with a razor blade.

4 Float *film-1* onto deionized water.

5 Dip *film-2* into water and pick *film-1* up.

6 Dry stepped film at ambient conditions and then transfer them into a 24-well plate for future use.

2.2 Ellipsometry

Ellipsometry is an optical technique to study the dielectric properties of thin films as it is very sensitive to the thickness and refractive index changes of thin films. In our lab, a self-nulling ellipsometer is used to determine the thickness of polymer thin films. Moreover,

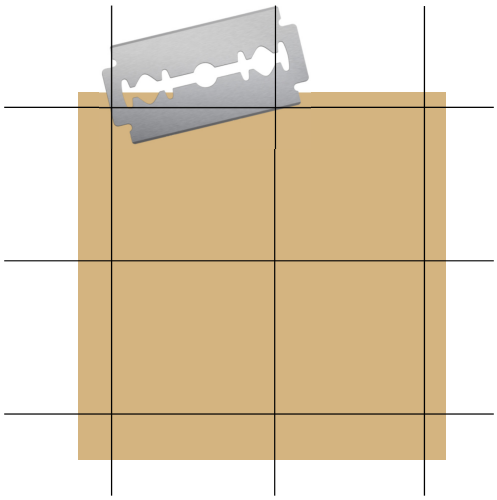

Figure 2.2: Schematic diagram of drawing lines on mica supported films. Modified from [131].

due to the different expansivities of polymer thin films between the melt and glass states, the glass transition temperature of polymer thin films can also be determined by the ellipsometer. The ellipsometer in our lab is a faraday-modulated self-nulling ellipsometer. Fig. 2.3 shows the optical path of the ellipsometer. The laser generates linearly polarized light at 632 nm, which passes through the first quarter-wave plate (Q1) and becomes circularly polarized light. The fast axis of Q1 is set 45 ° with respect to the plane of polarization of the laser beam. After passing through the Polarizer (P) and the second quarter-wave plate (Q2), the elliptically polarized light is produced, where Q2 is set 45 ° with respect to the plane of incidence. As Q1 and Q2 are fixed, the only way to adjust the polarization state of the incident light beam is to adjust P. With a proper value of P, a linearly polarized reflected light is produced upon the reflection on the sample. Finally,

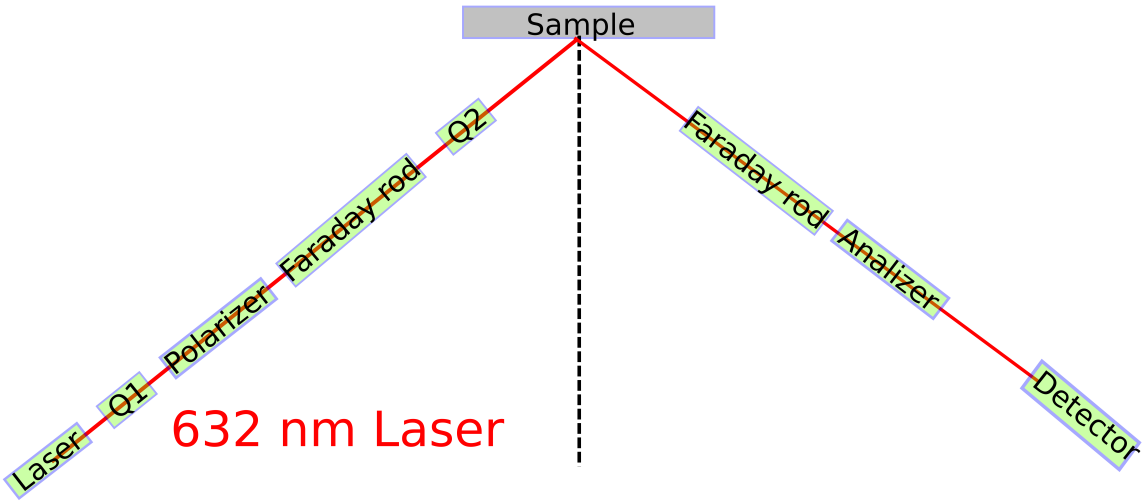

Figure 2.3: Schematic diagram of the faraday-modulated self-nulling ellipsometer.

the Analyzer (A) is used to produce a null condition (no light) at the detector. Both Faraday rods are used beside P and A to change the polarization state of the light slightly in a quadrature sinusoidal modulation. Then, the detected signal by the photodetector is demodulated and two signals are sent back to two stepper motors to adjust P and A. As a result, the ellipsometer always stays at a null condition. During the measurement, for a sample at a certain temperature, a pair of P and A values is obtained, which can be used to determine the physical properties of the sample with a proper model.

Thus, an important work is to make a model to describe the right optical path in the sample, which should include all reflections and refractions at all interfaces of the sample. In order to study the optical path and polarization state change of the light in the sample,

we should decompose the light into two components: the p component, oscillating parallel to the plane of incidence; and the s component, oscillating perpendicular to the plane of incidence. As these two components are perpendicular to each other, the change of these components are mutually independent. According to the Fresnel equations and Snell's law, the reflection coefficients of the p and s components at each interface of the sample can be given

$$r_p = \frac{N_1 \cos(\phi_0) - N_0 \cos(\phi_1)}{N_1 \cos(\phi_0) + N_0 \cos(\phi_1)} \tag{2.1}$$

$$r_s = \frac{N_0 \cos(\phi_0) - N_1 \cos(\phi_1)}{N_0 \cos(\phi_0) + N_1 \cos(\phi_1)} \tag{2.2}$$

where $N = \mathrm{n} + i\mathrm{k}$ is the complex refractive index, the subscript 0 stands for the refractive index of the upper layer, and the subscript 1 stands for the refractive index of the lower layer. Similar to the reflection coefficients, the transmission coefficients can be given by

$$t_p = \frac{2N_0 \cos(\phi_0)}{N_1 \cos(\phi_0) + N_0 \cos(\phi_1)} \tag{2.3}$$

$$t_s = \frac{2N_0 \cos(\phi_0)}{N_0 \cos(\phi_0) + N_1 \cos(\phi_1)} \tag{2.4}$$

In fact, if there are more than two layers in the sample, the total reflection is not contributed by the reflection at the first interface but the sum of all reflected lights at all interfaces. In consequence, the total reflection coefficients of the p and s components for a three-layer system can be given by:

$$R_p = \frac{r_{p01} + r_{p12} \exp(-i2\beta)}{1 + r_{p01} r_{p12} \exp(-i2\beta)} \tag{2.5}$$

$$R_s = \frac{r_{s01} + r_{s12} \exp(-i2\beta)}{1 + r_{s01} r_{s12} \exp(-i2\beta)} \tag{2.6}$$

where $\beta = 2\pi(\frac{d_1}{\lambda})N_1 cos(\phi_1)$, d_1 is the thickness of the second layer. Knowing the total reflection coefficients, we can determine both the thickness and refractive index of the film. However, the ellipsometer cannot directly measure these two components. Thus, the ratio of those two components is used.

$$\frac{R_p}{R_s} = \tan\Psi e^{i\Delta} \tag{2.7}$$

For the ellipsometer in our lab, the relations between P, A and Δ, Ψ are

$$\Delta = 2P + 90^\circ \tag{2.8}$$

$$\Psi = A \tag{2.9}$$

2.2.1 Determination of h and n

In reality, there are multiple layers in the sample. For each layer, there are two parameters: the thickness h and the refractive index n. In consequence, the main target is to solve for these h and n; however, it is not possible to analytically solve for h and n with one single wavelength and one fixed incident angle. As a result, we need to calculate P and A values with different h and n combinations and then compare these P and A values to the experimental P and A values to determine the real h and n values. Fig. 2.4 shows a typical three-layer system, which is used to demonstrate how to determine h and n values. The refractive index of air, film, and substrate are denoted by n_0, n, and n_2, and the thickness of the film is h. In general, $n_0 = 1$, and the substrate is Si, having a refractive index of

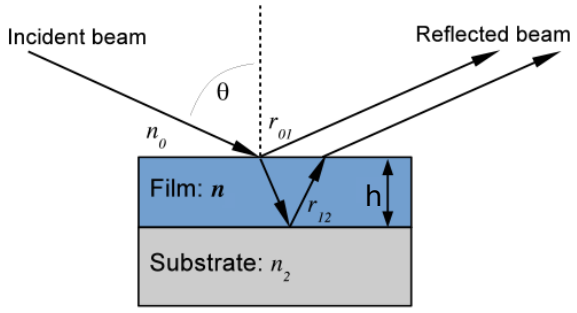

Figure 2.4: Three-layer system and its optical path. Figure from [132].

3.875 - 0.023i. For polystyrene films, the refractive index is about 1.583. In fact, there is always a native silicon dioxide layer on the Si substrate and the thickness of this layer is about 2 nm. A Matlab script with the formulas mentioned above is used to calculate P and A values with given h and n. For temperature independent measurements, n is fixed as a constant. With different h values, a series of P and A combinations can be obtained. Fig. 2.5 shows the P vs. A curve with a fixed n. In order to find the thickness of the sample, the experimental P and A values can be plotted on the same figure and the closest P and A pair on the curve can give a good estimation of the experimental data. As this P and A pair gives a unique film thickness h, the thickness of the film h_{exp} should be equal to the simulated film thickness h.

Because of the high sensitivity of ellipsometry to film thickness, it can be used to study the glass transition of polymer thin films [133]. In this thesis, all glass transition temperatures of thin films are measured with the self-nulling ellipsometer. A typical procedure is

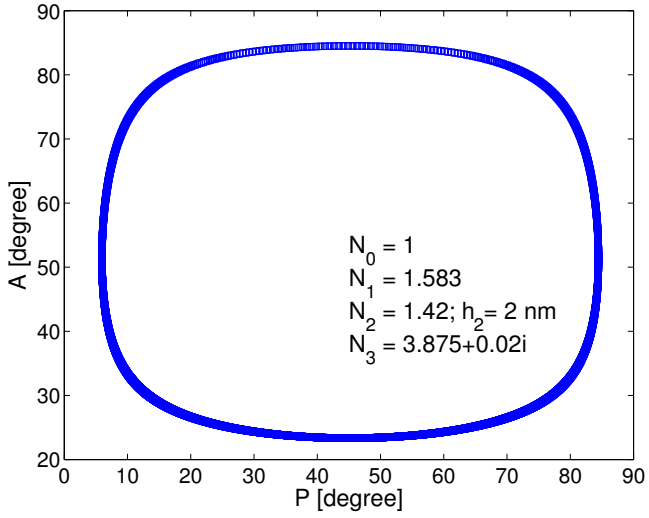

Figure 2.5: P and A simulation data of polystyrene films with different film thicknesses based on the four-layer model.

1 Mount a sample on a Linkam heating/cooling stage.

2 Turn on the ellipsometer and find P and A at a null condition.

3 Turn on the Linkam stage, hold temperature above bulk glass transition temperature.

4 Slowly cool down with a cooling rate of 2 K/min.

5 Repeat process [3] and [4] if necessary.

After experiments, P, A vs. temperature profiles can be obtained. There are several ways to determine the glass transition temperature. The easiest way is to fit either P and A data in both the glassy state and melt state, where the intersection of these two fits is

the glass transition temperature. Although finding temperature dependent film thickness and refractive index provides a better estimation on the glass transition temperature, the method above is good enough in most cases.

Fig. 2.6 shows the glass transition temperature determined by P profile and A profile respectively, in which the difference of T_g is less than 2 K (2 %).

2.3 Atomic-force microscopy

Atomic-force microscopy (AFM) is a type of scanning probe microscopy, and it has very high resolution and low requirement of the operating environment. Due to the diffraction limit, light based techniques become less useful at the nanoscale; however, AFM can overcome the diffraction limit and provide a resolution in the order of Angstrom. In this thesis, AFM is the most frequently used experimental equipment as it is the best tool to study the surface dynamics of polymers.

2.3.1 Components of AFM

There are four major components of AFM: tip and cantilever, piezoelectric element, laser and detector, and controller. In general, the laser beam is reflected off the back of the cantilever and detected by the photodiode detector. The piezoelectric element is used to adjust the height of the tip and cantilever based on the signal collected from the detector.

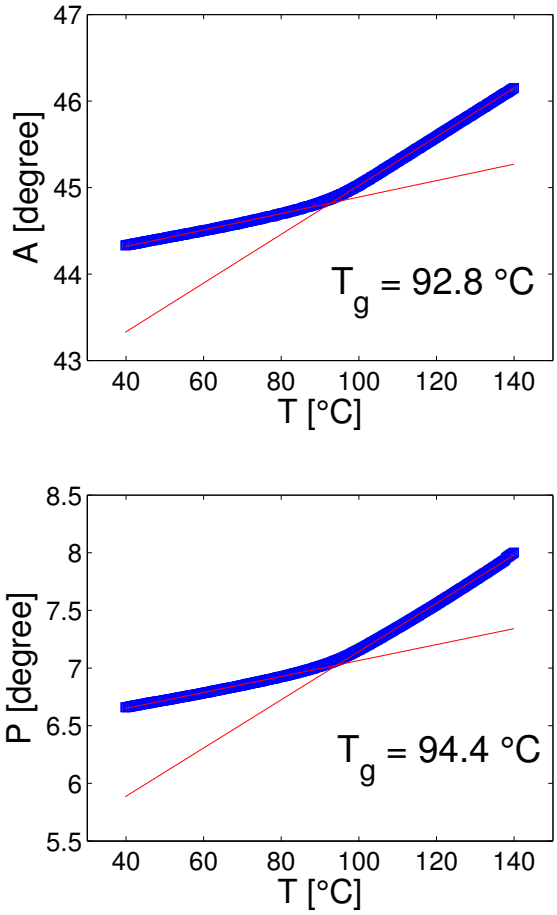

Figure 2.6: Glass transition temperature measurement on a polystyrene thin film, where the molecular weight is 11.9 kg/mol.

- The end of the cantilever is attached to the piezoelectric element, which can oscillate the cantilever and adjust the height of the cantilever in a very short range (1.5 μm to 15 μm).
- The tip at the front of the cantilever can *touch* the surface and *feel* how rough the surface is.
- The photodiode detector detects the shift of the reflected laser beam and tells the status of the cantilever.
- The controller adjusts the piezoelectric element according to the signal from the photodiode detector.

2.3.2 How AFM works

AFM can probe the weak force between the tip and the sample; thus, it is able to provide a true 3D image of the sample surface, which is different from the 2D image produced by traditional optical microscopes and electron microscopes. The interaction between the tip and the sample can be approximately characterized by the Lennard-Jones potential. At a long distance, the Van der Waals attraction dominates; at a short distance, the Pauli repulsion dominates. Fig. 2.7 demonstrates the interaction described above. During the scan, the interaction between the tip and the sample is maintained as a constant with a feedback loop. The deflection of the cantilever is the input of the feedback loop and the output of the feedback loop is used to adjust the piezoelectric element. If there is a bump

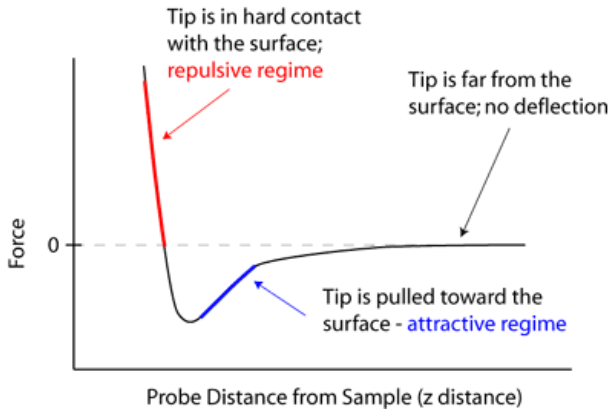

Figure 2.7: Net force between the tip and the sample. Figure from [134].

or dip on the sample, the tip moves up or down, which results in the deflection of the cantilever. The feedback loop then quickly responds and adjusts the piezoelectric element to restore the original interaction (setpoint) between the tip and the sample. At the same time, the topography of the sample surface is recorded by the system.

Fig. 2.8 shows the AFM images of atactic polystyrene (aPS) single crystals from aPS crystallization experiment, where (a) is the height image and (b) is the phase image. The difference in colour in the height image means the height difference between the amorphous domain and the crystalline domain; while, the colour difference in the phase image implies the mechanical property difference between two domains.

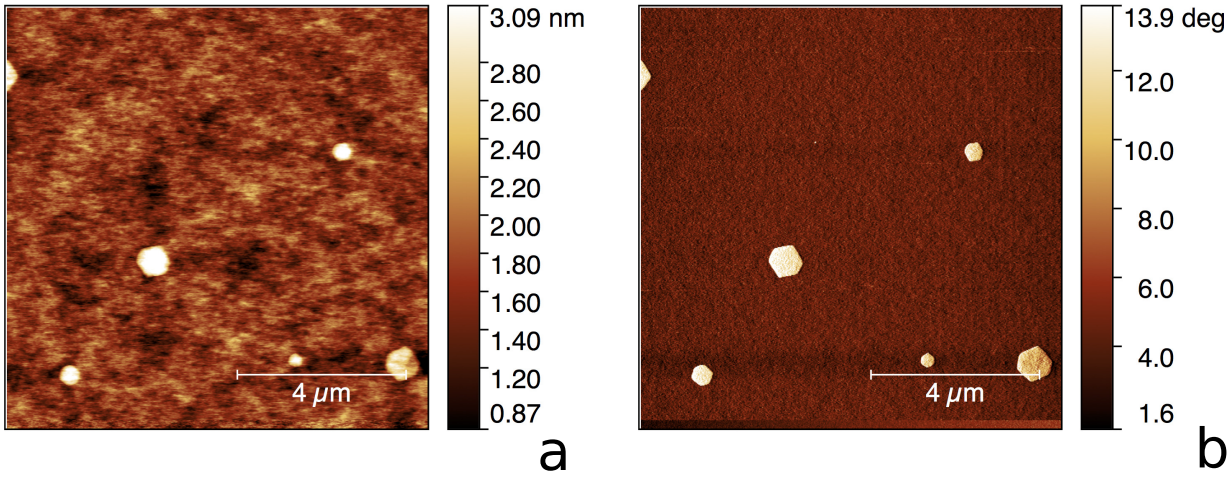

Figure 2.8: AFM images of a M_w 600 g/mol atactic polystyrene, (a) the height image, (b) the phase image.

2.3.3 Contact mode and AC mode

As mentioned previously, AFM uses a feedback loop to keep a constant interaction between the tip and the sample. In general, there are two ways of doing this. It leads to two operation modes: contact mode and AC mode.

Contact mode means that the AFM tip is in contact with the sample during the entire scan. The interaction between the tip and the sample is maintained as a constant by adjusting the piezoelectric element. Due to Hooke's law, the cantilever deflection is proportional to the interaction F and the reciprocal of the spring constant k. Accordingly, in order to achieve a strong signal and also keep the interaction small (too large interaction may cause the sample and tip damages), a low stiffness cantilever should be used (a typical

k value is about 0.2 N/m). When the tip approaches the sample surface, due to the large attractive force, the AFM tip snaps into the surface, which means the tip is in hard contact with the sample surface. In this condition, the interaction between the tip and the sample is repulsive due to the overlapping electron orbits (Pauli repulsion at the short distance in Fig. 2.7). The contact mode is easy to operate as there are not too many adjustable parameters (PID control), and it has a fast scanning speed. However, due to the hard contact between the tip and the sample, it may easily damage soft samples, such as most biological materials and polymer materials. Thus, another working mode, AC model, is more commonly used in these studies.

Unlike contact mode, in AC mode, the AFM tip is not in contact with the sample surface all the time during the scan. Instead, the AFM tip is oscillated at a constant frequency. In AC mode, the tip is in contact with the sample surface for only a part of the oscillation period or even not in contact with the sample surface. The first case is called tapping mode and the latter case is called non-contact mode. In either case, it dramatically reduces the risk of the sample and tip damages. In AC mode, the free amplitude varies from several nm to several hundreds nm and the driving frequency is always chosen to be near the resonance frequency. When the cantilever is oscillated in the open air, there is no external force exerted on the tip. As a result, the amplitude of the oscillation does not change. However, when the tip approaches the sample, due to the interaction between the tip and the sample, the frequency and the amplitude of the oscillation change. The setpoint is the threshold of the amplitude change, beyond which the feedback loop starts to react.

Accordingly, possible lateral damages can be dramatically reduced. In addition, due to the nature of oscillation, the phase information can also be obtained in AC mode. If there is no interaction, there is no phase difference between the driving signal and detected signal. When the tip approaches the sample, the phase shift caused by the interaction should be observed. The phase shift highly depends on the viscoelastic properties of the sample. As a result, phase images can be used to study the blend system because there is no significant height difference between two different domains and a significant contrast can be observed in the phase. In this thesis, the crystallization behaviours of aPS are studied with AFM phase imaging (the phase difference between the amorphous and crystalline domains Fig. 2.8).

2.4 Raman spectroscopy

When a laser beam illuminates on a sample, most of the light is scattered elastically, which is known as Rayleigh scattering (no frequency change between the incident light and the scattered light). However, a small fraction of the light scattered inelastically has different frequencies, which is known as Raman scattering. If the frequency of the scattered light is lower than that of the incident light, the light is deemed to have undergone a Stokes shift; in contrast, if the frequency is higher than that of the incident light, the light has undergone an anti-stokes shift. In general, anti-Stokes shift has a much lower intensity than Stokes shift.

Raman spectroscopy is a technique to detect inelastic scattering (Stokes shift or anti-Stokes shift). As a result, Raman spectroscopy can be used to determine the physical properties of the samples in different physical conditions, such as crystallization [133, 135, 136] and glass transition [137].

The Raman shift is typically expressed in terms of wavenumber, which can be written as

$$\Delta w(cm^{-1}) = (\frac{1}{\lambda_0(nm)} - \frac{1}{\lambda_1(nm)}) \times \frac{10^7 nm}{(cm)} \tag{2.10}$$

where λ_0 is the wavelength of incident light, and λ_1 is the Raman spectrum wavelength. Because Raman spectroscopy is able to measure low frequency modes, it is very suitable to study polymers. In addition, with some enhancement techniques, Raman spectroscopy is also a good candidate in studying the surface properties of polymer thin films, such as Surface-enhanced Raman spectroscopy (SERS) and Tip-enhanced Raman spectroscopy (TERS).

2.5 Annealing ovens

We designed five vacuum ovens, which are used to anneal polymer thin films in vacuum. The vacuum ovens have four major parts: temperature controller, vacuum chamber, hot stage, and lid.

- The temperature controller is made with Omega CN 7500 [138], which has two dual relay outputs.

- The vacuum chamber is made from stainless steel and connected to a dry scroll pump [139].
- The hot stage has three layers. The insulated flexible heater [140] is sandwiched by two aluminum plates.
- The lid is used to cap the heat stage. Without the lid, the temperature on the hot stage is not stable.

Chapter 3

Surface dynamics of glassy polymer films

3.1 Introduction

In the past two decades, the dynamic properties of glassy materials [15, 141] have attracted much attention owing to the significant impact on industrial fabrications [142]. These studies can be classified into two groups, in bulk system and in special systems [143], such as thin films [91], materials confined in porous media [144], and colloids [145], where the surface-volume ratio is relatively larger than that in the bulk. On the other hand, there has been accumulated evidence demonstrating that the glass transition temperature depression as the film thickness decreases is caused by the enhanced surface mobility. Thus,

to understand how polymers move and how they are distributed near the free surface below the bulk glass transition temperature are important as they may change our understanding of *solids*. For example, if there is a layer near the free surface with enhanced mobility, it may flow even when the bulk is still solid. This phenomenon has a significant impact on industrial manufactures, such as moulding polymers below T_g, which saves energy and reduces manufacturing cost. Another intuitive but striking example is the ion conducting polymers, in which conductivity depends on the dynamics of the system through the function $\sigma\tau_s T = \text{const}$ [146, 147]. Hence, a VFT type of behaviour is normally observed when $T > T_g$ [148]. If a layer near the free surface with enhanced mobility exists, it could result in the surface with higher conductivity when the bulk remains non-conductive. This is phenomenologically similar to topological insulators (totally different mechanisms). Therefore, a quantitative study on the surface dynamics of glassy materials is necessary.

In this chapter, we use a novel experiment, levelling of stepped films [149–153], to study the surface dynamics of polymer thin films in their glassy state. The study can be divided into four parts: low molecular weight polystyrene, different molecular weights polystyrene, different confinement conditions, and ultra-thin films.

The first part of the study focuses on how polymers flow below T_g. It involves providing a physical picture, developing a mathematic model, data analysis, comparison between the experimental and numerical flow profiles, and calculating the effective surface mobility.

In the second part, polystyrene stepped films with different molecular weights are used to study how polymer chains are distributed near the free surface, and how polymers flow

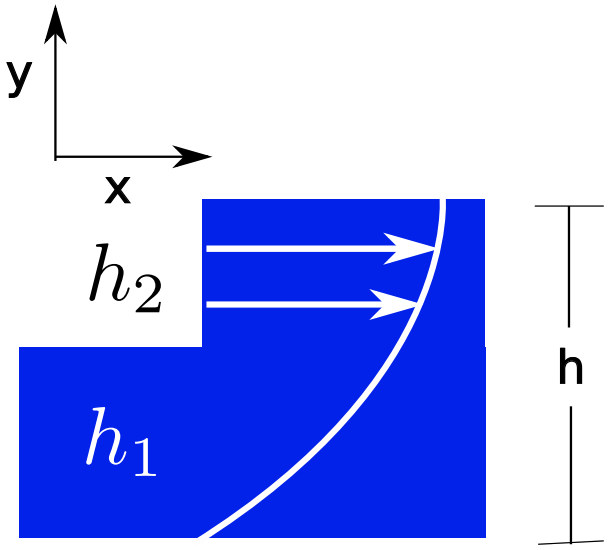

Figure 3.1: Schematic diagram of a stepped film, where the total film thickness is h, the bottom layer has a thickness h_1, and the top layer has a thickness h_2.

in the early stage, where the assumptions made in the model proposed in the first part are not valid.

In the third part, stepped films are immersed in different liquids. Whether the free surface effect can be removed by liquids is tested.

In the last part, the levelling of ultra-thin stepped films is studied to demonstrate whether the T_g reduction is caused by the existence of a liquid-like layer in glassy polymer films.

3.1.1 Theory and simulation

Above T_g, polymer melts can be considered as viscous liquids. Due to the unstable surface geometry, a levelling process, the Laplace pressure driven flow, occurs when stepped films are annealed above T_g. Consequently, by studying the levelling of stepped films, we are able to study the rheological properties of polymers at the nanoscale.

On the other hand, below T_g, stepped films cannot be considered as viscous fluids as they are solids in the experimental time window. However, if there is a liquid-like layer in glassy polymers, the levelling process is still possible as the liquid-like layer can flow.

In this section, the levelling processes above and below T_g are modelled in terms of fluid flows. However, above T_g, the entire film flows; while, below T_g, only the liquid-like layer can flow. Intuitively, they should behave differently.

Whole film flow

In general, above T_g, polymer melts are viscoelastic objects. However, we use low molecular weight polystyrene and a relatively long experimental time. Accordingly, the experimental time is longer than the Maxwell time $\frac{\eta}{E}$. As a result, polymer melts can be considered as pure viscous liquids. Then, we can use fluid dynamics to model the levelling process. Before the derivation, some assumptions are made

1. The fluid is incompressible and the inertia is negligible.

2. There is no slip at the substrate-polymer interface.

3. There is no shear at the polymer-air interface.

4. Gravity is negligible as the capillary length $l_c = \sqrt{\frac{\gamma}{\rho g}} >> h$ [154].

5. There is no long-range interaction between the substrate and the polymer film [155].

6. The lubrication approximation (flow in y direction is negligible, see Fig. 3.1) is used.

According to the above assumptions, it is not hard to tell that we are modelling an incompressible viscous fluid flow with no inertia, no gravity, no substrate interaction, no slip, and no shear boundary conditions. This automatically leads to the Stokes equation.

$$\nabla P = \eta \nabla^2 \boldsymbol{v} \tag{3.1}$$

where P is the local pressure and $\boldsymbol{v}$ is the local velocity. According to the lubrication approximation (Fig. 3.1), Eq. 3.1 reduces to

$$\frac{\partial P}{\partial x} = \eta \frac{\partial v^2}{\partial y^2} \tag{3.2}$$

Since there is no shear at the polymer-air surface, the shear stress at the polymer-air interface equals to zero.

$$\eta \frac{\partial v}{\partial y}\bigg|_{y=h} = 0 \tag{3.3}$$

Integrating Eq. 3.2 and substituting it into the above equation, it yields:

$$\frac{\partial v}{\partial y}\bigg|_{y=h} = [\frac{1}{\eta}\frac{\partial P}{\partial x} y + c]\bigg|_{y=h} = 0 \tag{3.4}$$

This leads to the parameter c to be

$$c = -\frac{1}{\eta}\frac{\partial P}{\partial x}h \tag{3.5}$$

Similarly, as there is no slip at the polymer-substrate interface, the local velocity at the polymer-substrate is zero. Integrating Eq. 3.2 and $v(y = h) = 0$, it leads to

$$v(y = 0) = [\frac{1}{\eta}\frac{\partial P}{\partial x}y^2 + \frac{c}{y} + cy + d]\Big|_{y=0} = 0 \tag{3.6}$$

This gives the parameter $d = 0$. Hence, the velocity can be expressed as

$$v = \frac{1}{\eta}\frac{\partial P}{\partial x}[\frac{1}{2}y^2 - hy] \tag{3.7}$$

This demonstrates that the velocity profile in thin films is parabolic, and this is Poiseuille flow. As the fluid is incompressible, the total volume should be conserved. As a result, the lateral flow leads to the height change in y direction.

$$\frac{\partial h}{\partial t} + \frac{\partial Q}{\partial x} = 0 \tag{3.8}$$

where Q is the flow rate per unit length. The expression of the flow rate can be given by:

$$Q = \int_0^h v dy \tag{3.9}$$

Substituting Eq. 3.7, the flow rate can be expressed as

$$\begin{aligned} Q &= \int_0^h \frac{1}{\eta}\frac{\partial P}{\partial x}(\frac{1}{2}y^2 - hy)dy \\ &= \frac{1}{\eta}\frac{\partial P}{\partial x}(\frac{1}{6}y^3 - \frac{1}{2}hy^2)|_{y=0}^{y=h} \\ &= -\frac{1}{3\eta}\frac{\partial P}{\partial x}h^3 \end{aligned} \tag{3.10}$$

Then the evolution equation (Eq. 3.8) becomes

$$\frac{\partial h}{\partial t} - \frac{1}{3\eta}\frac{\partial}{\partial x}(\frac{\partial P}{\partial x}h^3) = 0 \tag{3.11}$$

Due to the Young-Laplace equation, the local pressure can be written as:

$$P - P_0 = -\gamma\frac{\partial_x^2 h}{(1+(\partial_x h)^2)^{3/2}} \tag{3.12}$$

With the small slope approximation $\partial_x h^2 < 1$, the above expression reduces to:

$$\Delta P = -\gamma\frac{\partial^2 h}{\partial x^2} \tag{3.13}$$

Substituting the pressure expression into Eq. 3.11, it gives:

$$\frac{\partial h}{\partial t} + \frac{\gamma}{3\eta}\frac{\partial}{\partial x}(h^3\frac{\partial^3 h}{\partial x^3}) = 0 \tag{3.14}$$

The above equation is called the thin film equation (TFE) [149–152]. Clearly, there is a h^3 in the partial differential term, which implies the flow profile should somehow depend on the height of the film.

Surface flow

Below T_g, if there is a liquid-like layer, polymers can still flow within this layer and the surface flow occurs. In this case, we assume this thin layer has a viscosity η and a thickness h^*. The bulk film underneath is glassy and the viscosity is infinity. With this assumption, the TFE equation is not valid anymore; instead, we develop a new mathematic model, the glassy thin film equation (GTFE) . Fig. 3.2 shows the schematic diagrams of two types of

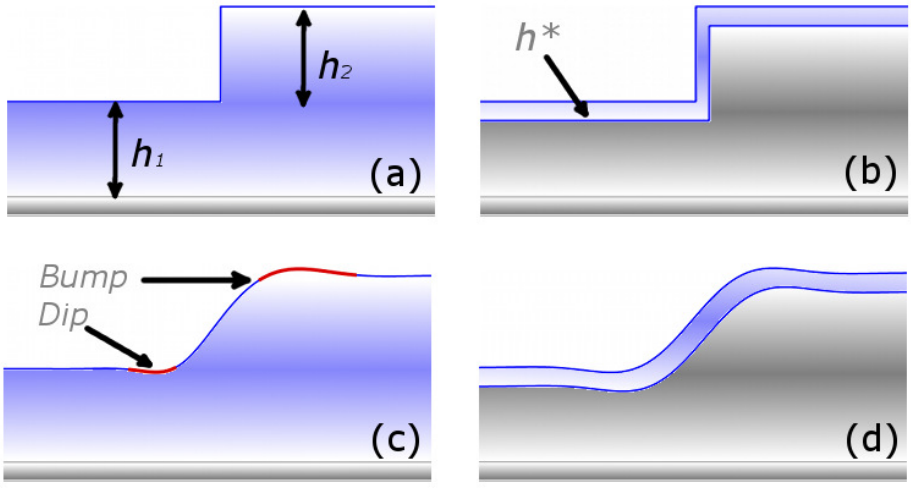

Figure 3.2: Schematic diagrams of two types of levelling processes, where the bump and dip are shown.

levelling processes, (a,c) the whole film flow, (b,d) the surface flow. The derivation of the GTFE is very similar to the TFE but with different boundary conditions. In the TFE, the polymer-substrate interface has a no-slip condition; in contrast, in the GTFE, there is a new interface between the liquid-like layer and the glassy film underneath. Similarly, a no slip condition is still used. According to the above hypothesis, the polymer/air surface with no shear condition leads to

$$\eta \frac{\partial v}{\partial y}\Big|_{y=h^*} = 0 \tag{3.15}$$

Then Eq. 3.4 becomes

$$\frac{\partial v}{\partial y}\Big|_{y=h^*} = [\frac{1}{\eta}\frac{\partial P}{\partial x} y + c]\Big|_{y=h^*} = 0 \tag{3.16}$$

This leads to the parameter c to be

$$c = -\frac{1}{\eta}\frac{\partial P}{\partial x}h^* \tag{3.17}$$

As a result, the expression of the velocity becomes

$$v = \frac{1}{\eta}\frac{\partial P}{\partial x}(\frac{1}{2}y^2 - h^* y) \tag{3.18}$$

The Volume conservation is still valid and the volumetric flow rate per unit length is reduced to

$$\begin{aligned} Q &= \int_0^h \frac{1}{\eta}\frac{\partial P}{\partial x}(\frac{1}{2}y^2 - h^* y)dy \\ &= \frac{1}{\eta}\frac{\partial P}{\partial x}(\frac{1}{6}y^3 - \frac{1}{2}h^* y^2)\Big|_{y=0}^{y=h^*} \\ &= -\frac{1}{3\eta}\frac{\partial P}{\partial x}h^{*3} \end{aligned} \tag{3.19}$$

The Young-Laplace equation and small slope approximation are still used. Finally, the expression of the GTFE is

$$\frac{\partial h}{\partial t} + \frac{\gamma h^{*3}}{3\eta}\frac{\partial^4 h}{\partial x^4} = 0 \tag{3.20}$$

Surprisingly, the form of the GTFE is very simple. It is a simple fourth order differential equation, which is mathematically identical to the surface diffusion model proposed by Mullins [156]. In Mullins' model, the flattening of a nearly plane solid surface is considered as the combination of four mechanisms: viscous flow, evaporation-condensation, volume diffusion and surface diffusion, where the surface diffusion mechanism in one dimension leads to the equation

$$\frac{\partial W}{\partial t} + B\frac{\partial^4 W}{\partial x^4} = 0 \tag{3.21}$$

where W is the surface height, $B = \frac{\gamma D_s \Omega \nu}{kT}$ is the mobility constant, D_s is the surface diffusion coefficient, γ is the surface tension, Ω is the molecular volume, and ν is the number of molecules per unit area on the surface. In Mullins' description, the surface diffusion is considered as the hopping motion of surface atoms in solids. If the two models are equal, it leads to

$$\frac{\gamma D_s \Omega \nu}{kT} = \frac{\gamma h^{*3}}{3\eta} \tag{3.22}$$

This implies that the Stokes-Einstein equation $D \sim \frac{kT}{\eta r}$ may still be valid in this condition. Of course, whether these two mechanisms are conceptually identical and whether Stokes-Einstein equation is still valid in this condition need to be verified.

Step levelling in the early stage

Both the TFE and GTFE assume that the lubrication approximation is valid and a small slope approximation is used. However, in the extremely early stage, this may not be true. In order to simulate the early state levelling process, the pressure term should be in the form of Eq. 3.12, which leads to a full GTFE

$$\frac{\partial h}{\partial t} + \frac{\gamma h^{*3}}{3\eta} \frac{\partial^2}{\partial x^2} [\frac{\partial_x^2 h}{(1 + (\partial_x h)^2)^{3/2}}] = 0 \tag{3.23}$$

which gives an exponent n between the width w and time t ($w \sim t^n$) bigger than 1/4 when $(\partial_x h)^2$ is not much smaller than 1.

3.1.2 Experimental procedures

In this section, the experimental procedures and details are introduced. In addition, the data analysis is also demonstrated. All stepped films were made with 3 kg/mol polystyrene, except for the molecular weight dependent levelling experiment.

Low molecular weight levelling experiment

In this project, all polystyrene stepped films were made following the procedure described in the previous chapter. Two types of experiments were conducted.

The first experiment is the width evolution experiment, where three different types of stepped films were made, which had the same bottom layer thickness $h_1 = 90$ nm and three different top layer thicknesses $h_2 = 14$, 23, and 42 nm. These samples were collectively heated in an oven flushed with N_2 for various times and removed from the oven for measurements. All stepped films were measured at room temperature with the AFM in tapping mode. Both topography and phase images were collected.

In the second part, the profile experiment was conducted where symmetric stepped films were used, which had the top layer thickness $\sim$ 90nm and the bottom layer thickness $\sim$ 90 nm as well. At each temperature, a single sample was measured on an AFM hot stage at room temperature. Then the sample was annealed at a predetermined temperature for a predetermined time and cooled back to room temperature for the AFM measurement. This process was repeated several times until the total annealing time reached 90 hours for

the annealing temperatures below or near the bulk glass transition temperature or until the profile satisfied the self-similar behaviour for the annealing temperatures above the bulk glass transition temperature.

Molecular weight dependent levelling experiment

In this project, two additional molecular weights of polystyrene were studied, 11.9 kg/mol and 22.2 kg/mol. The stepped films with $h_1 \sim 90$ nm, $h_2 \sim 90$ nm were made, except for one run on a ~ 41 nm on ~ 41 nm stepped film (M_w 11.9 kg/mol). Most of the experiments were similar to the low molecular weight profile experiment. Samples were annealed on the AFM hot plate and measured with the AFM at room temperature. In addition, there were two runs, where the stepped films (~ 90 nm on 90 nm stepped film and ~ 41 nm on 41 nm stepped film) were annealed at 90 °C (a second thermocouple sensor read 91 °C) in a homemade oven rather than on the AFM hot plate.

Liquid confinement levelling experiment

In this project, all polystyrene stepped films were made by following the procedure described in the previous section, except for the air/N_2 atmosphere replaced by different liquids: deionized water and corn syrup. All stepped films were configured with $h_1 \sim 90$ nm and $h_2 \sim 90$ nm and then annealed in a home made oven at 60 °C (a second thermocouple sensor read 61 °C) for various times. After annealing, samples were removed from the oven and quenched down to room temperature. For deionized water runs, after

Table 3.1: Experimental details of the ultra-thin films levelling project

Run	Sample	h_1	h_2	Temperature	Time	Oven or hotplate
1	1	7 nm	14 nm	65 °C	21 hours	hotplate
2	2	7 nm	7 nm	60 °C	50 hours	hotplate
3	3	8 nm	8 nm	65 °C	1, 2, 3 hours	hotplate
4	4	8 nm	8 nm	65 °C	1 hour	hotplate

annealing, samples were dried at ambient conditions before AFM measurements. For corn syrup runs, after annealing, the samples were rinsed with deionized water and dried at ambient conditions before AFM measurements.

Ultra-thin films levelling experiment

In this project, ultra-thin stepped polystyrene films with different geometries were made. After sample preparation, samples were annealed either on an AFM hot plate or in a homemade oven at either 60 °C or 65 °C for various times. The experimental details for each sample are shown in Table 3.1.2.

3.1.3 AFM measurement

All experimental profiles were obtained with a JPK AFM. AFM ran in tapping mode with Tap150-G tips from Budget Sensors, which have a resonant frequency of 150 ± 75 kHz,

length 125 μm, mean width 25 μm, thickness 2.1 μm, tip height 17 μm, and tip radius 15 nm. During measurements, the parameters were adjusted to make the trace and retrace profiles match. A typical scan resolution is 512 $\times$ 512, which leads to 512 single lines in each image.

3.1.4 Data analysis

One of the most important parts of the levelling experiments is data analysis. In this section, data analysis and analysis tools are introduced. The general data analysis for the levelling project followed the procedure described below:

1. Level AFM topology raw images with Gwyddion [157].
2. Export the images as text files with all data points.
3. Read the text files and fit each line in the images with a tanh function.
4. Find the distribution of the width and determine the most probable width for each image.
5. Shift and average all single lines to achieve the mean profile.
6. Fit the mean profile with a tanh function and determine the width of the mean profile.

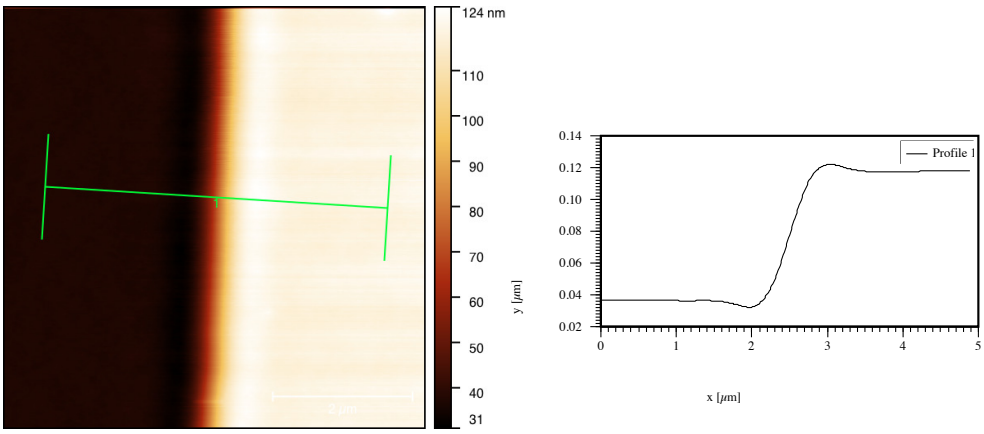

Figure 3.3: A typical AFM height image of a stepped film and an averaged line profile.

7. Check whether the width determined from the distribution and that from the mean profile are the same.

8. Level the mean profile with a quadratic function if necessary.

9. Compare the experimental profile with the TFE profile to extract the viscosity when the annealing temperature is higher than the bulk glass transition temperature.

10. Compare the experimental profile with the GTFE profile to extract the surface mobility when the annealing temperature is lower than the bulk glass transition temperature.

11. Compare the experimental profile with both the TFE and GTFE profiles to determine the correlation function (χ).

Fig. 3.3 shows a typical AFM height image after levelling with Gwyddion, where the line

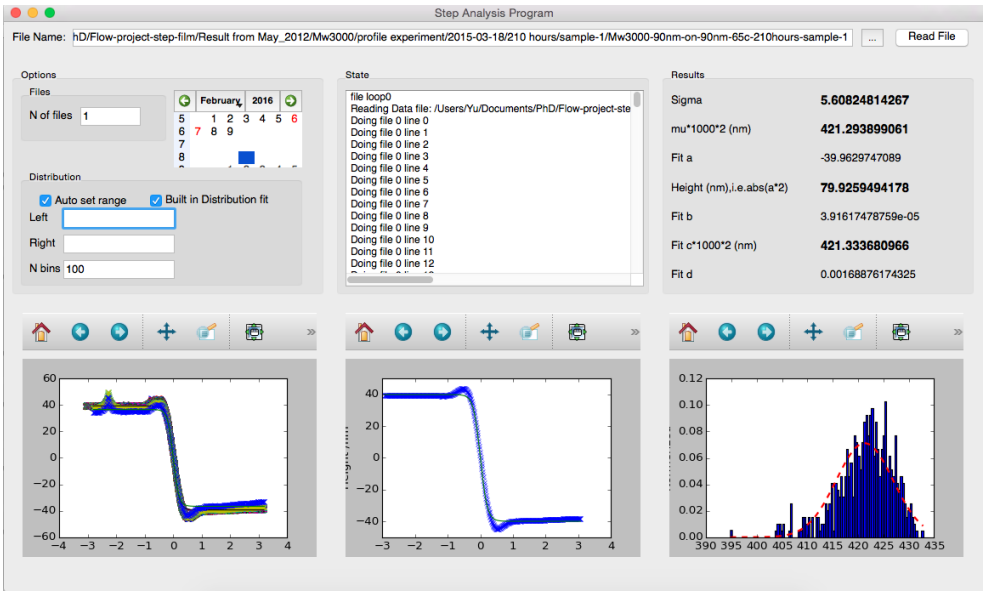

Figure 3.4: Step analysis program with a GUI (PyQt4 [158]) written in Python.

profile is also presented. Fig. 3.4 shows the step analysis program, which was written in Python. The program has three columns, where the left one shows all individual lines in an AFM height image, the middle one shows the mean profile produced by shifting and averaging of all lines, and the right one shows the width distribution of all individual lines as well as the Gaussian fit of the distribution. In addition, all fitting parameters are listed. From the figure, one can tell that the term *mu*1000*2* and the term *Fit c*1000*2* have the same value, indicating that the width of the mean profile and the most probable width of all lines in the image are consistent.

3.2 Discussion

3.2.1 Low molecular weight levelling

Width evolution

It has been well studied that above T_g, the stepped films tend to be flat. We first examine whether the levelling process can happen below the bulk glass transition temperature. As described in the experimental part, three different types of stepped films are annealed at temperatures at which they are expected to be immobile. Surprisingly, we find that the shape of these stepped films changes as the annealing time increases. This observation indicates that levelling process still happens below the bulk glass transition temperature. In order to determine whether this levelling process is due to the fluid flow, the width of each sample is extracted by fitting the profile with a tanh function.

Fig. 3.5 (a) shows the time evolution of the width of the stepped films ($h_1 \sim 90$ nm and $h_2 \sim 42$ nm) annealed at different temperatures, where the dashed lines stand for the $w = at^{1/4}$ fits. The results demonstrate that, whether above or below the glass transition, the time evolution of the width agrees with a 1/4 power law, which is a strong indication of a capillary-driven flow. In addition, the bulk TFE gives $w \propto \frac{1}{\eta_{eff}} t^{1/4}$. Hence, the effective viscosity at different temperatures can be obtained through the relationship $\eta_{eff} \propto a^{-1}$, where a is the pre-factor determined from the 1/4 power law fits. This effective viscosity should be understood as how viscous the film is if the entire film can undergo

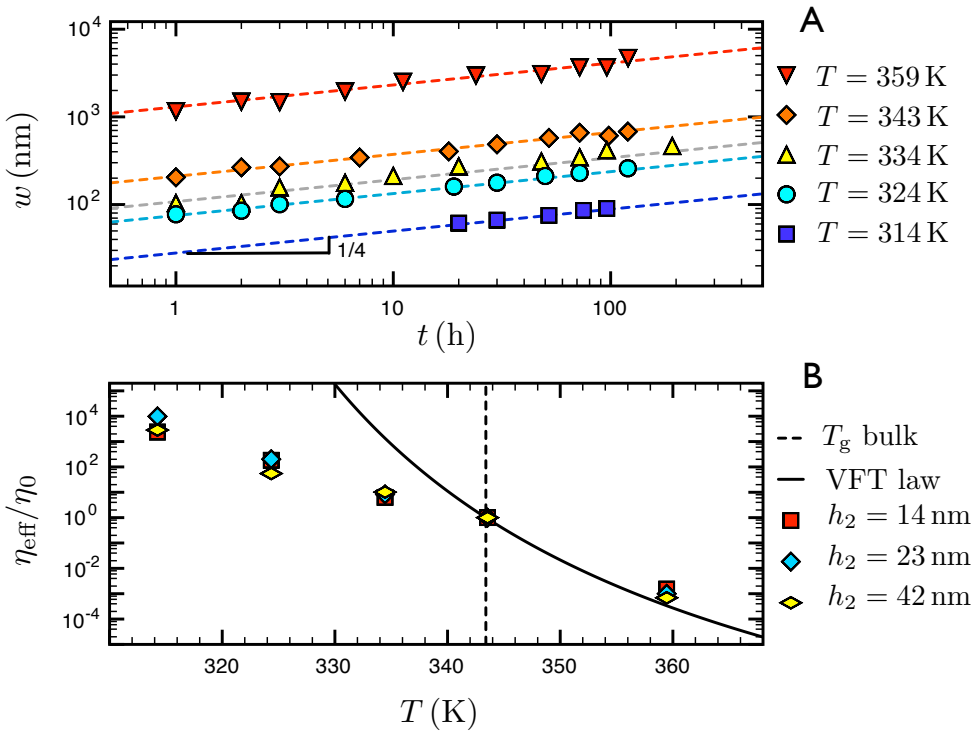

Figure 3.5: (a) Time evolution of the width of the stepped films with $h_1 \sim 90$ nm and $h_2 \sim 42$ nm. (b) Normalized effective viscosity as a function of temperature for three different geometries. Figure from [159].

flow as it does above T_g. On top of this, if we define η_0 as the effective viscosity at T_g, all effective viscosities at different temperatures for a given geometry can be normalized through $\eta_{eff}/\eta 0 = a_0/a$. By doing this, the difference due to sample geometry can be eliminated as they all have the same effective viscosity ratio 1 at T_g. Fig. 3.5 (b) shows the time dependent η_{eff}/η_0 for three different geometries, where the solid line stands for the VFT curve. Clearly, above the glass transition temperature, data follows the bulk VFT behaviour. However, below the glass transition temperature, data deviates from the bulk VFT behaviour. To account for the deviation, there are two possible explanations. The first one is that the entire film can still take part in the flow process below the glass transition temperature, but the viscosity of the entire film deviates from the VFT law. In contrast, the second explanation assumes that only a thin layer can flow below the glass transition temperature. If the second explanation is correct, the simulation profile based on the TFE would not be able to match the experimental profiles obtained below the glass transition temperature. As a result, we conduct a profile experiment to distinguish the levelling profiles obtained above and below the glass transition temperature.

Profile comparison experiment

Experimental details have been discussed in the experimental part. Here we take two typical runs and test whether the second explanation is valid. Fig. 3.6 shows the profile experiment. In the figure, both above and below the glass transition temperature, the flattening of steps can be observed. In (A and B), the width of steps increases as the

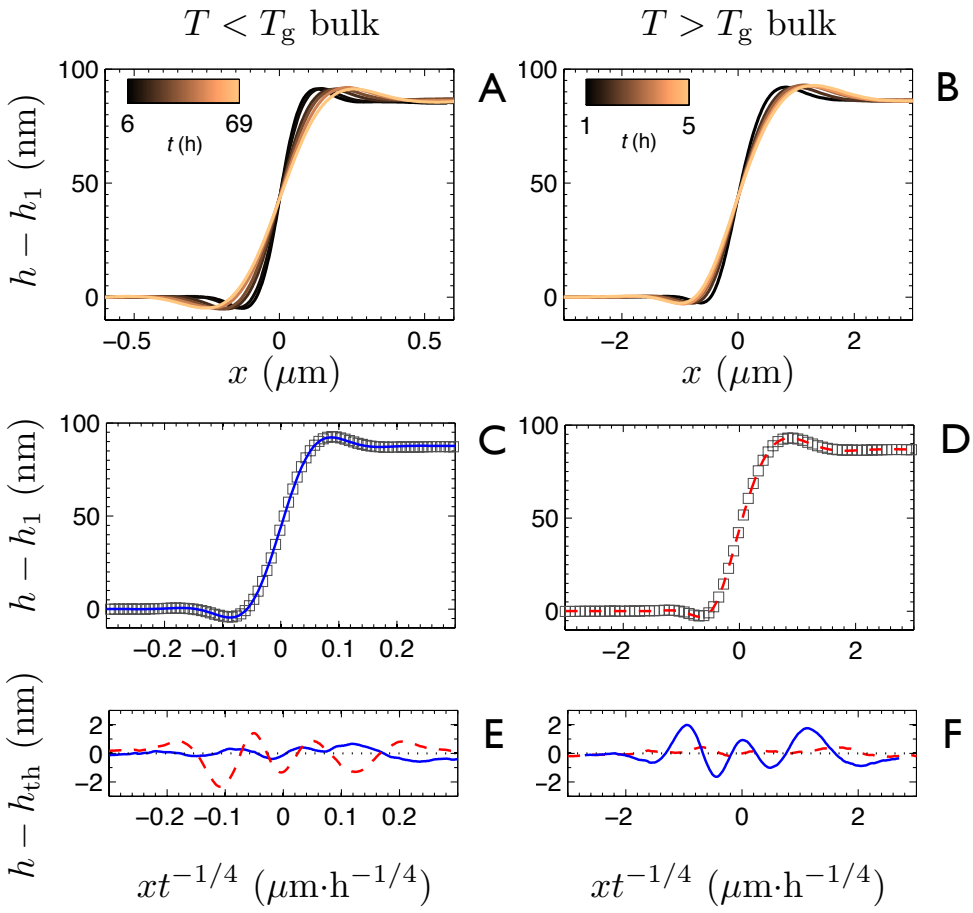

Figure 3.6: (A and B) Experimental profiles for 90 nm on 90 nm stepped films annealed for various times. (C and D) self-similar profiles (open squares) and simulation profiles (GTFE: blue solid line, TFE: red dashed line). (E and F) Goodness of the fit of experimental profiles to either the TFE profile or the GTFE profile. (A, C, E) are the profiles annealed below the glass transition temperature (T = 333 K) , while (B, D, F) are the profiles annealed above the glass transition temperature (T = 353 K). Figure from [159].

annealing time increases. As discussed in the previous sections, both above and below T_g, a 1/4 power law can be observed. In consequence, if we replace x by $x/t^{1/4}$, the experimental profiles should collapse into a master curve, a self-similar process. Fig. 3.6 C and D show the self-similar profiles above and below T_g. Although they both satisfy the self-similar behaviour, their shapes look different. One can see that annealed below T_g, the self-similar profile looks symmetric (the bump and the dip have the same size); while annealed above T_g, the self-similar profile looks more asymmetric (a bigger bump and a smaller dip). This simple difference demonstrates that below T_g, the levelling process does not agree with the hypothesis that the entire film can flow. In contrast, this levelling process should be described by the GTFE, which assumes that only a thin layer can flow while the rest of the materials underneath cannot. The detailed derivation has been already discussed previously. In order to validate the GTFE, we fit the self-similar experimental profiles to the simulation profiles generated from the GTFE and TFE. Fig. 3.6 E and F show the goodness of the fit of the experimental profile to either the GTFE profile or the TFE profile, where the blue-solid line represents the fit to the GTFE; while the red-dashed line stands for the fit to the TFE. Clearly, below T_g, the red-dashed line has the systematic error, while the blue-solid line has a better fit. This observation is opposite when the temperature is higher than the glass transition temperature. This indicates that above T_g, the levelling process can be describe by the TFE model, while below T_g, the levelling process can be described by the GTFE model. In order to make the conclusion more solid, we conduct another run at 338 K (T_g - 5 K), which has a bigger time range from 1 hour

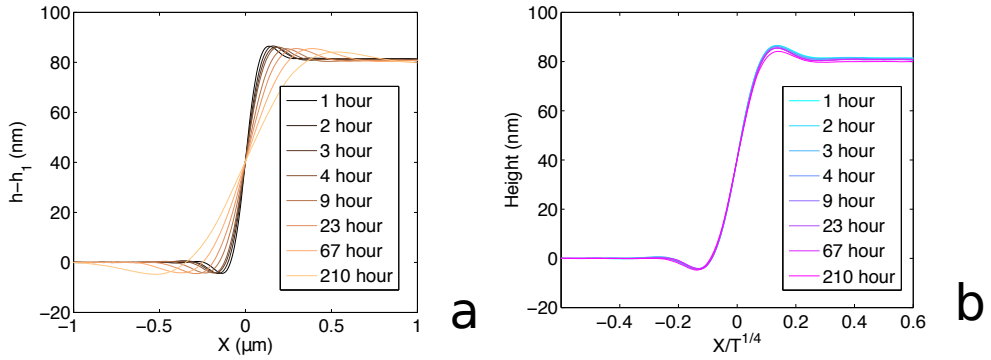

Figure 3.7: Time dependent levelling profiles of a stepped film annealed at 338 K, (a) time dependent profiles, (b) collapsed self-similar profiles.

up to 210 hours. From Fig. 3.7, the symmetric self-similar profile can still be observed.

Correlation function and the glass transition

The intuitive question now is then how to describe the transition from the GTFE to TFE. In other words, is there a sharp transition or a broad transition from the surface flow to the bulk flow? As a result, defining a variable that can quantify the transition is necessary. Accordingly, we define a correlation function χ to quantitatively describe how close the experimental profile is to the simulation profile and use it to study the transition from the surface flow to the bulk flow. Since there are two models, the GTFE and TFE, there are two correlation functions. Here we define χ_{GTFE} as

$$\chi_{GTFE} = \frac{\int dx (h_{EXP} - h_{TFE})^2}{\int dx (h_{GTFE} - h_{TFE})^2} \tag{3.24}$$

where h_{EXP} is the experimental profile, and h_{TFE} and h_{GTFE} are simulation profiles calculated based on the TFE and GTFE models respectively. The other correlation function is

$$\chi_{TFE} = \frac{\int dx(h_{EXP} - h_{GTFE})^2}{\int dx(h_{GTFE} - h_{TFE})^2} \tag{3.25}$$

In this way, the correlation function is called χ_{TFE}. In principle, if an experimental profile fits the simulation GTFE profile perfectly, it gives $\chi_{GTFE} = 1$ and $\chi_{TFE} = 0$. In the other case, it should give $\chi_{GTFE} = 0$ and $\chi_{TFE} = 1$. Although the flat areas cannot provide any information of distinguishing the two models, they can affect the value of the correlation function. In consequence, we only calculate χ_{GTFE} of the profile in the range of $-7w$ and $7w$, where w is the width of the profile. Fig. 3.8 shows the temperature dependent correlation function for the 90 nm on 90 nm stepped films. In order to make a direct comparison, the thermal expansivity data obtained from ellipsometry is also shown in the plot, which is normally used to determine the glass transition temperature in thin films. In the plot, the correlation function χ_{GTFE} is used, while χ_{TFE} gives a similar but inverted plot. Clearly, there is a transition of the correlation function and the transition temperature is very close to the glass transition temperature determined by ellipsometry. At low temperatures, χ_{GTFE} are close to 1; in contrast, at high temperatures, χ_{GTFE} shift to 0. In addition, in two regimes, χ_{GTFE} is temperature independent, which means the experimental profiles can be correctly described by the TFE model when $T < T_g$ and the GTFE model when $T > T_g$. The result is striking as it directly confirms the hypothesis that only a thin layer can flow below T_g proposed previously. In addition, the inset shows the

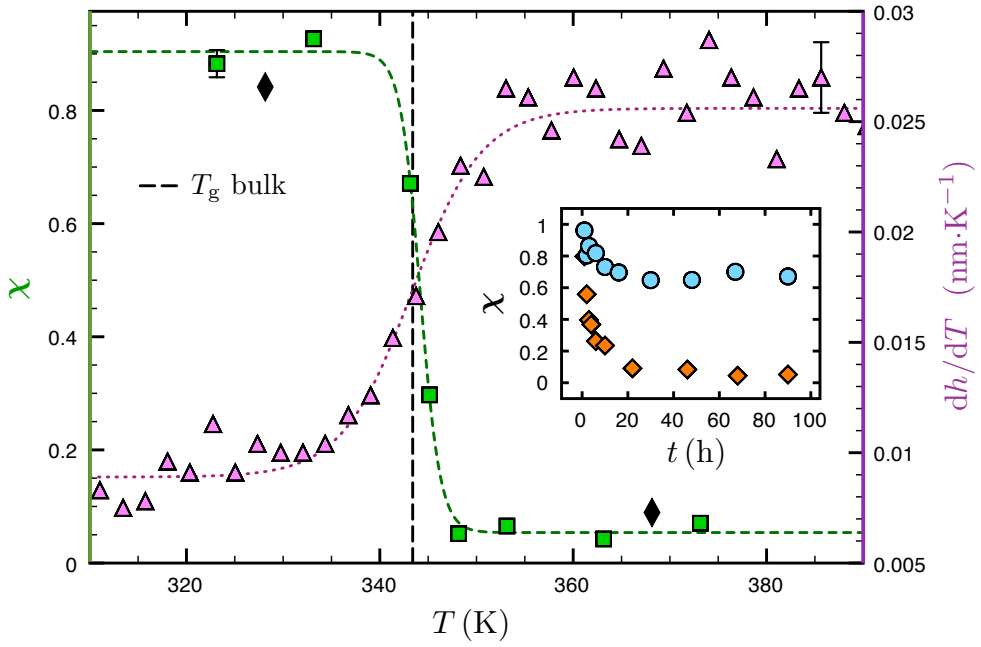

Figure 3.8: Correlation function χ_{GTFE} (green squares and black diamonds) as a function of temperature (left axis), and thermal expansivity data based on ellipsometry (purple triangles, right axis). The inset shows the correlation function χ_{GTFE} as a function of time at T = 343 K (blue circles) and at T = 348 K (orange diamonds). The black diamonds show the correlation function of a stepped film firstly annealed below T_g for 90 hours, then measured; and annealed above T_g, then measured. Figure from [159].

temporal evolution of the correlation function at two temperatures near the glass transition temperature. For T = 343 K, in the early stage, χ_{GTFE} is close to 1, which means the levelling process is dominated by the surface flow; however, in the late stage, χ_{GTFE} tends to be 0, which means the levelling process tends to be the entire film flow like. At T = 348 K, this phenomenon is more pronounced. This also implies that one can use a single sample to probe both the surface flow and the entire film flow. The black diamonds in the Fig. 3.8 correspond to the stepped film annealed below and above the glass transition temperature. After the first annealing below the glass transition temperature for 90 hours, the experimental profile gives $\chi_{GTFE} \sim 1$. Then the sample is annealed above the glass transition temperature, which leads to $\chi_{GTFE} \sim 0$. In most surface dynamics experiments (embedding and nanoholes recovery), probing with one sample is not possible due to the rapid saturation above the glass transition temperature.

Surface mobility near the glass transition temperature

By fitting the experimental profiles to the simulation profiles, the pre-factors can be extracted, which contain the information of the samples. As the simulation profiles are generated with dimensionless equations, the fitting process is actually to find the stretching parameter. Assuming the surface tension γ is temperature independent and $h = h_1 + h_2/2$, above the glass transition temperature, bulk viscosity η_b can be obtained with the TFE fitting parameter. However, as the h_m (h^*) and η_m are coupled together, only the surface mobility $h_m/(3\eta_m)$ can be obtained with the GTFE fitting parameter. In order to make a

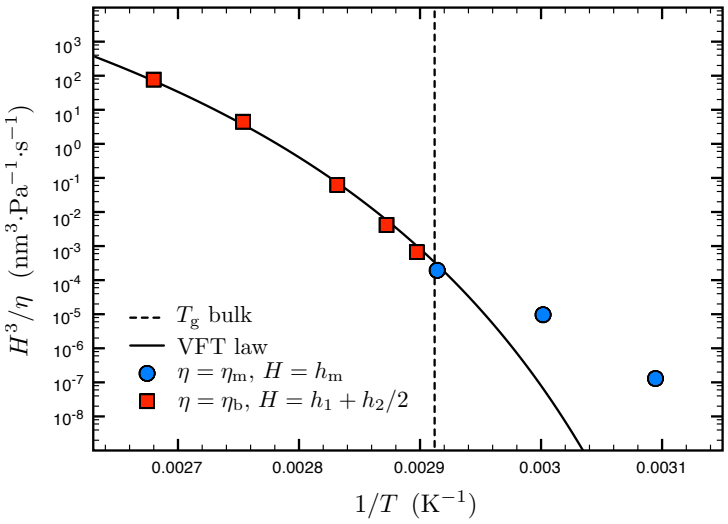

Figure 3.9: Mobility as a function of temperature, above T_g, $H = h_1 + h_2/2$, $\eta = \eta_b$; below T_g, $H = h_m$, $\eta = \eta_m$. Figure from [159].

direct comparison, even though above the glass transition temperature bulk viscosity can be obtained, we prefer to use the mobility $(h_1 + h_2/2)(3\eta_b)$ in the plot. In this way, one can intuitively tell that above T_g, the entire film can flow with a mobile layer $h_1 + h_2/2$; however, below T_g, only a thin layer h_m can undergo flow. As a result, it is convenient to define the mobility in a general expression $H/(3\eta)$: above T_g, $H = h_1 + h_2/2$, $\eta = \eta_b$ and below T_g, $H = h_m$, $\eta = \eta_m$.

Fig. 3.9 shows the mobility of the stepped films at different temperatures, from which above T_g the mobility follows the bulk VFT curve [160] (no shift), while below T_g, similar to Fig. 3.5, there is a strong deviation from the bulk VFT curve and it exhibits an Arrhenius type of temperature dependence. In this temperature range, the mobility is defined as

$h_m/(3\eta_m)$, which is the combination of two physical quantities. As a result, it is not possible to find the actual temperature dependence of these two quantities independently.

Surface diffusion and surface flow

From introduction, we know that the surface diffusion model and surface flow model have the same mathematical equation. In addition, from the experimental results, we can find that the surface flow model can describe the flow behaviour of polymer films below T_g. Consequently, it is reasonable to ask whether these two models are the same and whether polymers move as the models described.

In the surface diffusion picture, molecules do hopping motions at the free surface. As a result, this process is limited at the free surface. In the surface flow picture, molecules can flow in a layer with a finite thickness (a few of nm). Consequently, this process can still be considered as a fluid flow. From this point of view, these two models are different. However, in a real system, the motion of molecules is much more complicated as there might be a continuous distribution of dynamics in thin films. Consequently, to comment on the correctness of these two models is not fair as both of them are just coarse-grained models of a real system. The only thing we can conclude is that both of these models have the same mathematical equation and the levelling process of stepped films below T_g can be characterized by the equation.

Summary

To summarize, by performing the stepped film levelling experiment, we analyze the flow behaviours above and below the glass transition temperature. The results confirm the existence of a liquid-like layer in glassy polystyrene films. To account for these two different flow behaviours, we develop the GTFE to describe the surface flow below T_g and used the TFE to describe the flow above T_g. In order to quantify the transition from the surface flow to the entire film flow, we define two correlation functions χ_{GTFE} and χ_{TFE} to demonstrate that there is a sharp transition from the surface flow to the entire film flow with a transition temperature close to the bulk T_g. Lastly, we define a general mobility, which follows the bulk VFT curve above T_g and the Arrhenius behaviour below T_g.

3.2.2 Molecular weight dependent levelling

From the previous section, we can tell that for low molecular weight polymers, there is a thin liquid-like layer, which can flow even when $T < T_g$. Intuitively, the next question is how thick this layer is. Since thick films always exhibit bulk dynamics, one should expect that the free surface effect can only extend over a limited distance. Accordingly, it is possible to reach a situation where the size of the polymers is comparable to or bigger than that of the liquid-like layer. Do we still expect a surface flow in this situation? Consequently, a molecular weight dependent levelling experiment near the glass transition temperature is necessary.

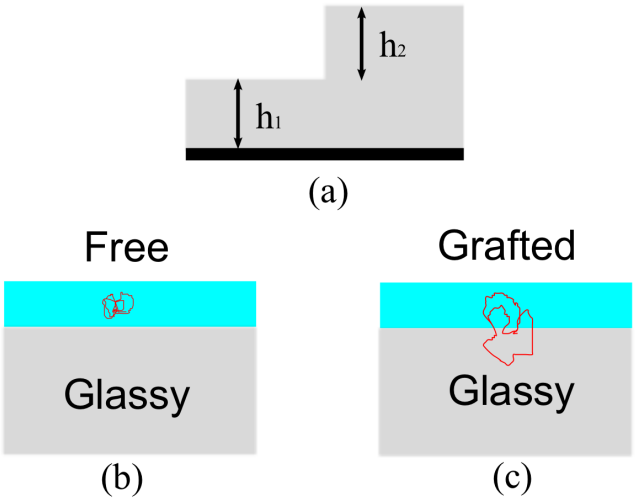

Figure 3.10: Schematic diagram of the molecular weight dependent levelling experiment. (b) The size of the liquid-like layer is bigger than that of the polymers. (c) The size of the liquid-like layer is smaller than that of the polymers.

Fig. 3.10 shows a schematic diagram of the molecular weight dependent levelling experiment. In case (b), the size of the polymers is smaller than that of the liquid-like layer; thus, polymers can easily flow in the liquid layer (without chain confinement). While, in case (c), the size of the polymers is bigger than that of the liquid layer. As a result, it may lead some polymer chains partially anchored in the glassy part (with chain confinement).

Before the experiment, we need to roughly estimate what molecular weight is required to have the chain confinement effect. In the embedding experiments [114, 115, 161], the result shows an initial embedding plateau, which is about 5 nm and decreases as the temperature decreases. A similar conclusion can be found in the dye reorientation measurement [162]. Thus, it is possible to assume the liquid-like layer has a thickness of a few nanometers. If we take 5 nm as the size of the liquid-like layer and $2R_g$ as the size of polymers, a molecular weight of 8.5 kg/mol is required to have the chain confinement effect. In addition, it is better to stay in the non-entangled regime, as the entanglement effect may lead the model to be more complicated. Accordingly, three molecular weights were chosen, 3 kg/mol, 11.9 kg/mol, and 22.2 kg/mol, where the size of the 3 kg/mol polymers is smaller than the size of the liquid-like layer, and the sizes of the other two polymers are bigger than the size of the liquid-like layer. See Table 3.2.

Temporal evolution of the stepped films near T_g with higher molecular weights

In order to understand the flow behaviour under confinement, we first measured the levelling profiles above and below T_g for various times. Fig. 3.11 shows the temporal evolution

Table 3.2: Polystyrene with three different molecular weights.

PS	M_w	R_g	$2R_g$
1	3.0 kg/mol	1.5 nm	3.0 nm
2	11.9 kg/mol	3.0 nm	6.0 nm
3	22.2 kg/mol	4.0 nm	8.0 nm

of the levelling profiles for M_w = 11.9 kg/mol stepped films at T_g - 3 °C and T_g + 12 °C, respectively. Surprisingly, even under confinement, the levelling is still observed, implying that the polymers can still flow below the bulk T_g with $2R_g \sim h_m$. The levelling process is also observed for 22.2 kg/mol polystyrene below T_g, where $2R_g > h_m$. See Fig. 3.12. The results imply that the stepped films can even flow below T_g with their size comparable or bigger than that of the liquid-like layer. Similar to the lower molecular weight levelling experiment, there are also two possible interpretations. The first one is that the levelling of stepped films is the bulk behaviour. This means we probe the bulk dynamics of polymers in their glassy state. The second one is that even though some segments are grafted in the glassy layer underneath, it is possible that there are still some polymer chains with all their segments in the liquid-like layer and these polymers can flow below T_g.

Time dependent correlation function near T_g for three different polymers

In order to determine which explanation is correct, we fit the experimental profiles to both the GTFE and TFE, which yields both χ_{GTFE} and χ_{TFE} for each experimental profile.

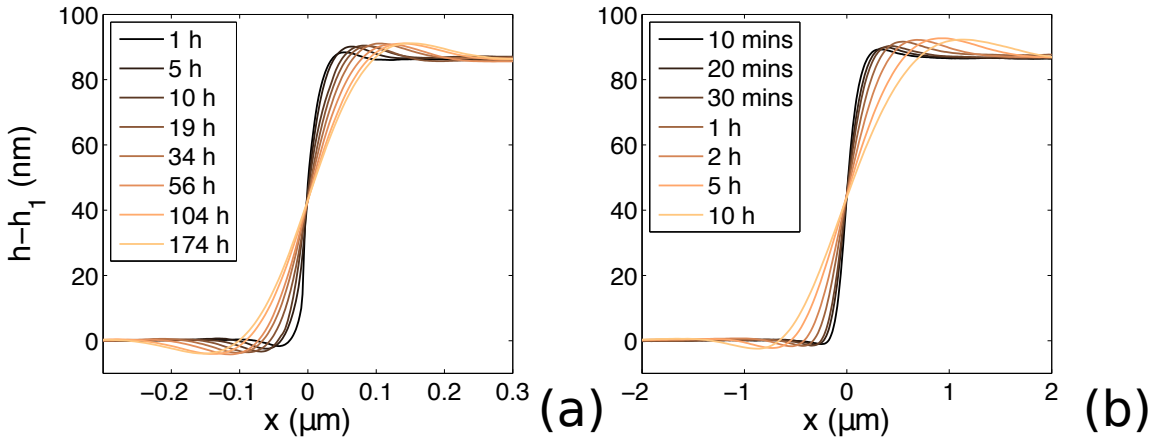

Figure 3.11: Temporal evolution of the levelling profiles for M_w = 11.9 kg/mol stepped films above and below the bulk T_g, (a) T = T_g - 3 °C, (b) T = T_g + 12 °C.

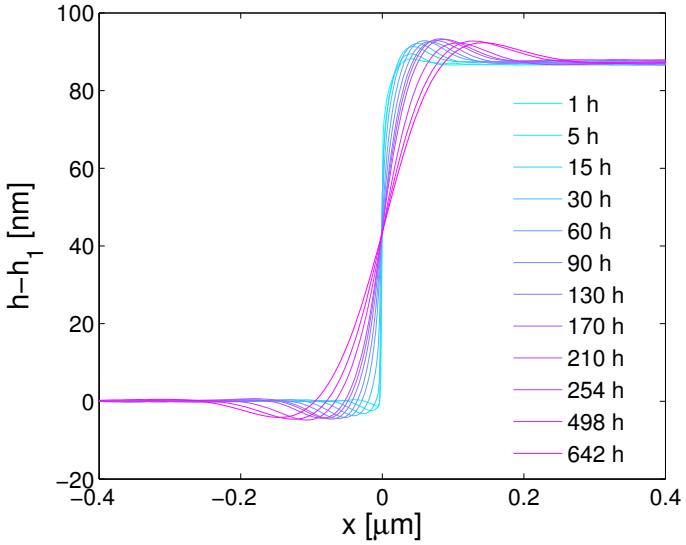

Figure 3.12: Temporal evolution of the levelling profiles for M_w = 22.2 kg/mol stepped films annealled at 90 °C (T_g - 6 °C).

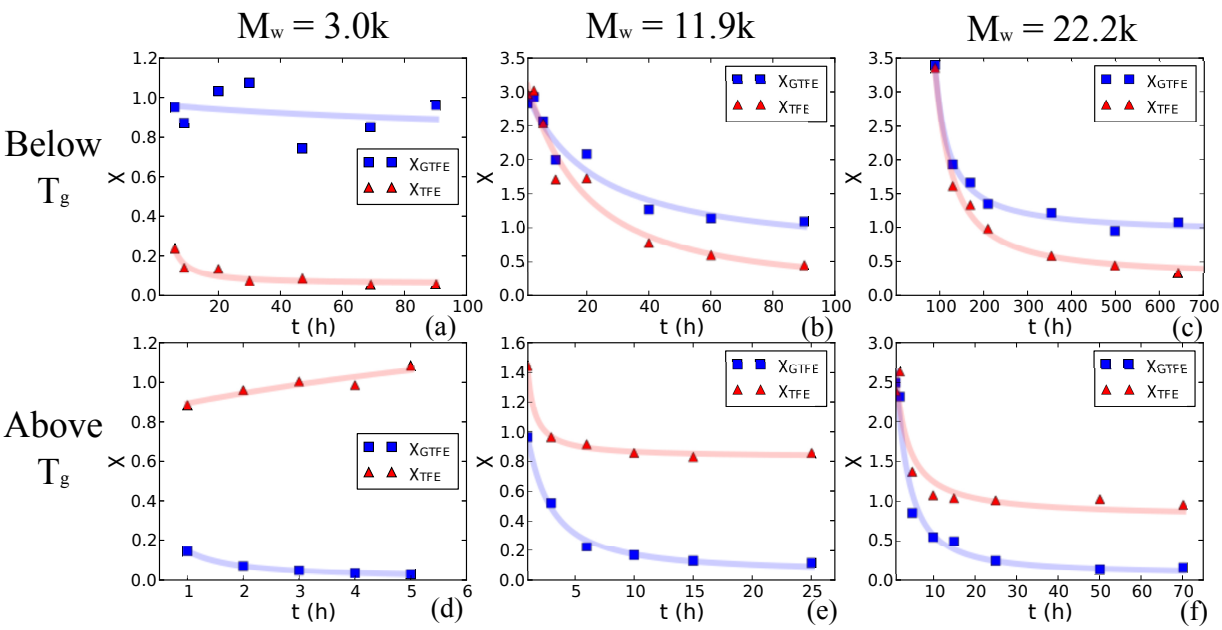

Figure 3.13: Temporal evolution of the correlation functions near T_g for three different polymers.

Fig. 3.13 shows both χ_{GTFE} and χ_{TFE} of stepped films near T_g with three different molecular weights. Clearly, for $M_w = 3$ kg/mol, above T_g, χ_{GTFE} are close to 0 and χ_{TFE} are close to 1; however, below T_g, χ_{TFE} are close to 0 and χ_{GTFE} are close to 1. This indicates that in the experimental time window the surface flow can be found below T_g, and the entire film flow can be observed above T_g.

For higher molecular weights, both χ_{GTFE} and χ_{TFE} do not saturate in the early stage; instead, χ_{GTFE} slowly approaches to 1, χ_{TFE} slowly approaches to 0 at $T < T_g$, and χ_{GTFE} slowly approaches to 0, χ_{TFE} slowly approaches to 1 at $T > T_g$. This implies that in the early stage, the experimental profile can be described by neither the GTFE nor the TFE.

Although both correlation functions do not saturate in the early stage, it is still possible to conclude that below T_g, the experimental profiles tend to be the GTFE type, while above T_g, they tend to be the TFE type. This result can directly confirm the second interpretation proposed in the previous section because the surface flow dominates in the stepped films where $2R_g > h_m$ below T_g.

Polymer conformations near the free surface below T_g

According to the experimental observations above, there must be some polymers that are completely free in the liquid-like layer below T_g as the grafted polymers cannot flow. It should be noted that these free polymers are not the result of the segregation effect (of course it might be) but pure randomness. It is widely accepted that polymers in their melts satisfy random walk statistics. Thus, conducting a random work simulation, one should be

able to determine the fraction of polymers with all their segments located in the liquid-like layer. For the simulation, we use the Kuhn length as the basic unit, in other words, one random step stands for one Kuhn length. For polystyrene, the Kuhn length b = 1.8 nm and the Kuhn monomer (M_0) is about 0.72 kg/mol [3]. Accordingly, it is reasonable to set h_m = 3b ($\sim$ 5.4 nm) based on gold nanoparticle embedding experiments [114, 115, 161]. In addition, we use the reflecting boundary condition for the polymer-air surface. Technically the simulation itself has no physical meaning and is very straightforward. For the simulation, there are two basic values, n_f and n_s, where n_f stands for the number of polymers that all their segments are located in the mobile layer and n_s represents the total fractions of polymers within the mobile layer. The inset in Fig. 3.15 portrays three different situations in the simulation. In case (a), all segments of the polymer are in the mobile layer. As a result, $n_f + 1$ while n_s remains unchanged. In case (b), only a fraction (60 %) of the polymer is in the mobile layer. Consequently, $n_s + 0.6$ while n_f remains the same. In case (c), the entire polymer is in the glassy region. Accordingly, both n_s and n_f do not change. Although the random walks are generated in the three-dimensional space, x, y locations do not contribute to our statistics. Hence, for each molecular weight, the initial location in x and y directions can be set as 0, but z_i varies. It can be expressed as $[x, y, z]_{t=0} = [0, 0, z_i]$. For each initial point (z_i), 10,000 random walks are generated to get enough data for accurate statistics, where z_i varies from 0 to the fully extended chain length N. Fig. 3.14 shows 10 walks generated by the simulator. During the simulation, the end-to-end distance is also monitored to check the validity of the simulator.

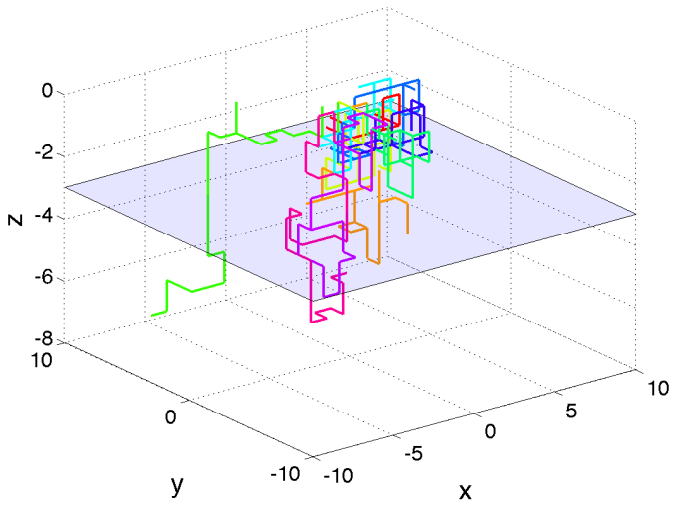

Figure 3.14: 10 random walks generated by the simulation program, where different colours stand for different polymer chains.

Fig. 3.15 shows the probability $\phi = \frac{n_f}{n_f+n_s}$ of having a polymer chain with all its segments in the mobile layer (*free polymer*) as a function of molecular weight. It is surprising that, even for high molecular weight polymers where $2R_g >> h_m$, a lot of polymers can still fit in the mobile layer. Taking the $M_w = 22.2$ kg/mol ($2R_g \sim 1.5h_m$) as an example, it gives $\phi = 46$ %, which means half of the polymers can still flow. This is probably why we still observe a surface type of flow below T_g under confinement.

Levelling in the early stage

In the previous sections, we compared the experimental levelling profiles to the simulation profiles and determined that even under confinement, the surface type of flow can still be

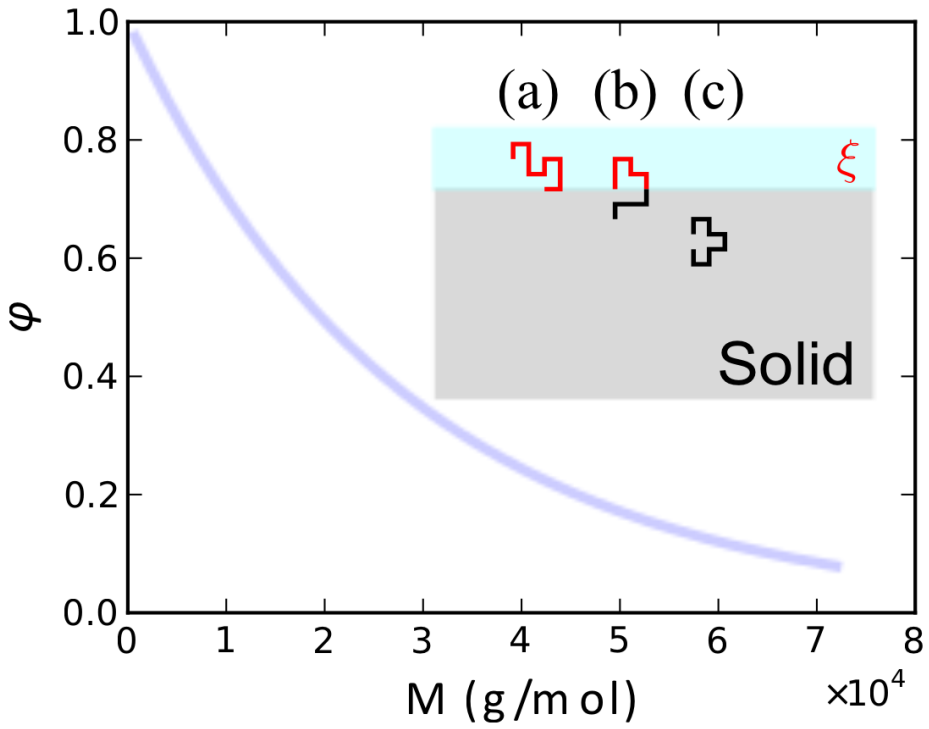

Figure 3.15: Fraction of *free polymers* as a function of molecular weight. The inset shows three different cases in the simulation.

observed. However, due to the relatively high viscosity, the stepped films take a long time to reach the self-similar regime, which results in a non 1/4 power law. In order to check whether this non 1/4 power law between the width of the step and time ($w \sim t^{1/4}$) is caused by the invalidity of the small slope approximation in the early stage, we compare our experimental profiles to the full GTFE profile (details see the simulation section).

The bottom plot in Fig. 3.16 demonstrates the non 1/4 power law in the early stage of the levelling process below T_g, where the big symbols are the experimental data. Clearly, the experimental data roughly follows the simulation data, indicating that the non 1/4 power law is indeed caused by the invalidity of the small slope approximation. The simulation results also suggest that the 1/4 power law can be recovered when $b > h$, which means a stepped film with $h_2 = 90$ nm requires a width wider than 90 nm. In addition, it indicates that thinner stepped films should reach the self-similar regime earlier than thick films do. Fig. 3.17 and Fig. 3.18 show the levelling process of a ~ 41 nm on ~ 41 nm stepped film annealed below T_g, where in the early stage 1 to 3 hours, there is a small deviation from the 1/4 fit, but over a longer time, the 1/4 power law and the self-similar behaviour can be observed. The results also indicate that the correlation functions can provide a good estimation on whether the profile is the GTFE type or the TFE type even when the self-similar regime is not reached.

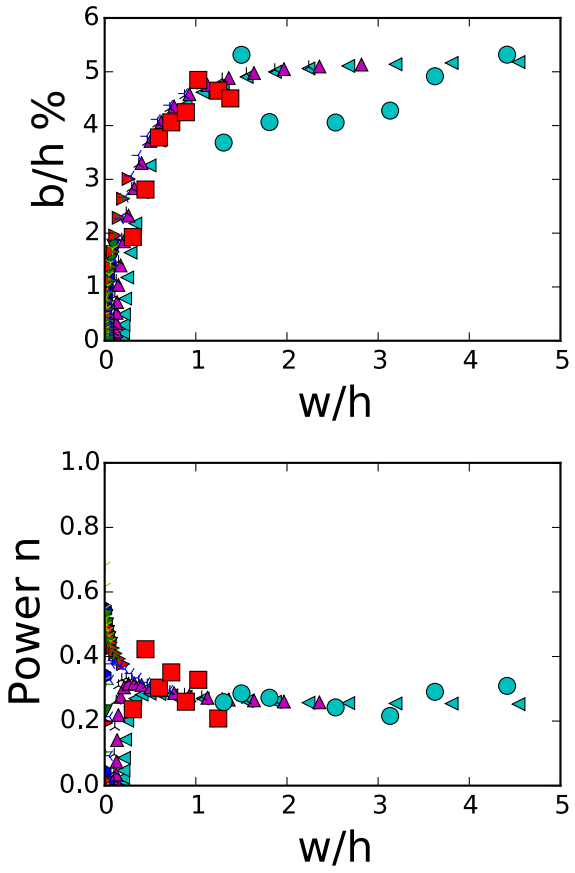

Figure 3.16: $b/h\%$ and n as a function of $w/h\%$, where w is the width of the steps, h is the height of the steps, b is the height of the bumps and n is the power law between the width w and annealing time t. The red squares are based on the 87 nm on 87 nm M_w = 11.9 kg/mol stepped film and the blue circles are based on the $\sim$ 41 nm on $\sim$ 41 nm M_w = 11.9 kg/mol stepped film. The remaining data is based on the full GTFE simulation, where different colours stand for the different initial aspect ratios ($w(t = 0)/h$).

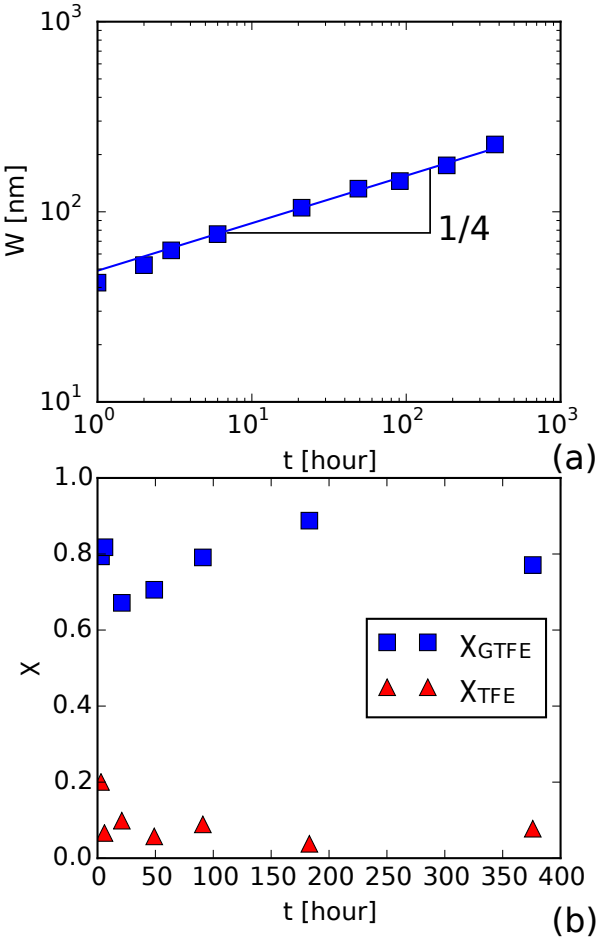

Figure 3.17: Time dependent width (a) and correlation functions (b) of a 41 nm on 41 nm stepped film annealed below T_g

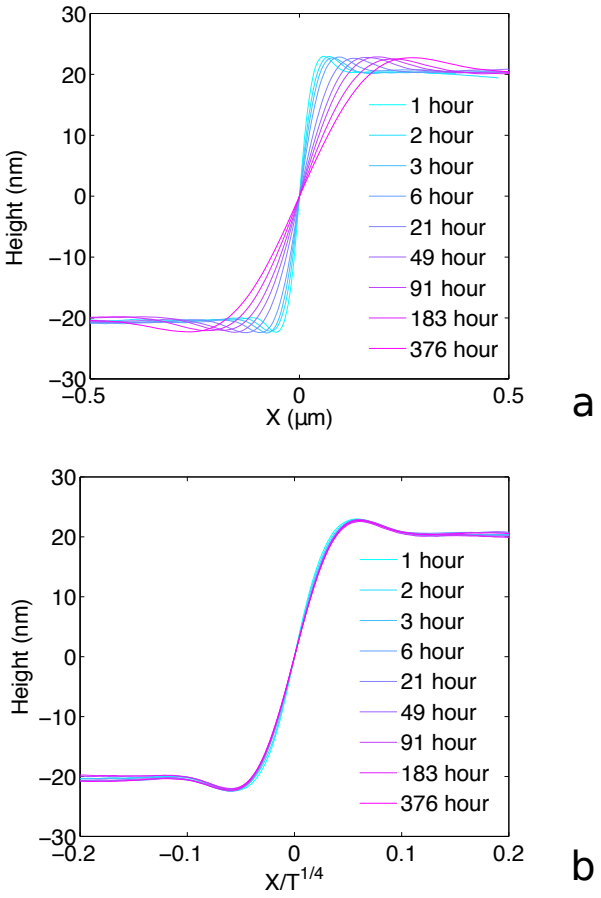

Figure 3.18: Temporal evolution of the experimental profiles (a) and the collapsed self-similar profiles (b) for a 41 nm on 41 nm film annealed below T_g.

Summary

We study the levelling process of high molecular weight polystyrene stepped films near their bulk glass transition temperatures. Above T_g, the entire film flow is observed and below T_g the surface flow is observed even under confinement where $2R_g > h_m$. In order to account for this phenomenon, a random walk simulation is conducted. The simulation shows that even for high molecular weight polymers where $2R_g > h_m$, a significant fraction of polymers can still fit in the liquid-like layer and flow. Lastly, it is found in the early stage, the levelling process does not agree with the 1/4 power law. We explain that this non 1/4 power is caused by the invalidity of the small slope approximation in the GTFE. A comparison between the experimental profiles and the simulation profiles based on the full GTFE is conducted and the results confirm the original hypothesis.

3.2.3 Levelling under soft confinement

It is widely accepted that there is a thin layer in glassy polymers with enhanced dynamics. The phenomenon has been studied by various techniques including the levelling experiment discussed previously. In addition, the ellipsometry study on capped films showing no T_g reduction [82] indicates that the free surface effect induced T_g reduction can be removed by removing the free surface. Thus, it is interesting to examine at what condition this free surface effect can be removed. In other words, if we immerse glassy polymers in liquids, can the free surface effect be removed? In order to answer this question, we conduct a soft

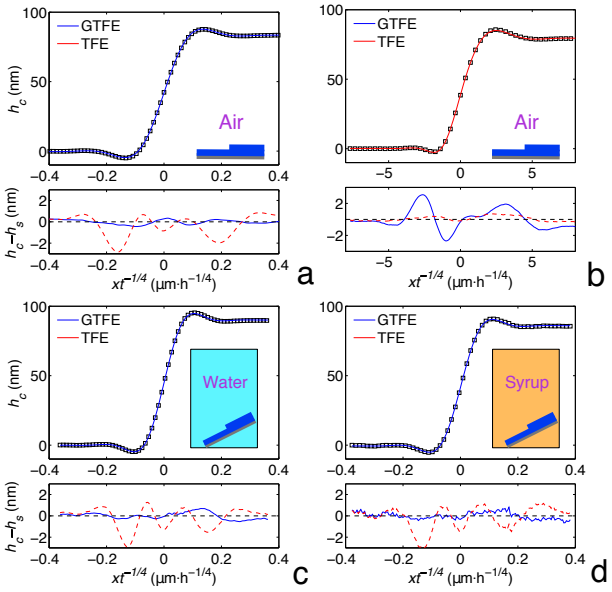

Figure 3.19: Experimental profiles and their fits to both the GTFE and TFE profiles in different conditions, (a) air below T_g, (b) air above T_g, (c) water below T_g, (d) syrup below T_g.

confinement levelling experiment. In this experiment, we immerse the stepped films in two different liquids, water and corn syrup, to study the levelling process of these stepped films in their glassy state.

Fig. 3.19 shows the experimental profiles and their fits to both the GTFE and TFE profiles in different conditions. Clearly, whether confined in water or in syrup, the surface type of flow is always observed. The observation implies that the liquids on the top of the stepped films cannot remove the free surface and a mobile layer still exists in glassy polymer films. This result is in excellent agreement with the T_g reduction experiment of

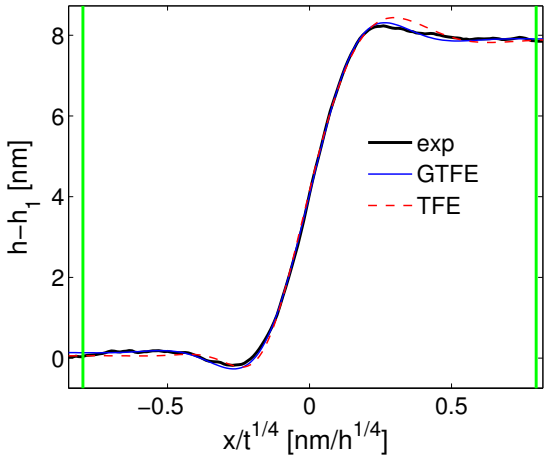

Figure 3.20: Experimental profile (black solid line) of an ultra-thin stepped film ($h_1 = h_2 = 8nm$) annealed at 338 K (T_g - 5 K) on a hotplate for 3 hours, the GTFE simulation profile (blue solid line), and the TFE simulation profile (red dashed line).

polymer nanoparticles in aqueous solutions [163].

3.2.4 Ultra-thin stepped film levelling

As discussed above, there is a transition from the surface flow to the entire film flow at the bulk glass transition temperature of relatively thick stepped films. If the T_g reduction in thin films is caused by a thin liquid-like layer in polymer thin films, the transition from the surface flow to the bulk flow should remain the bulk value as the liquid-like layer does not depend on the film thickness. In order to test this hypothesis, we conduct a levelling experiment with ultra-thin stepped films.

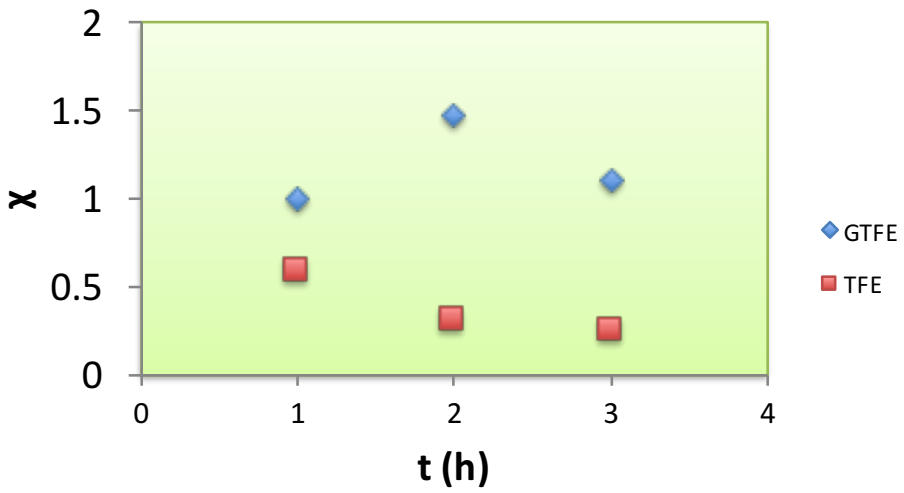

Figure 3.21: Time dependent correlation functions of an ultra-thin stepped film ($h_1 = h_2 = 8nm$) annealed at 338 K, where the blue symbols represent χ_{GTFE} and red symbols stand for χ_{TFE}.

Fig. 3.20 shows the experimental profile of an ultra-thin stepped film annealed below T_g, where the GTFE and TFE simulation profiles are presented as well. Although the experimental profile is a little bit rough, it is still possible to find that in the bump area, the experimental profile better matches the GTFE profile than the TFE profile. This implies that at $T = T_g - 5K$, the surface flow is still observable even in ultra-thin films.

As long as the stepped film reaches the self-similar regime, the correlation function should remain unchanged. Fig. 3.21 shows the time dependent correlation functions of the same stepped film mentioned above. Clearly, χ_{GTFE} remains ~ 1 and χ_{TFE} remains 0. This is a good indication that the result we got is not an artifact. This is very important in

ultra-thin films as the correlation function dependents on how accurate the measurement is. Based on the preliminary results, we can say that there is no significant reduction of the transition temperature (less than 5 K) for an 8 nm on 8 nm stepped film.

3.3 Summary

To summarize, we use the novel stepped film levelling experiment to study the surface dynamics of glassy polymers. Four projects in this chapter focus on different aspects of the surface dynamics of glassy polymers.

In the first project, we focus on the low molecular weight polystyrene system, where $2R_g < h_m$. We first demonstrate that the stepped films can flow even below T_g and use the newly developed GTFE model to describe the observations. By fitting the experimental profiles to both the GTFE and TFE simulation profiles, it is found that below T_g, the GTFE can give a better fit; while above T_g, the TFE is better. In order to quantify the transition from the surface flow to the bulk entire film flow, we define the correlation function and find a sharp transition near the bulk T_g. Lastly, the temperature dependent mobility is extracted by fitting the experimental profiles to either the GTFE or TFE.

In the second project, we study the levelling process of glassy stepped films with higher molecular weights, where $2R_g > h_m$. We find that even when the size of polymers is bigger than that of the liquid-like layer, the surface flow is still observed below T_g. Then, we conduct a random walk simulation to demonstrate even under confinement, a significant

fraction of polymers can still fit in the liquid-like layer and flow. In addition, a non 1/4 power law in the levelling process is found due to the invalidity of the small slope approximation. Thus, a simulation with the full GTFE is conducted and the result shows a good agreement with the experimental data.

In the third project, the stepped films are immersed in different liquids. The levelling process of the stepped films in different liquids also shows the surface flow behaviour below T_g, which is in good agreement with the ellipsometry study on T_g reduction of polystyrene nanoparticles in aqueous solutions.

In the last project, ultra-thin stepped films are used to test whether there is a reduction of the correlation transition temperature as the film thickness decreases. It is found that even at $T_g(bulk) - 5°\mathrm{C}$, the surface flow is still observed. It indicates that there is no significant reduction of the transition temperature for a 8 nm on 8 nm stepped film.

Chapter 4

Crystallization of atactic polystyrene

4.1 Introduction

Solid polymers can be either amorphous or crystalline. Polystyrene is one of the most commonly used polymers all over the world. There are three different isomers of polystyrene, atactic polystyrene (aPS), isotactic polystyrene (iPS), and syndiotactic polystyrene (sPS). iPS and sPS are semicrystalline, and aPS is often described as amorphous because the big randomly oriented phenyl groups hinder the crystallization of aPS. As a result, aPS is often used as an example model to study the properties of amorphous solids. However, is this correct? Or is there any chance to form crystals of aPS? Before answering this question, let's take a look at a relevant study, the gelation of aPS. Gels are solid jelly-like materials. The 3D network in gels can trap solvent molecules. Polymers can physically

form gels without chemical bonds. In physical gels, polymer chains are considered physically connected to each other, in other words, these connections are reversible. The most probable way to achieve physical gels is through the interchain crystallization [164]. As a result, it is reasonable to see gels formed from crystallizable polymers dissolved in poor solvents. Taking polystyrene as an example, Xue *et al.* studied the gelation of isotactic polystyrene in different solvents with different molecular weights [165]; while Daniel *et al.* studied the thermoreversible gelation of syndiotactic polystyrene in toluene and chloroform [166]. It is not hard to understand these observations as both isotactic and syndiotactic polystyrene can crystallize. However, Tan *et al.* [167] found even atactic polystyrene can form physical gels, which is very surprising. There are two possible interpretations, either aPS can crystallize, or there is another mechanism of forming gels. In addition, theoretical physicists also predicated the crystallization of aPS. Semenov [168] gave a detailed study on the cluster formation in homopolymers melts, where the crystallization of aPS can happen due to local stereoregularity. As a result, we need to rethink about the conclusion that aPS cannot crystallize as it may not be correct. In this project, we use low molecular weight aPS as a test model to examine whether these polymers can form crystals.

4.2 Experimental details

In this project, low molecular weight atactic polystyrene was used. The molecular weights were 600 g/mol and 890 g/mol, where aPS with M_w = 600 g/mol was purchased from

two companies, Polymer Source and Polysciences, while aPS with M_w = 890 g/mol was purchased from Polymer Source. T_g of these two polymers are -10 °C and 0 °C respectively. All samples were made by spin coating aPS solutions in toluene onto Si substrates and all measurements were conducted with a JPK AFM on a hot plate. Due to the low T_g of aPS, we actually scanned the liquid surfaces at room temperature. Hence, low driving amplitude and high set point were used during the scans. Another important feature of low molecular weight aPS is the evaporation, which may cause problems during the AFM scans at high temperatures. In order to conduct AFM experiments at high temperatures, a rubbery layer was used to cover the PS layer, which can prevent the possible evaporation.

4.3 Discussion

Fig. 4.1 (a) shows three different isomeric structures of polystyrene. From the structure, one can tell that two adjacent monomers can have different phenyl group orientations. In chemistry, two adjacent monomers constitute a diad. If two monomers orient in the same direction, the diad is called a meso diad (m). In contrast, if two monomers orient in opposite directions, the diad is called a racemo diad (r). Clearly, for pure iPS, it should have a $mm...mm$ structure. In contrast, for pure sPS, it should have a $rr...rr$ structure. NMR is very sensitive to the tacticity of samples, different stereoregular segments exhibit different NMR peaks. Fig. 4.1 (b) shows the C13 NMR spectra of the aliphatic carbons of aPS, iPS, and sPS. Clearly, in the methylene regime (42 to 47 ppm), iPS and sPS only

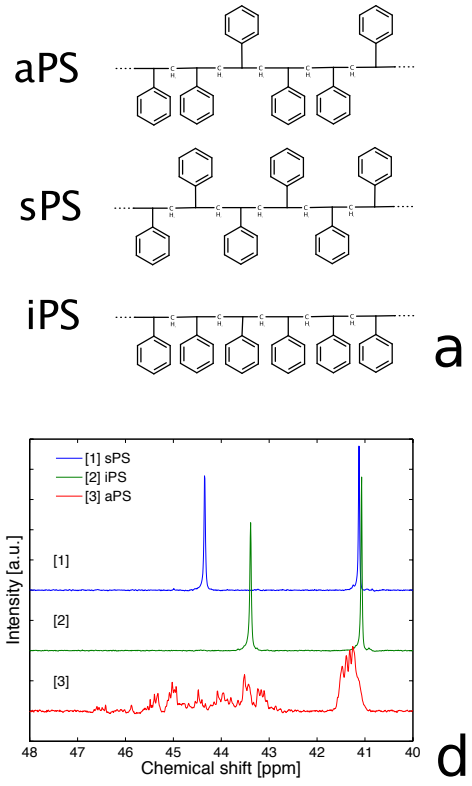

Figure 4.1: (a) Isomeric structures of polystyrene, (b) NMR spectra of iPS, sPS, and aPS.

have one single peak but aPS has many small peaks. It indicates that iPS and sPS are composed of one type of diads, but aPS is composed of random sequences of meso and racemo diads. Each small peak in the spectrum is a sequence of meso and racemo diads. As a result, one can tell that the low molecular weight aPS we used has random orientations of phenyl groups compared to iPS and sPS.

First, we demonstrate low molecular weight aPS can form crystals. Fig. 4.2 shows two sets of AFM images of M_w 600 g/mol aPS samples, where b and e are height images;

while c and f are phase images. Clearly, two pieces of crystals are observed, which is the first direct evidence of the crystallization of aPS. Now the question becomes why aPS can crystallize. If we take a look at the composition of aPS, we can find that in aPS, polymer chains have their phenyl groups randomly oriented on either side of the backbone. However, it is also true that we can get some polymer chains with all their phenyl groups on one side or alternate on both sides. This means in aPS, due to random statistics, there are some stereoregular chains. This can be demonstrated through a simple calculation. If a polymer chain is composed of N monomers, and the probability of a phenyl group oriented on one side is 1/2, then the probability of having stereoregular chains in a system with many polymer chains can be expressed as

$$P = P_i + P_S = 2 \times (\frac{1}{2})^{N-1} = (\frac{1}{2})^{N-2} \tag{4.1}$$

where P_i is the probability of having iso-stereoregular chains, and P_s is the probability of having syndio-stereoregular chains. If we take $N = 6$, it gives $P = (\frac{1}{2})^4 = \frac{1}{16}$. Clearly, the probability is not small. As a result, the crystals we observed are composed of these stereoregular chains. In order to understand the crystallization behaviour of aPS, we conduct an in-situ experiment with the AFM.

As mentioned previously, low molecular weight polystyrene has low T_g values, especially for $M_w = 600$ g/mol. This can be seen from the rough sample surfaces in the AFM height images at room temperature. Moreover, it is found that the crystals in height images do not have good contrast. However, a significant contrast can be observed between the amorphous and crystalline domains in phase images. As a result, in this project, we use

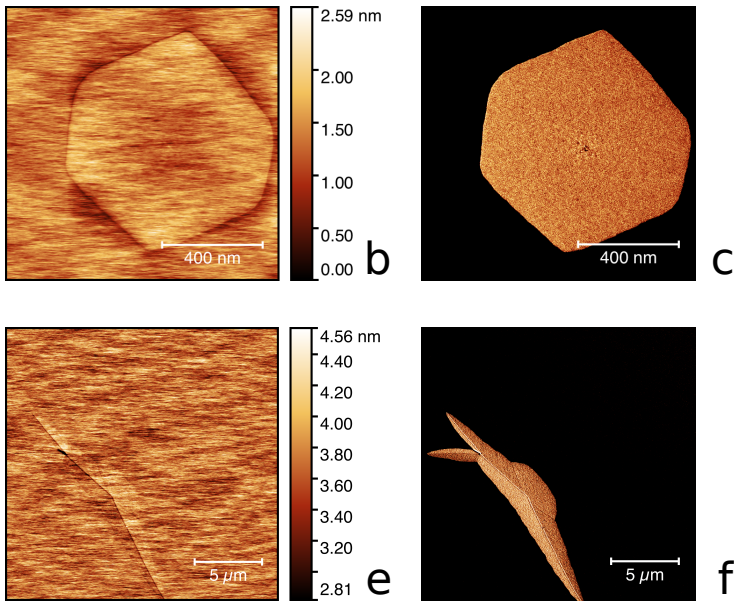

Figure 4.2: AFM images of aPS single crystals, where (b) and (e) are height images, (c) and (f) are phase images.

phase images rather than height images. First, we study the growth kinetics of aPS. After many tests, it is found that aPS with molecular weight 600 g/mol can grow at room temperature. Thus, we measure the growth of aPS crystals in-situ with AFM at 20 °C. Well prepared M_w = 600 g/mol sample is first annealed on a hot plate at 90 °C for 1 hour to remove the thermal history and then quickly quenched down to 20 °C. Fig. 4.3 shows the crystal growth at 20 °C, where the x-axis is the time elapsed from the first data point, and y-axis is $A^{1/2} - A_0^{1/2}$ (A is the area of the crystal), which represents the size change of crystals in one dimension. Clearly, the linear size of crystals increases as the time increases, which can be observed in the phase images. A very striking feature of this

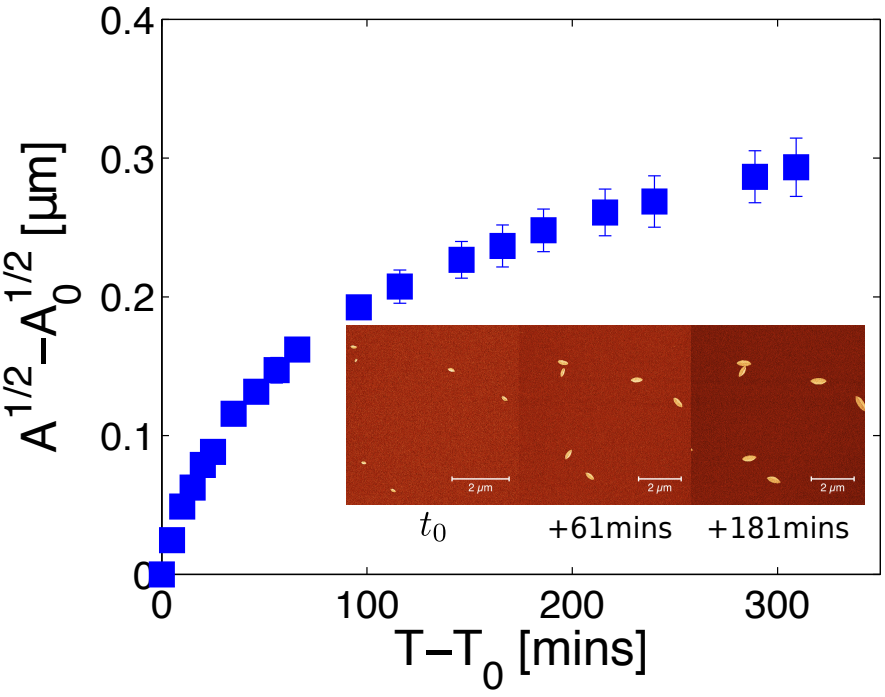

Figure 4.3: Growth of aPS crystals at 20 °C, where the inset shows three AFM phase images of the crystals at different periods of crystallization time.

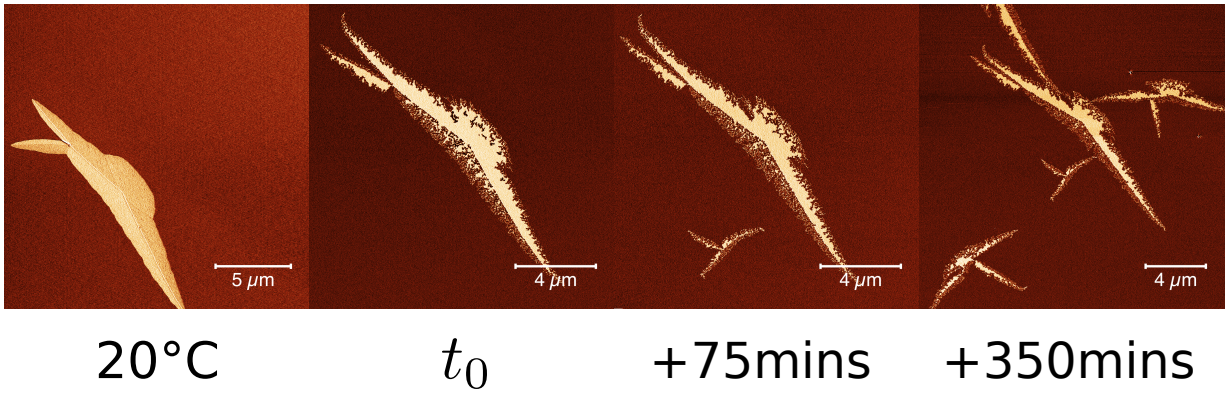

Figure 4.4: Real-time images of the melting of aPS crystals at 40 °C.

growth curve is the non-linear time dependence. In general, the linear time dependence of the crystal size is observed in melt crystallization. The non-linear time dependence implies that there is a different mechanism from the normal melt crystallization. Why does it exhibit a different mechanism? As mentioned previously, the polymer chains in aPS have their phenyl groups oriented randomly and only a subset of polymer chains have regularly oriented phenyl groups. This means that some stereoregular chains are dissolved in aPS melts and the crystallization occurs in a "solution" of aPS. It has been widely studied that the crystallization from dilute solutions or under a vapour condition highly depends on the local concentration and diffusion process (Fick's law) [60]. In these conditions, a non-linear growth curve is typically observed. As a result, the non-linear growth kinetics in our experiment might be caused by the lack of crystallizable materials and the dominance of a diffusion controlled process.

On top of the growth study, we also study the melting behaviours of these aPS crystals.

In the first melting experiment, the sample is first heated on a hot plate at 70 °C for 24 hours and held at room temperature. Before the melting experiment, the sample is measured with the AFM at 20 °C (the left figure in 4.4). Following that, the sample is placed on a hot plate at 40 °C and measured with the AFM in real-time. Fig. 4.4 shows a series of phase images of aPS crystals melting at 40 °C. From the images, we can see that there are some parts of the crystal that melt quickly in the early stage, while the remaining parts melt slowly in the late stage. This indicates that either the crystals have different degrees of defects or there are different melting points. In addition, from the images, the aggregation of aPS crystals can be also observed. This indicates that crystals tend to stay together in some situations. The reason why they exhibit this aggregation behaviour is still unclear. Some possible interpretations are: the Marangoni effect induced flow due to the evaporation, the attraction between crystals that have not melted.

From Fig. 4.4, we can see that even after 350 minutes of annealing at 40 °C, there are still some parts of the crystals that have not melted. Thus, it is reasonable to increase the temperature and determine at what temperature these crystals can completely melt. In order to conduct this experiment, we need to scan at temperatures significantly higher than T_g. However, low molecular weight aPS is very liquid and can even evaporate, it makes the in-situ AFM experiment at high temperatures difficult. To overcome this problem, we float a 10 nm Poly(butyl methacrylate) (PBMA) layer (T_g 20 °C) onto the aPS sample because it has been shown that AFM is able to probe the interfaces buried in polymers [169] in tapping mode. By doing this, the rubbery thin layer can prevent possible evaporation

effect and also enhance the mechanical strength of the sample. As a result, we are able to scan these samples at high temperatures. Fig. 4.5 shows the time dependent melting experiment of aPS sample coated with a 10 nm PBMA layer. The sample is first heated at 70 °C for 1 hour and quenched down to room temperature for growth. After growth, the sample is covered with 10 nm PBMA thin layer to cover the liquid surface. Clearly, one can find that at 20 °C, the PBMA layer is in the glassy state, which leads to a weak contrast between the amorphous and crystalline domains. As temperature increases, the PBMA layer becomes rubbery-like, and it results in a more significant contrast between the amorphous and crystalline domains. At 30 °C, the onset of melting is observed, although the melting speed is relatively slow. Similar to Fig. 4.4, from 35 to 50 °C, some parts of the crystals melt fast, while the remaining parts melt slowly. At high temperatures (60, 70 °C), all crystals have completely melted. The different melting behaviours in the melting experiment imply that these aPS crystals have different thermal stabilities. Some possible explanations are: different degrees of defects, different local tacticities (melting point depends on tacticity), and different stereoregular structures (iso or syndio). Of course, whether both the iso-stereoregular and syndio-stereoregular chains with a small degree of polymerization are able to crystallize is still unclear as the 3/1 helical structure, a crystalline structure of iPS, is not easy to form (too short chains).

Semenov [168] proposed a simple model to describe the cluster formation in homopolymer melts. In this model, the stereoregular segments in polymer chains can form clusters, which can be considered as lamellar crystals. The following derivation comes from Se-

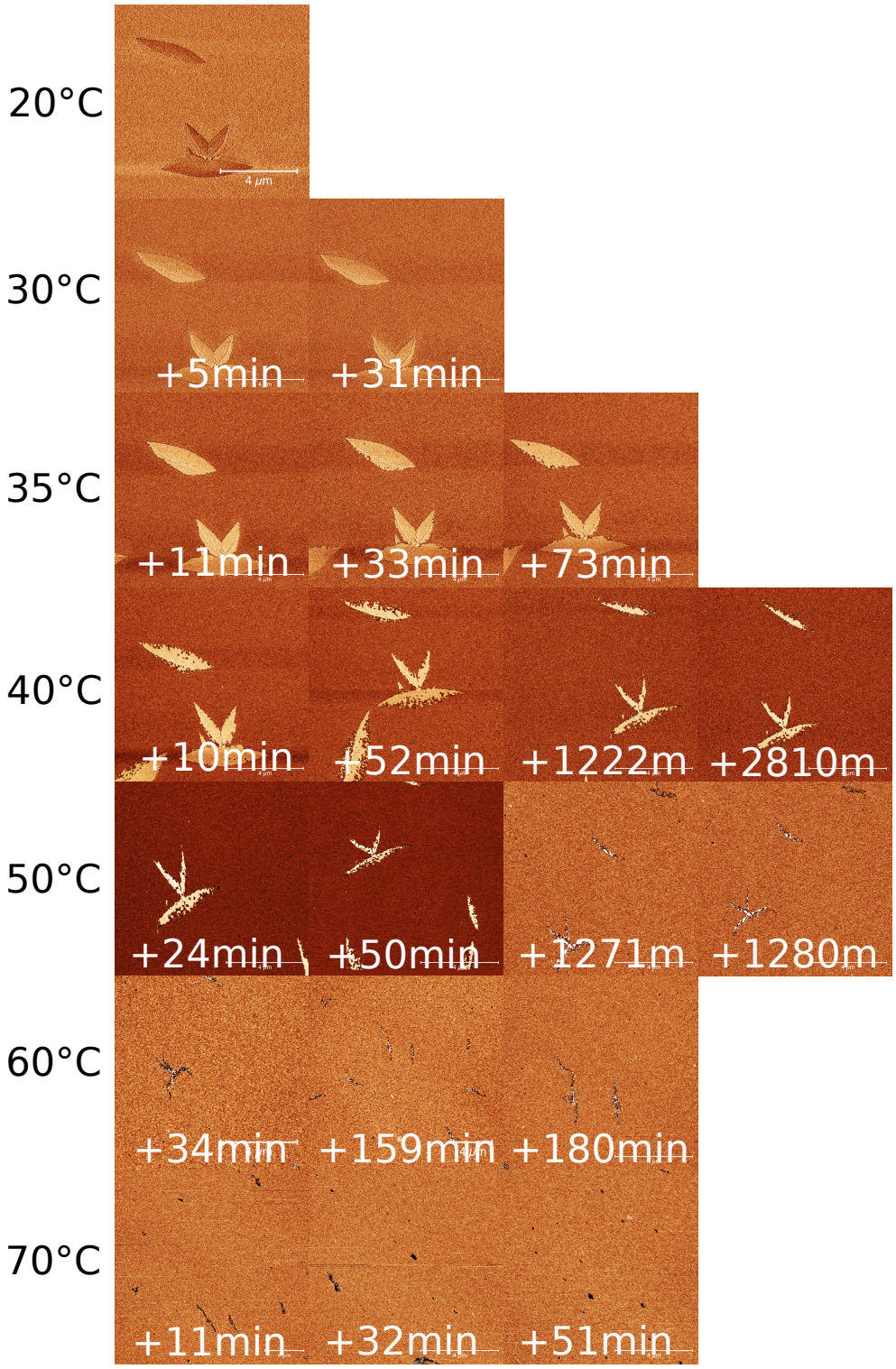

Figure 4.5: Temperature dependent melting of aPS with a thin PBMA layer.

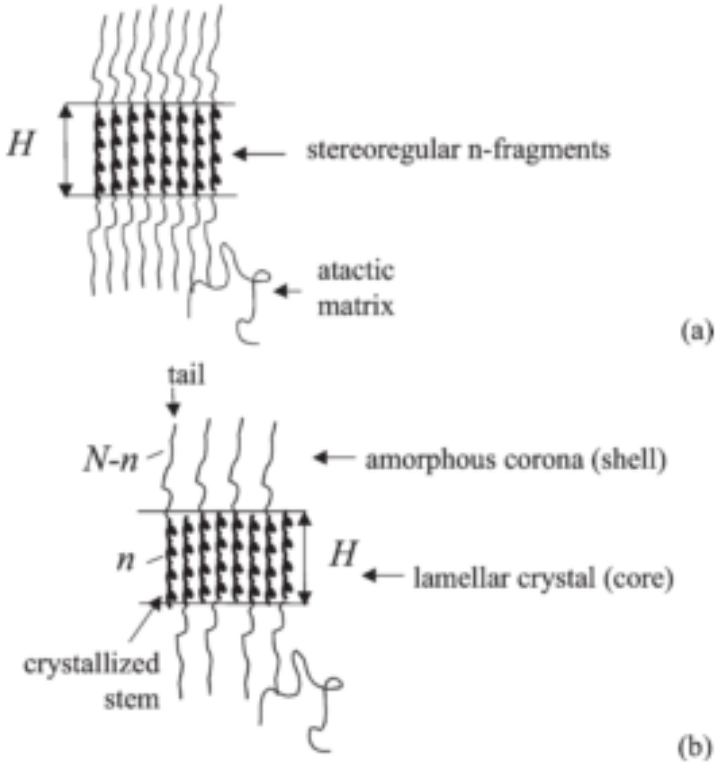

Figure 4.6: Schematic diagram of core/shell lamellar micelles. Figure from [168].

menov's paper. The free energy change per chain upon the cluster formation is composed of four terms.

$$F_{lam} \approx \Delta F_{crystal} + F_{entr} + F_{face} + F_{conf} \tag{4.2}$$

$\Delta F_{crystal}$ is the free energy gain on crystallization, which can be expressed as

$$\frac{\Delta F_{crystal}}{kT} \approx -S_m n\tau \tag{4.3}$$

where $\tau = \frac{T_m}{T} - 1$, S_m is the entropy of melting per monomer, T_m is the ideal crystallization temperature, and T is the current temperature.

F_{entr} is the free energy caused by the entropy loss, which can be expressed as

$$\frac{F_{entr}}{kT} \approx -\ln(\frac{2}{N}\phi) = \ln(N/4) + (n-1)\beta \tag{4.4}$$

where N is the number of monomers per chain, n is the number of monomers per chain in the crystalline domain, $\beta = \ln(1 + e^{-|\Delta\epsilon|})$, and $\Delta\epsilon$ is a measure of tacticity ($f_m/f_r = e^{\Delta\epsilon}$).

Of course, the degree of tacticity can be expressed in a more intuitive way

$$d_t = |f_m - f_r| = \tanh(|\Delta\epsilon|/2) \tag{4.5}$$

where f_m and f_r are the fractions of meso diads and racemo diads respectively.

F_{face} is the interfacial energy between the amorphous and crystalline domains, which can be expressed as

$$\frac{F_{face}}{kT} = 2J = 2J_0(1+\tau) \tag{4.6}$$

where $J = A_1\gamma/(kT)$, γ is the interfacial tension and can be considered as no temperature dependence (the simplest case), A_1 is the area per chain at the amorphous-crystalline interface and $J_0 = J|_{T=T_m}$.

F_{conf} is the conformational free energy due to the elongation of the amorphous domain, which can be expressed as

$$\frac{F_{conf}}{kT} = \frac{3}{2}\frac{\tilde{H}^2}{\tilde{N}b^2} = \frac{3}{2}\frac{\tilde{L_1}^2}{b^2}\tilde{N} \tag{4.7}$$

where $\tilde{N} = N - n$ is the number of segments in an amorphous tail, $\tilde{H} = \tilde{L_1}\tilde{N}$ corresponds to the thickness of a tail, b is the length of one polymer segment and the mean projection of a tail, $\tilde{L_1}$, can be expressed as:

$$\tilde{L_1} = \frac{\rho_c}{2\rho_m}L_1 \tag{4.8}$$

where ρ_c is the crystalline density and ρ_m is the amorphous density, and L_1 is the stem length per polymer segment. Given $S_m \approx 2.1$ and $J_0 \approx 1.95$ (based on the equilibrium melting temperature of iPS $T_m \approx 266$°C), the theoretical melting point of aPS can be calculated.

In our experiment, we assume the entire polymer chain is in the crystalline domain. In consequence, only $\Delta F_{crystal}$, F_{entr}, and F_{face} in need to be considered in our system.

Fig. 4.7 shows the theoretical melting point of aPS as a function of tacticity with different N, where $d_t = 0$ stands for purely atactic polystyrene, $d_t = 0.5$ stands for either isotactic or syndiotactic polystyrene. Taking $N = 6$ as an example, it is clear that the theoretical melting point of aPS with $N = 6$ is in the range of 18 °C and 61 °C, which is

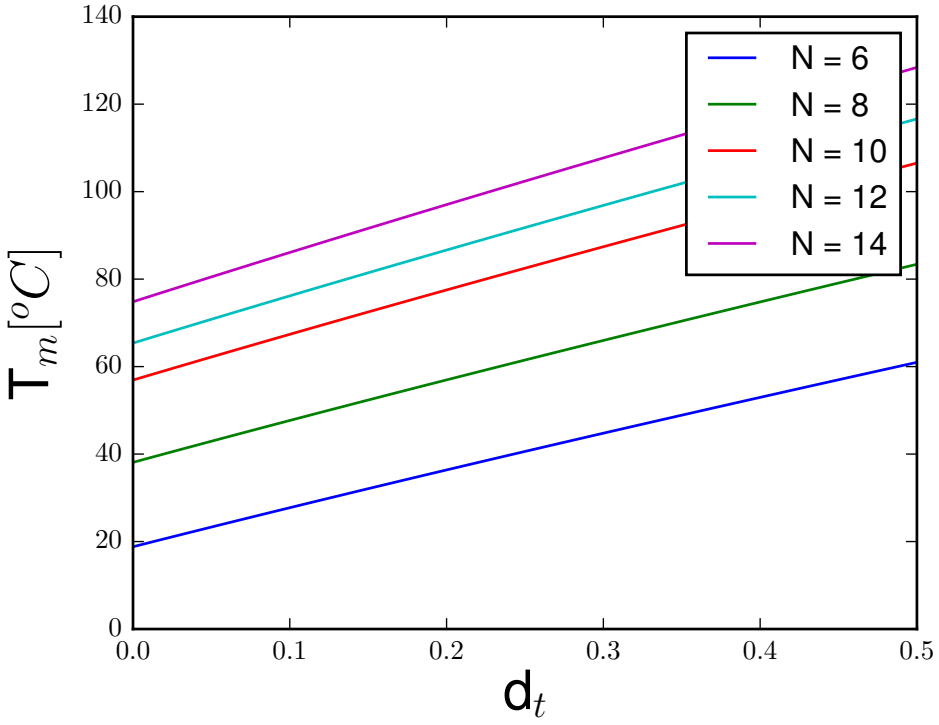

Figure 4.7: Theoretical melting point of aPS as a function of tacticity with different N, based on Semenov's model [168].

in good agreement with our experimental observations.

4.3.1 Interesting observations

During the experiment, there are many interesting observations. The first interesting observation is the wetting property of low molecular weight polystyrene films change upon heating above 110 °C. When samples are annealed below 100 °C, polystyrene films dewet from Si substrates; however, when samples are annealed above 110 °C, polystyrene films stop dewetting. More importantly, it seems that more crystals form upon heating above 110 °C and their shapes are more hexagonal, see Fig. 4.8. We use the same sample in Fig. 4.8 and conduct a temperature dependent measurement. In this experiment, the sample is first annealed at the pre-determined temperature for 10 minutes and cooled down to room temperature for the measurement. All AFM images are obtained at room temperature. Fig. 4.9 shows the temperature dependent measurement. From the figure, we can say that these crystals start to melt at 40 °C because the crystals change their shapes when they are annealed above 40 °C for 10 minutes. In addition, it is also found that these crystals can grow at room temperature as they melt first and regrow during AFM imaging periods. Moreover, no location change of these crystals annealed below 70 °C indicates that these crystals cannot completely melt in 10 minutes below 70 °C. On the other hand, the location change of these crystals annealed above 70 °C demonstrates that the highest melting point of these crystals is 70 °C. At high temperatures, there are two regimes. From 70 °C to 110 °C, the total area of these crystals increases as the annealing temperature increases.

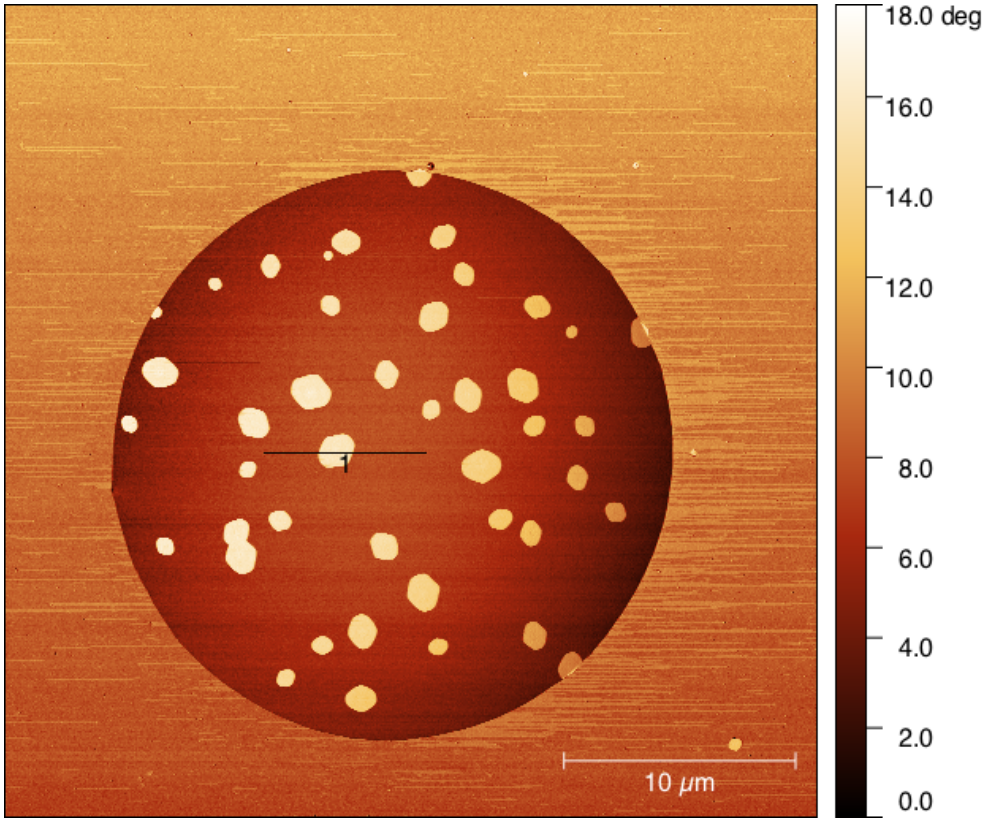

Figure 4.8: A polystyrene (M_W600 g/mol) droplet on a Si substrate. The sample is annealed at 130 °C first and kept at room conditions.

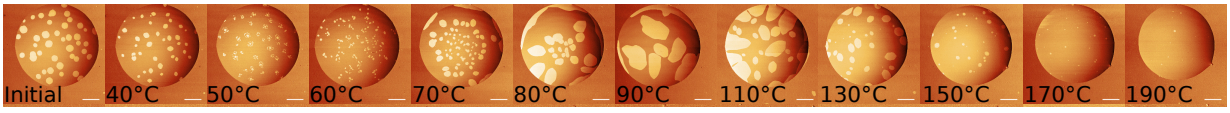

Figure 4.9: Temperature dependent measurement of a polystyrene (M_W 600 g/mol) droplet on a Si substrate. The sample is annealed at 130 °C first and kept at room conditions. During the experiment, the sample is annealed at each temperature for 10 minutes and measured at room temperature. This process is repeated from 40 °C to 190 °C.

This might be the memory effect of these crystals. When the sample is annealed at high temperatures ($>$ 70 °C), crystallizable materials are still around even though they have completely melted. When the sample is cooled down, these crystallizable materials can easily form new crystals. From 130 °C to 190 °C, the total area of these crystals decreases as the annealing temperature increases. This might be caused by the evaporation mentioned in the previous section. High temperatures lead to high evaporation rates, which result in the loss of crystallizable materials. In consequence, the surface coverage of these crystals decreases. Fig. 4.10 shows the AFM phase images of a polystyrene sample (M_W 600 g/mol) with different temperature profiles. The sample is first annealed at 110 °C, cooled to a predetermined temperature, and measured at that temperature. (Before the measurement, the sample is heated and cooled between 110 °C and room temperature for several times.) In A and B, the sample has a temperature profile: 110 °C to 40 °C (scan at 40 °C) to 25 °C (scan at 25 °C); while, in C and D, the sample has a temperature profile 110 °C to 25 °C (scan at 25 °C) to 40 °C (scan at 40 °C). Clearly, in A, there are some crystals that are the cores of the crystals in B. In addition, a significant phase contrast between the cores and the surroundings in B implies that there are two components: one can grow at 40 °C and the other one can grow at 25 °C. However in C, homogeneous crystals are observed when the temperature is directly cooled from 110 to 25 °C. Moreover, in D, some parts of the crystals melt and the remaining parts cannot melt within the experimental time window. This indicates that these two components can also stay together to form homogeneous crystals.

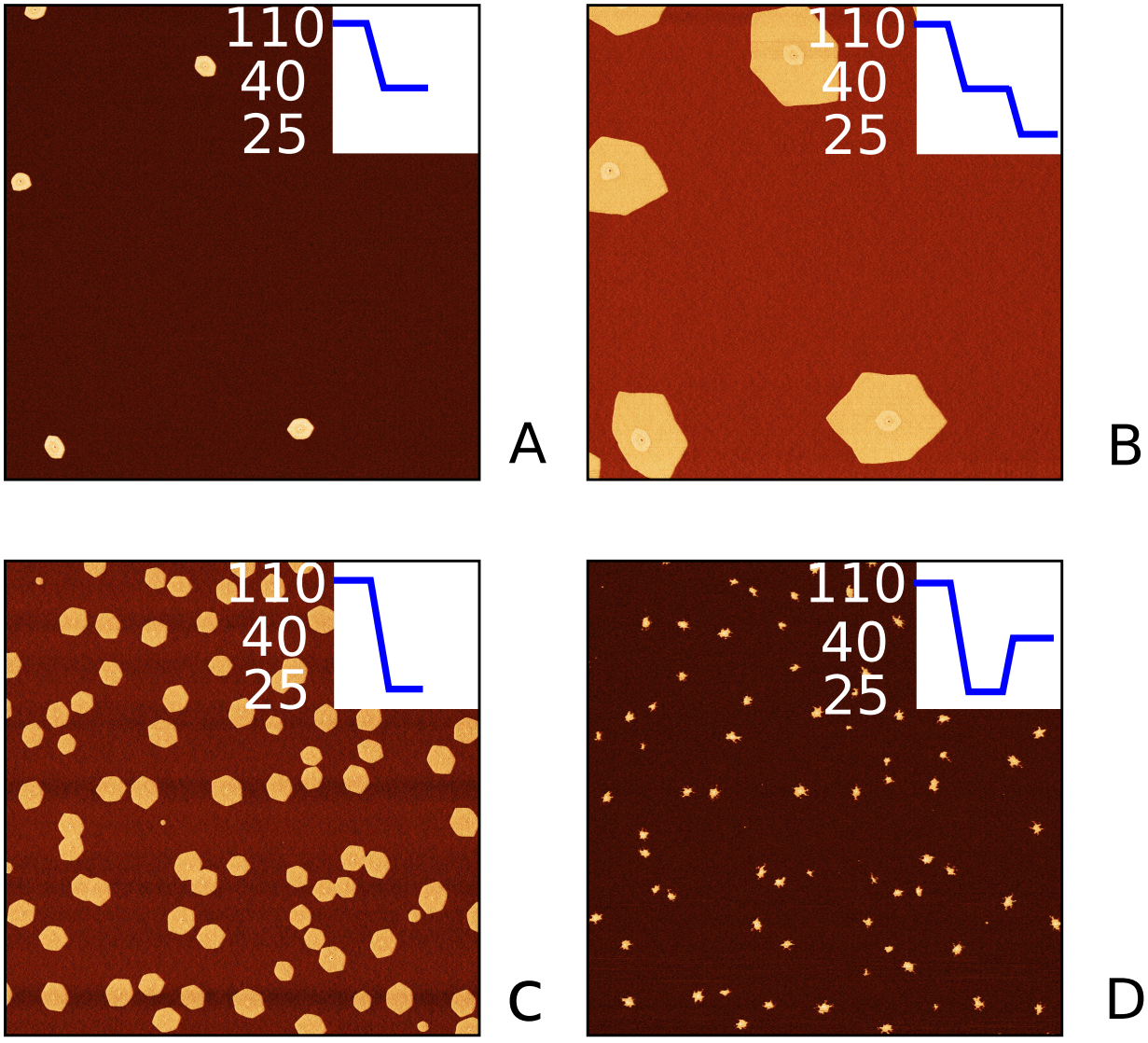

Figure 4.10: AFM phase images of the two components of aPS crystals. Insets show the temperature profiles.

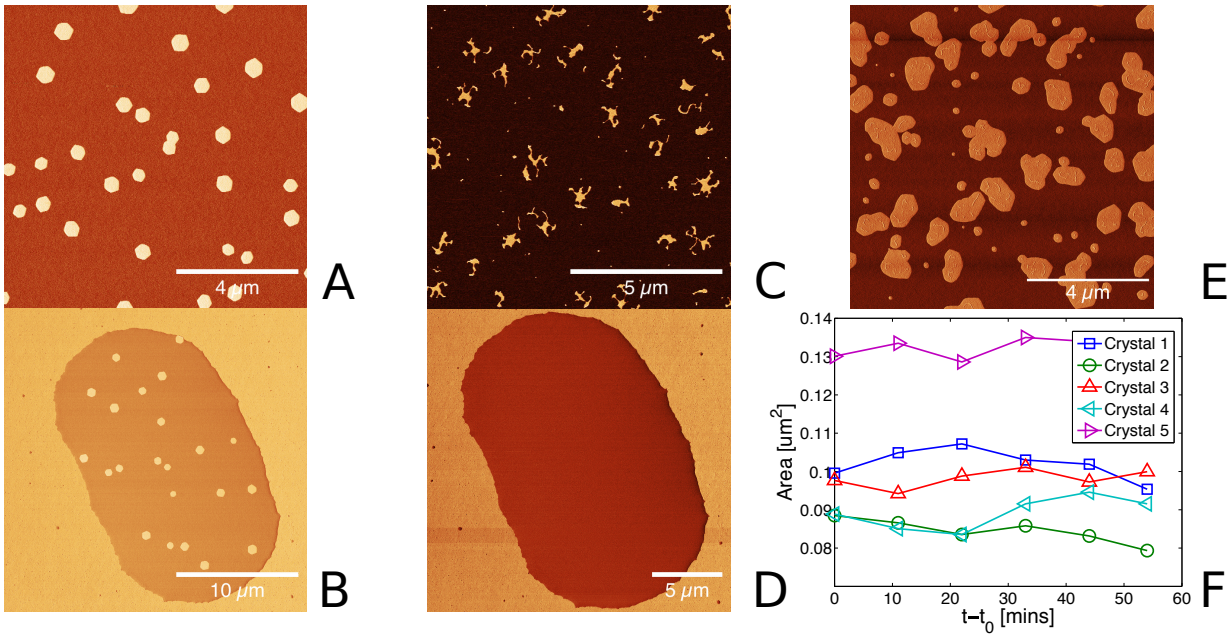

Figure 4.11: AFM phase images of atactic polystyrene crystals on one sample (A-E), where A, B and E are scanned at room temperature; C and D are scanned at 40 °C. F shows the size of the crystals in C as a function of time annealed at 40 °C.

Another experiment also exhibits a similar result. The sample in Fig. 4.11 is first annealed at 110 °C and kept at room temperature. A and B are the phase images of two different locations on the same sample at room temperature. One can tell that they all have similar crystals. However, when the temperature increases to 40 °C, all crystals are disappeared in D. This indicates that they completely melt at 40 °C. In contrast, some parts of crystals in C melt and some parts do not. F shows the size of the remaining parts in C as a function of time and these remaining parts seem to be stable within the experimental time window. The result directly reveals that these crystals are different.

Either they have different melting points or they have different thermal stabilities. When the heater is turned off, a similar core-surrounding pattern as shown in Fig. 4.10 (B) is recovered, which is shown in E.

4.4 Summary

To summarize, in this project, we demonstrate the crystallization of low molecular weight aPS and then systematically study the growth and melting behaviours of these aPS crystals. For the growth kinetics study, a non-linear growth is observed. It might be caused by the lack of crystallizable materials and the dominance of the diffusion controlled growth. For the melting kinetics study, some parts are observed with a fast melting speed, while the remaining parts are observed with a relatively slow melting speed. This indicates that these aPS crystals have different thermal stabilities. Lastly, some interesting observations are also presented. Here, we have made the first observation of the crystallization of aPS, which is just a starting point. There is no doubt that to understand why and how aPS crystallizes are important. Consequently, more comprehensive and detailed studies need to be done in the future as they may totally change our understanding on semicrystalline polymers and may have a huge impact on polymer processing.

Chapter 5

Expansivity study on polymer thin films

5.1 Introduction

The glass transition is one of the deepest and unsolved questions in condensed matter physics [170]. One particularly interesting phenomenon of the glass transition is the glass transition temperature reduction observed in polymer thin films at the nanoscale, which has attracted much attention in the past two decades. For polystyrene, as the film thickness is less than 40 nm, the glass transition temperature is often observed lower than the bulk value. Although there are some contradictory reports, the T_g reduction in polymer thin films is always considered as the cause of the existence of a free surface with enhanced

mobility. Consequently, Forrest and Dalnoki-Veress [128] proposed a simple model that links the enhanced surface mobility to the T_g reduction in thin films. The following derivation is based on the simple model. In the model, polymer thin films are not uniform and there is a continuous distribution of dynamics near the free surface. Thus, it is necessary to use a variable that can describe the local dynamics in polymer thin films. Consequently, the rheological temperature R is used, which is defined as the temperature at which a bulk system exhibits the same dynamics. It is clear that R depends on the location in polymer thin films. Assuming the bulk thermal expansivity only depends on temperature, a distribution of R in polymer thin films implies that the temperature dependent local expansivity curve depends on the location in polymer thin films. As a result, the thermal expansivity of a polymer thin film can be expressed as the summation of all R dependent expansivity profiles

$$\alpha = \frac{1}{h}\int_0^h \alpha(R(z))dz \tag{5.1}$$

where z is the distance from the free surface, R is the rheological temperature and h is the thickness of the film. If we assume the local rheological temperature decreases from the free surface with a function $f(z/\xi(T))$, where $\xi(T)$ is defined as the characteristic length scale from the surface-like to the bulk-like, the local rheological temperature can be expressed as

$$R(z) = T + (R_s - T)f(z/\xi(T)) \tag{5.2}$$

where R_s is the rheological temperature of the free surface. In fact, this characteristic length scale is temperature dependent, which can be expressed as

$$\xi(T) = a_0 + a_1(T_g - T) \tag{5.3}$$

where T_g is the bulk glass transition temperature, a_0 and a_1 are temperature independent variables. In order to get the temperature dependent surface rheological temperature, Forrest and Dalnoki-Veress used the bulk temperature dependent relaxation in the model. It is reasonable to assume that the bulk relaxation time is given by the VFT equation $\tau \sim \exp(B/(T - T_0))$, where B is the activation energy and T_0 is the Vogel temperature. In addition, the surface relaxation time can be described by a simple activated process $\tau \sim \exp(E_s/T)$, where E_s is the surface activation energy. Assuming the surface relaxation time at T is equal to the bulk relaxation time at R_s, the temperature dependent rheological temperature can be expressed as

$$R_s(T) = T_0 + \frac{BT}{E_s} \tag{5.4}$$

where T_0 is the Vogel temperature, and E_s is the activation energy. In general, the bulk thermal expansivity is always expressed as the tanh function

$$\alpha = \frac{1}{2}[(\alpha_m + \alpha_g) + (\alpha_m - \alpha_g)\tanh((T - T_g)/w)] \tag{5.5}$$

Accordingly, the local expansivity can be expressed as

$$\alpha(R(z)) = \frac{1}{2}[(\alpha_m + \alpha_g) + (\alpha_m - \alpha_g)\tanh((R(z) - T_g)/w)] \tag{5.6}$$

where α_m is the melt expansivity, α_g is the glass expansivity, and w the width of the transition. Substituting the above expression into Eq. 5.1, the total expansivity can be expressed as

$$\alpha = \frac{1}{h}\int_0^h \frac{1}{2}[(\alpha_m + \alpha_g) + (\alpha_m - \alpha_g)\tanh((R(z) - T_g)/w)]dz \tag{5.7}$$

Considering Eq. 5.2 and assuming $f(x) = \exp(-x)$, the total expansivity can be expressed as

$$\alpha = \frac{1}{h}\int_0^h \frac{1}{2}[(\alpha_m + \alpha_g) + (\alpha_m - \alpha_g)\tanh((T + (R_s - T)\exp(-z/\xi(T)) - T_g)/w)]dz \tag{5.8}$$

where $\xi(T)$ and $R_s(T)$ are given by Eq. 5.3 and 5.4. If the variable of integration $z \in [0, h]$ is replaced by $x \in [0, 1]$, where $z = xh$, the total expansivity of the film reduces to

$$\alpha = \int_0^1 \frac{1}{2}[(\alpha_m + \alpha_g) + (\alpha_m - \alpha_g)\tanh((T + (R_s - T)\exp(-xh/\xi(T)) - T_g)/w)]dx \tag{5.9}$$

This implies that if the bulk values $(\alpha_m, \alpha_g, w, E_s, a_0, a_1, T_0)$ are used, the only free parameter is the film thickness h. In the model, the apparent T_g is defined as the temperature at which $\alpha = \frac{1}{2}(\alpha_m + \alpha_g)$. To verify the model, we conduct a thermal expansivity experiment of polymer thin films

5.2 Experimental details and data analysis

All experiments were conducted with a WDE ellipsometer. Polystyrene films (M_w = 599 kg/mol, PDI = 1.10) were made by spin coating polymer solutions dissolved in toluene

onto Si substrates. All samples were annealed above T_g before use. During the experiment, the sample was placed on a Linkam stage and was held at 130 °C for at least 10 minutes. The expansivity profiles were obtained on the cooling runs from 130 °C to 0 °C with a cooling rate of 2 $\mathrm{K\,min^{-1}}$ or 1 $\mathrm{K\,min^{-1}}$.

For the calculation, a four-layer model is used. The details of each layer are listed below

Layer 1 Media: air, $n = 1$

Layer 2 Media: polystyrene, $n(T = 20°\mathrm{C}) = 1.583$

Layer 3 Media: SiO_x, $n = 1.42$, $h = 2\ nm$

Layer 4 Media: Si, $n = 3.875 - 0.023i$

For each dataset, the P and A pair at 20 °C is first found. Then, assuming the refractive index of polystyrene at 20 °C is 1.583, a series of h, P, and A pairs can be generated based on the four-layer model. Accordingly, the film thickness is determined by finding the shortest distance between the experimental P and A pair and generated P and A. In order to find the temperature dependent film thickness in the entire range of temperatures, the Lorentz-Lorenz equation [171] is used to update the new refractive index at each temperature. The general expression of the Lorentz-Lorenz can be expressed as

$$\frac{n^2 - 1}{n^2 + 2} = \frac{4\pi}{3} N\alpha \tag{5.10}$$

where N is the number of molecules per unit volume, α is the mean polarizability, and n is the refractive index. In addition, we assume the expansion only occurs in the normal

direction to the substrate. Of course, it is not accurate for $T > T_g$, but it does not affect the width and shape of the expansivity curves. Accordingly, the relationship between the refractive index at T and 20 °C can be expressed as

$$\frac{\frac{n_n^2-1}{n_n^2+2}}{\frac{n_{20°C}^2-1}{n_{20°C}^2+2}} = \frac{h_{20°C}}{h_n} \tag{5.11}$$

where n_n is the new refractive index at T, n_{20}°C is the refractive index at 20 °C, h_n is the film thickness at T, and h_{20}°C is the film thickness at 20 °C. This leads to a new refractive index at T

$$n_n = \sqrt{\frac{2c+1}{1-c}} \tag{5.12}$$

where $c = (\frac{n_{20°C}^2-1}{n_{20°C}^2+2})/(\frac{h_n}{h_{20°C}})$. Repeating this process for the entire dataset, the temperature dependent film thickness h and refractive index n can be obtained. In order to make the expansivity profile meaningful, the temperature dependent h and n are smoothed by averaging every 20 data points. Following that, the expansivity profile is determined by $\frac{1}{h}\frac{dh}{dT}$. For the bulk expansivity profile, the 108 nm expansivity profile is fitted by the tanh function. From the fit, the bulk α_m, α_g, and w can be obtained and used in the calculation part.

5.3 Discussion

Before the comparison, it is worth to test the model with some different parameters. Thus, we conduct a series of calculations with different combinations of a_1 and E_s but enforcing

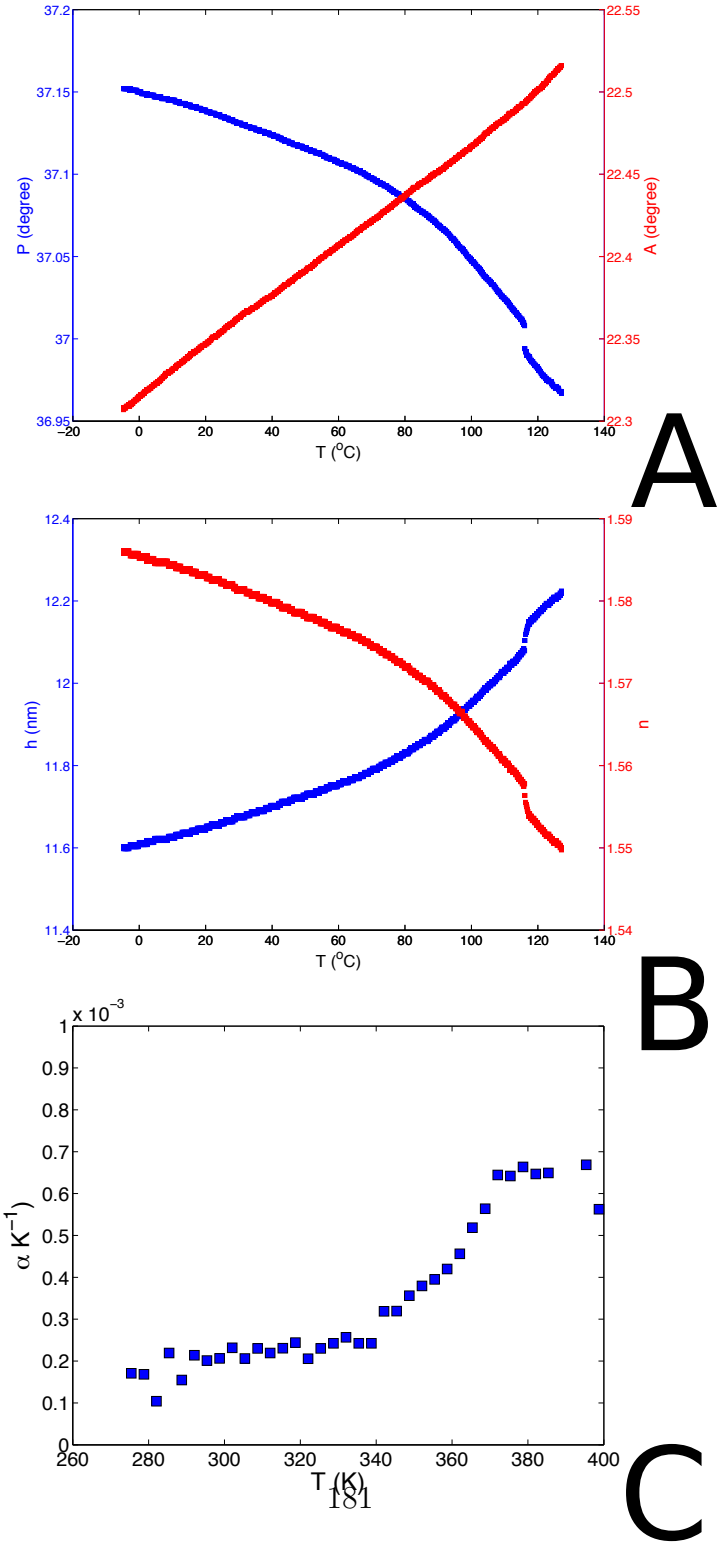

Figure 5.1: Raw data of a 11.6 nm thin film. (A) Temperature dependent P and A, (B) temperature dependent h and n, (C) thermal expansivity profile.

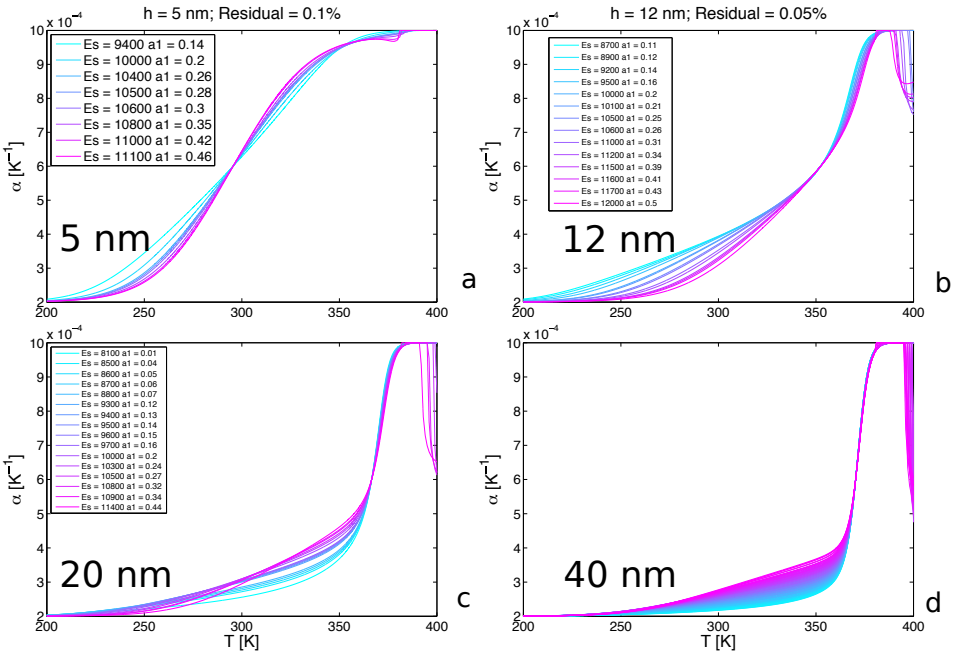

Figure 5.2: Thermal expansivity profiles of PS thin films calculated based on the simple model with different combinations of a_1 and E_s. (a) 5 nm, (b) 12 nm, (c) 20 nm, (d) 40 nm. The rest parameters are $w = 5\ K, T_0 = 331\ K, a_0 = 4\ nm, T_g = 373\ K, B = 1878K, a_g = 2 \times 10^{-4}\ K^{-1}, a_m = 10^{-3}\ K^{-1}$.

the apparent T_g to be constant for each film thickness h. Fig. 5.2 shows the calculated thermal expansivity profiles with different combinations of a_1 and E_s. Clearly, the value of these parameters can affect the shape of expansivity profiles even thought they all have the same apparent T_g. Thus, comparing the calculated expansivity profiles to the experimental expansivity profiles, the real values of a_1 and E_s can be extracted.

For the comparison, the bulk parameters are $w = 10$ K (from the 108 nm film mea-

surement), $T_0 = 331$ K, $a_0 = 4$ nm, $T_g = 373$ K, $B = 1878$ K, $E_s = 10000$ K, $a_1 = 0.05$ nm/K. The melt expansivity ranges from $6 \times 10^{-4}K^{-1}$ to $8 \times 10^{-4}K^{-1}$ and the glass expansivity ranges from $0.5 \times 10^{-4}K^{-1}$ to $2 \times 10^{-4}K^{-1}$ for different fits. A range of glass and melt expansivities rather than the constant glass and melt expansivities might be caused by several factors, such as the uncertainty of the experimental data (thermal drift), the approximation of updating the refractive index with the Lorentz-Lorenz equation, and the thermal expansion of the SiO_x layer. To be noted, the glass expansivity and melt expansivity in the calculation do not affect the width and the shape of the expansivity curves. Fig. 5.3 shows the experimental expansivity profiles of PS thin films with different h (11.6 nm, 12.5 nm, 36.3 nm, 108.5 nm), where the red-solid lines and blue-dashed lines represent the model calculated profiles and shifted bulk profiles respectively. Clearly, the model can provide a better fit than the bulk profile as the film thickness decreases, especially for the 11.6 nm and 12.5 nm expansivity profiles. In addition, the apparent T_g of thin films are calculated by $T_g = T$ at which $\alpha = \frac{1}{2}(\alpha_m + \alpha_g)$. It is not hard to see a thickness dependent T_g, which is consistent with the literature [30]. The good agreement of the experimental data with the model indicates that the simple model can describe the thermal expansivity data better than the bulk curve in thin films. More importantly, it reveals the relation between the free surface and the T_g reduction in thin films.

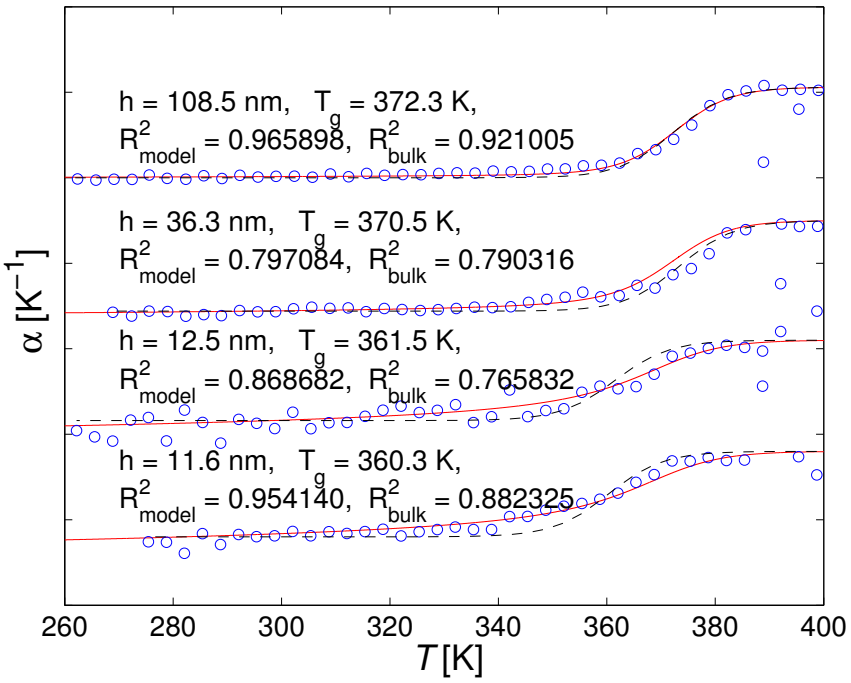

Figure 5.3: Thermal expansivity profiles of PS thin films with different h. All curves have been shifted vertically and tick labels on the y axis have been removed for clarity. The red solid lines stand for the model calculations and the blue dashed lines stand for the shifted bulk expansivity profiles. The R^2 of each fit is shown beside each profile.

Chapter 6

Concluding remarks and future work

In this thesis, we focus on studying the surface dynamics, glass transition, and the crystallization of atactic polystyrene by using some newly developed experimental techniques. The motivation of this thesis is to deeply understand how aPS behave near the glass transition temperature, especially for low molecular weight polystyrene. In order to gain insight into this topic, three different studies are conducted, where each of them focuses on a special area.

In the first part, the surface dynamics of polymer films is systematically studied by using the novel stepped film levelling experiment. This part is composed of four subsections, (1) low molecular weight levelling, (2) molecular weight dependent levelling, (3) levelling under soft confinement, and (4) ultra-thin stepped film levelling. For subsection (1), we find that polymers can even flow below the bulk T_g, and the flow profile is very different

from that above T_g. In order to account for the observation, the GTFE is developed, which can describe the flow behaviour below T_g. In addition, an Arrhenius type of temperature dependence of the surface mobility is observed below T_g, which deviates from the bulk VFT curve. For subsection (2), the stepped film levelling experiment is conducted with higher molecular weights. The result indicates that even for 22.2 kg/mol, the surface flow is still observed below T_g. Thus, a random walk simulation is conducted to demonstrate that even for $2R_g > \xi$, a lot of polymer chains still fit in the liquid-like layer and flow below T_g. For subsection (3), the levelling process is conducted under different soft confinement conditions. The results show that even under different soft confinement conditions, the surface flow is still observed below T_g, which is consistent with the T_g reduction experiment in aqueous colloidal system. For subsection (4), the ultra-thin stepped film levelling experiment is conducted. From the results, no transition temperature reduction is observed in an 8 on 8 nm stepped film.

In the second part, the crystallization of low molecular weight aPS is studied. We first demonstrate the experimental evidence of the crystallization of aPS. On top of this, a systematic study of aPS is conducted. The growth study reveals that the growth rate is not constant but time dependent, which is similar to the diffusion-controlled growth. In addition, the melting study of aPS crystals shows a range of melting from 30 °C to 70 °C, which is consistent with the theoretical calculation. Lastly, we show many interesting experimental observations that have not been fully understood yet.

In the third part, the thermal expansivity experiment is conducted in thin polymer films

to validate the recently developed simple model [128]. The thermal expansivity profiles of polystyrene films with different film thicknesses are measured by ellipsometry. Both the calculated profiles based on the simple model and the bulk shifted profiles are compared to the experimental thermal expansivity profiles. The result shows that the simple model provides a better fit than the bulk curve does. In addition, the apparent T_g reduction observed is in good agreement with the literature. More importantly, because the simple model is based on the hypothesis of the existence a liquid-like layer in glassy polymer thin films, a better fit of the simple model than the bulk curve directly confirms this hypothesis.

From these results, we can expect that there are some studies can be done in the future to extend current studies. Some possible experiments are listed here. For the levelling project under soft confinement, one can try more liquids (different viscosity, different interfacial energy) until the free surface is removed. In this condition, the whole film flow is expected.

For the thermal expansivity experiment, one can measure the thermal expansivity profile of free standing films, where large T_g reductions are always observed. The thermal expansivity profile of free standing films may show a wider transition as there are two free surfaces presented in free standing films.

For the crystallization experiment, more detailed studies are needed, such as temperature dependent morphology of aPS. In addition, one can artificially make polystyrene samples with different degree of stereoregularity. As a result, the crystallization of polystyrene with large molecular weights might be able to achieve. This may lead to many interesting

studies. In addition, a very interesting observation in crystallization study is the evaporation of low molecular weight polystyrene. This observation is really interesting as it might have a huge impact on industry. If the evaporation of low molecular weight polymers is a general feature, it might be possible to make polymer films via physical vapor deposition (PVD) and UV cross-linking, by which customized patterns can be made.

To summarize, this thesis provides some new observations and ideas of polymers near the glass transition temperature in both amorphous and crystalline states. These observations may help us to better understand the nature of glass transition as well as the concept of polymer crystallization. Although how polymers behave near the glass transition is still unclear, with efforts in the last several decades we are approaching the answer.

References

[1]H. Staudinger, "Über polymerisation", Berichte der deutschen chemischen Gesellschaft (A and B Series) **53**, 1073–1085 (1920).

[2]http://www.statista.com/statistics/282732/global-production-of-plastics-since-1950/.

[3]M. Rubinstein and R. H. Colby, *Polymer physics* (Oxford University Press, 2003).

[4]P. E. Rouse, "A Theory of the Linear Viscoelastic Properties of Dilute Solutions of Coiling Polymers", The Journal of Chemical Physics **21**, 1272 (1953).

[5]G. Strobl, *The physics of polymers* (Springer, 2007).

[6]J. Duhamel, A. Yekta, M. A. Winnik, T. C. Jao, M. K. Mishra, and I. D. Rubin, "A blob model to study polymer chain dynamics in solution", The Journal of Physical Chemistry **97**, 13708–13712 (1993).

[7]M. Doi, "Explanation for the 3.4-power law for viscosity of polymeric liquids on the basis of the tube model", Journal of Polymer Science: Polymer Physics Edition **21**, 667–684 (1983).

[8]D. T. Limmer and D. Chandler, "Theory of amorphous ices", Proceedings of the National Academy of Sciences **111**, 9413–9418 (2014).

[9]J.-Y. Chen and C.-S. Yoo, "High density amorphous ice at room temperature.", Proceedings of the National Academy of Sciences of the United States of America **108**, 7685–7688 (2011).

[10]M. D. Demetriou, M. E. Launey, G. Garrett, J. P. Schramm, D. C. Hofmann, W. L. Johnson, and R. O. Ritchie, "A damage-tolerant glass", Nature Materials **10**, 123–128 (2011).

[11]J. Schroers and W. L. Johnson, "Ductile Bulk Metallic Glass", Physical Review Letters **93**, 255506 (2004).

[12]P. G. Debenedetti and F. H. Stillinger, "Supercooled liquids and the glass transition", Nature **410**, 259–267 (2001).

[13]C. A. Angell, "Relaxation in liquids, polymers and plastic crystals strong/fragile patterns and problems", Journal of Non-Crystalline Solids **131-133**, 13–31 (1991).

[14]C. A. Angell, "Perspective on the glass transition", Journal of Physics and Chemistry of Solids **49**, 863–871 (1988).

[15]C. A. Angell, K. L. Ngai, G. B. McKenna, P. F. McMillan, and S. W. Martin, "Relaxation in glassforming liquids and amorphous solids", Journal of Applied Physics **88**, 3113 (2000).

[16]M. L. Williams, R. F. Landel, and J. D. Ferry, "The Temperature Dependence of Relaxation Mechanisms in Amorphous Polymers and Other Glass-forming Liquids", Journal of the American Chemical Society **77**, 3701–3707 (1955).

[17]T. G. Fox and P. J. Flory, "Second-Order Transition Temperatures and Related Properties of Polystyrene. I. Influence of Molecular Weight", Journal of Applied Physics **21**, 581 (1950).

[18]D. B. Macleod, "On a relation between surface tension and density", Transactions of the Faraday Society **19**, 38 (1923).

[19]A. K. Doolittle, "Studies in Newtonian Flow. I. The Dependence of the Viscosity of Liquids on Temperature", Journal of Applied Physics **22**, 1031 (1951).

[20]A. K. Doolittle, "Studies in Newtonian Flow. II. The Dependence of the Viscosity of Liquids on Free-Space", Journal of Applied Physics **22**, 1471 (1951).

[21]A. K. Doolittle, "Studies in newtonian flow. III. the dependence of the viscosity of liquids on molecular weight and free space (in homologous series)", Journal of Applied Physics **23**, 236–239 (1952).

[22]D. M. Colucci, G. B. McKenna, J. J. Filliben, A. Lee, D. B. Curliss, K. B. Bowman, and J. D. Russell, "Isochoric and isobaric glass formation: Similarities and differences", Journal of Polymer Science Part B: Polymer Physics **35**, 1561–1573 (1997).

[23]T. Czekaj and J. Kapko, "Theoretical calculations of glass transition temperatures of plasticized polymers", European Polymer Journal **17**, 1227–1229 (1981).

[24]L. Yang, D. J. Srolovitz, and A. F. Yee, "Molecular dynamics study of isobaric and isochoric glass transitions in a model amorphous polymer", The Journal of Chemical Physics **110**, 7058 (1999).

[25]G. Adam and J. H. Gibbs, "On the Temperature Dependence of Cooperative Relaxation Properties in Glass-Forming Liquids", The Journal of Chemical Physics **43**, 139 (1965).

[26]J. H. Gibbs and E. A. DiMarzio, "Nature of the Glass Transition and the Glassy State", The Journal of Chemical Physics **28**, 373 (1958).

[27]T. Salez, J. Salez, K. Dalnoki-Veress, E. Raphaël, and J. A. Forrest, "Cooperative strings and glassy interfaces", Proceedings of the National Academy of Sciences **112**, 8227–8231 (2015).

[28]J. A. Forrest, K. Dalnoki-Veress, J. R. Stevens, and J. R. Dutcher, "Effect of Free Surfaces on the Glass Transition Temperature of Thin Polymer Films", Physical Review Letters **77**, 2002–2005 (1996).

[29]J. L. Keddie, R. A. L. Jones, and R. A. Cory, "Interface and surface effects on the glass-transition temperature in thin polymer films", Faraday Discussions **98**, 219 (1994).

[30]J. L. Keddie, R. Jones, and R. Cory, "Size-Dependent Depression of the Glass Transition Temperature in Polymer Films .", Europhysics Letters **27**, 59–64 (1994).

[31]P. J. Flory, "On the Morphology of the Crystalline State in Polymers", Journal of the American Chemical Society **84**, 2857–2867 (1962).

[32]P. J. Flory, "Thermodynamics of Crystallization in High Polymers. I. Crystallization Induced by Stretching", The Journal of Chemical Physics **15**, 397 (1947).

[33]http://1.bp.blogspot.com/-12r4jDHVYak/UhYkkbnbGZI/AAAAAAAABgA/k6zlhhoP8JA/s1600/Fringed+Micelles.gif.

[34]R. Jaccodine, "Observations of Spiral Growth Steps in Ethylene Polymer", Nature **176**, 305–306 (1955).

[35]P. H. Till, "The growth of single crystals of linear polyethylene", Journal of Polymer Science **24**, 301–306 (1957).

[36]A. Keller, "A note on single crystals in polymers: Evidence for a folded chain configuration", Philosophical Magazine **2**, 1171–1175 (1957).

[37]K. H. Storks, "An Electron Diffraction Examination of Some Linear High Polymers", Journal of the American Chemical Society **60**, 1753–1761 (1938).

[38]A. P. de Boer and A. J. Pennings, "Polyethylene networks crosslinked in solution : preparation, elastic behaviour and oriented crystallization. Part 3.Oriented crystallization of swollen networks", Faraday Discuss. Chem. Soc. **68**, 345–364 (1979).

[39]G. Capaccio, I. M. Ward, and M. A. Wilding, "Morphology of isotropic and oriented linear polyethylene. Study by small-angle X-ray scattering, Raman spectroscopy and nitric acid etching", Faraday Discussions of the Chemical Society **68**, 328 (1979).

[40]D. J. Cutler, P. J. Hendra, and R. D. Sang, "Structure of polymers rapidly crystallized from their melts", Faraday Discussions of the Chemical Society **68**, 320 (1979).

[41]D. Y. Yoon and P. J. Flory, "Molecular morphology in semicrystalline polymers", Faraday Discussions of the Chemical Society **68**, 288 (1979).

[42]M. Stamm, E. W. Fischer, M. Dettenmaier, and P. Convert, "Chain conformation in the crystalline state by means of neutron scattering methods", Faraday Discussions of the Chemical Society **68**, 263 (1979).

[43]J. M. Guenet, C. Picot, and H. Benoit, "Chain conformation of semicrystalline isotactic polystyrene by small-angle neutron scattering", Faraday Discussions of the Chemical Society **68**, 251 (1979).

[44]S. Krimm and T. C. Cheam, "Mixed-crystal infrared studies of chain organization in solution-crystallized polyethylene", Faraday Discussions of the Chemical Society **68**, 244–250 (1979).

[45]A. J. Kovacs and C. Straupe, "Isothermal growth, thickening, and melting of poly(ethylene oxide) single crystals in the bulk", Journal of Polymer Science: Polymer Symposia **50**, 283–325 (2007).

[46]D. C. Bassett, A. M. Hodge, and R. H. Olley, "Lamellar morphologies in melt-crystallized polyethylene", Faraday Discussions of the Chemical Society **68**, 218–224 (1979).

[47]A. Keller, "Crystalline polymers; an introduction", Faraday Discussions of the Chemical Society **68**, 145 (1979).

[48]S. J. Organ, J. K. Hobbs, and M. J. Miles, "Reorganization and Melting of Polyethylene Single Crystals: Complementary TEM, DSC, and Real-Time AFM Studies", Macromolecules **37**, 4562–4572 (2004).

[49]R. D. Boyd and J. P. S. Badyal, "Adjacent reentry of folded polydimethylsilane polymer chains", Advanced Materials **9**, 895–896 (1997).

[50]J. Schelten, D. Ballard, G. Wignall, G. Longman, and W. Schmatz, "Small-angle neutron scattering studies of molten and crystalline polyethylene", Polymer **17**, 751–757 (1976).

[51]C. M. Guttman, E. A. DiMarzio, and J. D. Hoffman, "Calculation of SANS intensity for polyethylene: effect of varying fold planes and fold plane roughening", Polymer **22**, 597–608 (1981).

[52]G. Hauser, J. Schmidtke, and G. Strobl, "The Role of Co-Units in Polymer Crystallization and Melting: New Insights from Studies on Syndiotactic Poly(propene- co -octene)", Macromolecules **31**, 6250–6258 (1998).

[53]M. Tian, M. Dosière, S. Hocquet, P. J. Lemstra, and J. Loos, "Novel Aspects Related to Nucleation and Growth of Solution Grown Polyethylene Single Crystals", Macromolecules **37**, 1333–1341 (2004).

[54]D. C. Bassett and A. Keller, "On the habits of polyethylene crystals", Philosophical Magazine **7**, 1553–1584 (1962).

[55]M. Muthukumar, "Nucleation in Polymer Crystallization", in *Advances in chemical physics* (John Wiley & Sons, Inc., Hoboken, NJ, USA, 2004), pp. 1–63.

[56]J. D. Hoffman and R. L. Miller, "Kinetic of crystallization from the melt and chain folding in polyethylene fractions revisited: theory and experiment", Polymer **38**, 3151–3212 (1997).

[57]D. Turnbull and J. C. Fisher, "Rate of Nucleation in Condensed Systems", The Journal of Chemical Physics **17**, 71 (1949).

[58]N. S. Trasi and L. S. Taylor, "Effect of polymers on nucleation and crystal growth of amorphous acetaminophen", CrystEngComm **14**, 5188 (2012).

[59]M. V. Massa and K. Dalnoki-Veress, "Homogeneous Crystallization of Poly(Ethylene Oxide) Confined to Droplets: The Dependence of the Crystal Nucleation Rate on Length Scale and Temperature", Physical Review Letters **92**, 255509 (2004).

[60]N. Naga, Y. Yoshida, K. Noguchi, and S. Murase, "Crystallization of Amorphous Poly(Lactic Acid) Induced by Vapor of Acetone to Form High Crystallinity and Transparency Specimen", Open Journal of Polymer Chemistry **03**, 29–33 (2013).

[61]J. I. Lauritzen and J. D. Hoffman, "Theory of formation of polymer crystals with folded chains in dilute solution", Journal of Research of the National Bureau of Standards Section A: Physics and Chemistry **64A**, 73 (1960).

[62]J. D. Hoffman and J. I. Lauritzen, "Crystallization of bulk polymers with chain folding: theory of growth of lamellar spherulites", Journal of Research of the National Bureau of Standards Section A: Physics and Chemistry **65A**, 297 (1961).

[63]S. Z. D. Cheng and B. Lotz, "Enthalpic and entropic origins of nucleation barriers during polymer crystallization: The Hoffman-Lauritzen theory and beyond", Polymer **46**, 8662–8681 (2005).

[64]I. C. Sanchez, "Dilute Solution Theory of Polymer Crystal Growth: A Kinetic Theory of Chain Folding", The Journal of Chemical Physics **55**, 893 (1971).

[65]I. C. Sanchez and E. A. DiMarzio, "Dilute solution theory of polymer crystal growth: Fractionation effects", Journal of Research of the National Bureau of Standards Section A: Physics and Chemistry **76A**, 213 (1972).

[66]J. I. Lauritzen, "Effect of a finite substrate length upon polymer crystal lamellar growth rate", Journal of Applied Physics **44**, 4353–4359 (1973).

[67]J. I. Lauritzen and J. D. Hoffman, "Extension of theory of growth of chain-folded polymer crystals to large undercoolings", Journal of Applied Physics **44**, 4340–4352 (1973).

[68]F. C. Frank, "Nucleation-controlled growth on a one-dimensional growth of finite length", Journal of Crystal Growth **22**, 233–236 (1974).

[69]Y. Miyamoto, Y. Tanzawa, H. Miyaji, and H. Kiho, "Growth rate of isotactic polystyrene crystals in concentrated solutions and in the melt", Polymer **33**, 2496–2501 (1992).

[70]E. Passaglia and F. Khoury, "Crystal growth kinetics and the lateral habits of polyethylene crystals", Polymer **25**, 631–644 (1984).

[71]A. Toda, "Rounded lateral habits of polyethylene single crystals", Polymer **32**, 771–780 (1991).

[72]J. D. Hoffman, "Regime III crystallization in melt-crystallized polymers: The variable cluster model of chain folding", Polymer **24**, 3–26 (1983).

[73]J. P. Armistead and J. D. Hoffman, "Direct Evidence of Regimes I, II, and III in Linear Polyethylene Fractions As Revealed by Spherulite Growth Rates", Macromolecules **35**, 3895–3913 (2002).

[74]J. H. Magill, "Crystallization of Poly-(Tetramethyl-p-Silphenylene)-Siloxane Polymers", Journal of Applied Physics **35**, 3249 (1964).

[75]F. P. Price, "The Development of Crystallinity in Polychlorotrifluoroethylene", Journal of the American Chemical Society **74**, 311–318 (1952).

[76]J. Magill and H.-M. Li, "Crystallization kinetics and morphology of polymer blends of poly(tetramethyl-p-silphenylene siloxane) fractions", Polymer **19**, 416–422 (1978).

[77]M. Avrami, "Granulation, Phase Change, and Microstructure Kinetics of Phase Change. III", The Journal of Chemical Physics **9**, 177 (1941).

[78]M. Avrami, "Kinetics of Phase Change. II - Transformation-Time Relations for Random Distribution of Nuclei", Journal of Chemical Physics **8**, 212–224 (1940).

[79]M. Avrami, "Kinetics of Phase Change. I General Theory", The Journal of Chemical Physics **7**, 1103 (1939).

[80]L. A. Baldenegro-Perez, D. Navarro-Rodriguez, F. J. Medellin-Rodriguez, B. Hsiao, C. A. Avila-Orta, and I. Sics, "Molecular weight and crystallization temperature effects on poly(ethylene terephthalate) (PET) homopolymers, an isothermal crystallization analysis", Polymers **6**, 583–600 (2014).

[81]C. L. Jackson and G. B. McKenna, "The glass transition of organic liquids confined to small pores", Journal of Non-Crystalline Solids **131-133**, 221–224 (1991).

[82]J. S. Sharp and J. A. Forrest, "Free Surfaces Cause Reductions in the Glass Transition Temperature of Thin Polystyrene Films", Physical Review Letters **91**, 235701 (2003).

[83]O. Bäumchen, J. D. McGraw, J. A. Forrest, and K. Dalnoki-Veress, "Reduced Glass Transition Temperatures in Thin Polymer Films: Surface Effect or Artifact?", Physical Review Letters **109**, 055701 (2012).

[84]P. G. de Gennes, "Glass transitions in thin polymer films", European Physical Journal E **2**, 201–203 (2000).

[85]C. J. Ellison and J. M. Torkelson, "The distribution of glass-transition temperatures in nanoscopically confined glass formers", Nature Materials **2**, 695–700 (2003).

[86]R. P. White, C. C. Price, and J. E. G. Lipson, "Effect of Interfaces on the Glass Transition of Supported and Freestanding Polymer Thin Films", Macromolecules **48**, 4132–4141 (2015).

[87]M. D. Ediger and J. A. Forrest, "Dynamics near Free Surfaces and the Glass Transition in Thin Polymer Films: A View to the Future", Macromolecules **47**, 471–478 (2014).

[88]F. Kremer, M. Tress, and E. U. Mapesa, "Glassy dynamics and glass transition in nanometric layers and films: A silver lining on the horizon", Journal of Non-Crystalline Solids **407**, 277–283 (2015).

[89]F.-Y. Lin and W. Steffen, "Capillary wave dynamics of thin liquid polymer films", The Journal of Chemical Physics **141**, 104903 (2014).

[90]H. Kim, A. Rühm, L. B. Lurio, J. K. Basu, J. Lal, D. Lumma, S. G. J. Mochrie, and S. K. Sinha, "Surface Dynamics of Polymer Films", Physical Review Letters **90**, 068302 (2003).

[91]K. Fukao and Y. Miyamoto, "Glass transitions and dynamics in thin polymer films: Dielectric relaxation of thin films of polystyrene", Physical Review E **61**, 1743–1754 (2000).

[92]K. Fukao, S. Uno, Y. Miyamoto, A. Hoshino, and H. Miyaji, "Relaxation dynamics in thin supported polymer films", Journal of Non-Crystalline Solids **307-310**, 517–523 (2002).

[93]R. M. Papaléo, R. Leal, W. H. Carreira, L. G. Barbosa, I. Bello, and A. Bulla, "Relaxation times of nanoscale deformations on the surface of a polymer thin film near and below the glass transition", Physical Review B **74**, 094203 (2006).

[94]G. B. DeMaggio, W. E. Frieze, D. W. Gidley, M. Zhu, H. A. Hristov, and A. F. Yee, "Interface and Surface Effects on the Glass Transition in Thin Polystyrene Films", Physical Review Letters **78**, 1524–1527 (1997).

[95]L. Xie, G. B. DeMaggio, W. E. Frieze, J. DeVries, D. W. Gidley, H. A. Hristov, and A. F. Yee, "Positronium Formation as a Probe of Polymer Surfaces and Thin Films", Physical Review Letters **74**, 4947–4950 (1995).

[96]G. Reiter, "Dewetting of thin polymer films", Physical Review Letters **68**, 75–78 (1992).

[97]G. Reiter, "Mobility of Polymers in Films Thinner than Their Unperturbed Size", Europhysics Letters (EPL) **23**, 579–584 (1993).

[98]G. Reiter, "Dewetting of Highly Elastic Thin Polymer Films", Physical Review Letters **87**, 186101 (2001).

[99]C. Redon, F. Brochard-Wyart, and F. Rondelez, "Dynamics of dewetting", Physical Review Letters **66**, 715–718 (1991).

[100]D. J. Plazek and V. M. O'Rourke, "Viscoelastic behavior of low molecular weight polystyrene", Journal of Polymer Science Part A-2: Polymer Physics **9**, 209–243 (1971).

[101]G. Debrégeas, P. Martin, and F. Brochard-Wyart, "Viscous Bursting of Suspended Films", Physical Review Letters **75**, 3886–3889 (1995).

[102]K. Dalnoki-Veress, B. Nickel, C. Roth, and J. Dutcher, "Hole formation and growth in freely standing polystyrene films", Physical Review E **59**, 2153–2156 (1999).

[103]O. K. C. Tsui, X. P. Wang, J. Y. L. Ho, T. K. Ng, and X. Xiao, "Studying Surface Glass-to-Rubber Transition Using Atomic Force Microscopic Adhesion Measurements", Macromolecules **33**, 4198–4204 (2000).

[104]S. Ge, Y. Pu, W. Zhang, M. Rafailovich, J. Sokolov, C. Buenviaje, R. Buckmaster, and R. M. Overney, "Shear modulation force microscopy study of near surface glass transition temperatures", Physical Review Letters **85**, 2340–2343 (2000).

[105]J. A. Hammerschmidt, W. L. Gladfelter, and G. Haugstad, "Probing polymer viscoelastic relaxations with temperature-controlled friction force microscopy", Macromolecules **32**, 3360–3367 (1999).

[106]V. N. Bliznyuk, H. E. Assender, and G. A. D. Briggs, "Surface glass transition temperature of amorphous polymers. A new insight with SFM", Macromolecules **35**, 6613–6622 (2002).

[107]T. Kajiyama, K. Tanaka, and A. Takahara, "Study of the surface glass transition behaviour of amorphous polymer film by scanning-force microscopy and surface spectroscopy", Polymer **39**, 4665–4673 (1998).

[108]H. van Melick, A. van Duken, J. den Toonder, L. Govaert, and H. Meijer, "Near-surface mechanical properties of amorphous polymers", Philosophical Magazine A **82**, 2093–2102 (2002).

[109]Z. Fakhraai and J. A. Forrest, "Probing Slow Dynamics in Supported Thin Polymer Films", Physical Review Letters **95**, 025701 (2005).

[110]J. Teichroeb and J. A. Forrest, "Direct Imaging of Nanoparticle Embedding to Probe Viscoelasticity of Polymer Surfaces", Physical Review Letters **91**, 016104 (2003).

[111]J. S. Sharp, J. H. Teichroeb, and J. A. Forrest, "The properties of free polymer surfaces and their influence on the glass transition temperature of thin polystyrene films.", The European physical journal. E, Soft matter **15**, 473–87 (2004).

[112]S. A. Hutcheson and G. B. McKenna, "Comment on "the properties of free polymer surfaces and their influence on the glass transition temperature of thin polystyrene films" by J.S. Sharp, J.H. Teichroeb and J.A. Forrest", European Physical Journal E **22**, 281–286 (2007).

[113]S. A. Hutcheson and G. B. McKenna, "Nanosphere embedding into polymer surfaces: A viscoelastic contact mechanics analysis", Physical Review Letters **94**, 1–4 (2005).

[114]D. Qi, M. Ilton, and J. A. Forrest, "Measuring surface and bulk relaxation in glassy polymers", The European Physical Journal E **34**, 56 (2011).

[115]D. Qi, C. R. Daley, Y. Chai, and J. A. Forrest, "Molecular weight dependence of near surface dynamical mechanical properties of polymers", Soft Matter **9**, 8958 (2013).

[116]C. R. Daley, Z. Fakhraai, M. D. Ediger, and J. A. Forrest, "Comparing surface and bulk flow of a molecular glass former", Soft Matter **8**, 2206 (2012).

[117]Z. Fakhraai and J. A. Forrest, "Measuring the Surface Dynamics of Glassy Polymers", Science **319**, 600–604 (2008).

[118]D. Qi, Z. Fakhraai, and J. A. Forrest, "Substrate and Chain Size Dependence of Near Surface Dynamics of Glassy Polymers", Physical Review Letters **101**, 096101 (2008).

[119]T. Kerle, Z. Lin, H.-C. Kim, and T. P. Russell, "Mobility of Polymers at the Air/Polymer Interface", Macromolecules **34**, 3484–3492 (2001).

[120]W. Zhang and L. Yu, "Surface Diffusion of Polymer Glasses", Macromolecules **49**, 731–735 (2016).

[121]W. Zhang, C. W. Brian, and L. Yu, "Fast Surface Diffusion of Amorphous o -Terphenyl and Its Competition with Viscous Flow in Surface Evolution", The Journal of Physical Chemistry B **119**, 5071–5078 (2015).

[122]L. Zhu, C. W. Brian, S. F. Swallen, P. T. Straus, M. D. Ediger, and L. Yu, "Surface Self-Diffusion of an Organic Glass", Physical Review Letters **106**, 256103 (2011).

[123]Z. Jiang, H. Kim, X. Jiao, H. Lee, Y.-J. Lee, Y. Byun, S. Song, D. Eom, C. Li, M. H. Rafailovich, L. B. Lurio, and S. K. Sinha, "Evidence for Viscoelastic Effects in Surface Capillary Waves of Molten Polymer Films", Physical Review Letters **98**, 227801 (2007).

[124]K. J. Alvine, Y. Dai, H. W. Ro, S. Narayanan, A. R. Sandy, C. L. Soles, and O. G. Shpyrko, "Capillary Wave Dynamics of Thin Polymer Films over Submerged Nanostructures", Physical Review Letters **109**, 207801 (2012).

[125]C. M. Evans, S. Narayanan, Z. Jiang, and J. M. Torkelson, "Modulus, Confinement, and Temperature Effects on Surface Capillary Wave Dynamics in Bilayer Polymer Films Near the Glass Transition", Physical Review Letters **109**, 038302 (2012).

[126]Z. Yang, C.-H. Lam, E. DiMasi, N. Bouet, J. Jordan-Sweet, and O. K. C. Tsui, "Method to measure the viscosity of nanometer liquid films from the surface fluctuations", Applied Physics Letters **94**, 251906 (2009).

[127]Z. Yang, Y. Fujii, F. K. Lee, C.-H. Lam, and O. K. C. Tsui, "Glass Transition Dynamics and Surface Layer Mobility in Unentangled Polystyrene Films", Science **328**, 1676–1679 (2010).

[128]J. A. Forrest and K. Dalnoki-Veress, "When Does a Glass Transition Temperature Not Signify a Glass Transition?", ACS Macro Letters **3**, 310–314 (2014).

[129]http://polymersource.com/dataSheet/P4685-S.pdf.

[130]D. B. Hall, P. Underhill, and J. M. Torkelson, "Spin coating of thin and ultrathin polymer films", Polymer Engineering & Science **38**, 2039–2045 (1998).

[131]http://shavingrazorblade.blogspot.ca.

[132]http://www.film-sense.com/technology/advantages-of-ellipsometry/.

[133]J. H. Kim, J. Jang, and W. C. Zin, "Thickness dependence of the glass transition temperature in thin polymer films", Langmuir **17**, 2703–2710 (2001).

[134]http://www.teachnano.com/education/AFM.html.

[135]E. J. C. Kellar, C. Galiotis, and E. H. Andrews, "Raman Vibrational Studies of Syndiotactic Polystyrene. 1. Assignments in a Conformational/Crystallinity Sensitive Spectral Region", Macromolecules **29**, 3515–3520 (1996).

[136]Y. Hu, J. K. Liang, A. S. Myerson, and L. S. Taylor, "Crystallization Monitoring by Raman Spectroscopy: Simultaneous Measurement of Desupersaturation Profile and Polymorphic Form in Flufenamic Acid Systems", Industrial & Engineering Chemistry Research **44**, 1233–1240 (2005).

[137]H. Liem, J. Cabanillas-Gonzalez, P. Etchegoin, and D. D. C. Bradley, "Glass transition temperatures of polymer thin films monitored by Raman scattering", Journal of Physics: Condensed Matter **16**, 721–728 (2004).

[138]http://www.omega.ca/pptst_eng/CN7500.html.

[139]https://www.agilent.com/en-us/products/vacuum-technologies/primary-medium-vacuum-pumps/dry-scroll-pumps/sh-110.

[140]http://www.omega.ca/pptst_eng/KHR_KHLV_KH.html.

[141]P. A. O'Connell and G. B. McKenna, "Arrhenius-type temperature dependence of the segmental relaxation below T_g", The Journal of Chemical Physics **110**, 11054 (1999).

[142]Y. Guo, A. Morozov, D. Schneider, J. W. Chung, C. Zhang, M. Waldmann, N. Yao, G. Fytas, C. B. Arnold, and R. D. Priestley, "Ultrastable nanostructured polymer glasses", Nature Materials **11**, 337–343 (2012).

[143]J. Zhao, S. L. Simon, and G. B. McKenna, "Using 20-million-year-old amber to test the super-Arrhenius behaviour of glass-forming systems", Nature Communications **4**, 1783 (2013).

[144]A. Schnhals, H. Goering, C. Schick, B. Frick, and R. Zorn, "Glassy dynamics of polymers confined to nanoporous glasses revealed by relaxational and scattering experiments", The European Physical Journal E - Soft Matter **12**, 173–178 (2003).

[145]E. R. Weeks, "Three-Dimensional Direct Imaging of Structural Relaxation Near the Colloidal Glass Transition", Science **287**, 627–631 (2000).

[146]Y. Wang, A. L. Agapov, F. Fan, K. Hong, X. Yu, J. Mays, and A. P. Sokolov, "Decoupling of Ionic Transport from Segmental Relaxation in Polymer Electrolytes", Physical Review Letters **108**, 088303 (2012).

[147]M. A. Ratner and D. F. Shriver, "Ion transport in solvent-free polymers", Chemical Reviews **88**, 109–124 (1988).

[148]Y. Wang, N. A. Lane, C.-N. Sun, F. Fan, T. A. Zawodzinski, and A. P. Sokolov, "Ionic Conductivity and Glass Transition of Phosphoric Acids", The Journal of Physical Chemistry B **117**, 8003–8009 (2013).

[149]L. E. Stillwagon and R. G. Larson, "Leveling of thin films over uneven substrates during spin coating", Physics of Fluids A: Fluid Dynamics **2**, 1937 (1990).

[150]L. E. Stillwagon and R. G. Larson, "Fundamentals of topographic substrate leveling", Journal of Applied Physics **63**, 5251 (1988).

[151]J. D. McGraw, T. Salez, O. Bäumchen, E. Raphaël, and K. Dalnoki-Veress, "Self-Similarity and Energy Dissipation in Stepped Polymer Films", Physical Review Letters **109**, 128303 (2012).

[152]J. D. McGraw, N. M. Jago, and K. Dalnoki-Veress, "Capillary levelling as a probe of thin film polymer rheology", Soft Matter **7**, 7832 (2011).

[153]T. Salez, J. D. McGraw, O. Bäumchen, K. Dalnoki-Veress, and E. Raphaël, "Capillary-driven flow induced by a stepped perturbation atop a viscous film", Physics of Fluids **24**, 102111 (2012).

[154]H. E. Huppert, "Propagation of two-dimensional and axisymmetric viscous gravity currents over a rigid horizontal surface", Journal of Fluid Mechanics **121**, 43–58 (1982).

[155]R. Seemann, S. Herminghaus, and K. Jacobs, "Dewetting Patterns and Molecular Forces: A Reconciliation", Physical Review Letters **86**, 5534–5537 (2001).

[156]W. W. Mullins, "Flattening of a Nearly Plane Solid Surface due to Capillarity", Journal of Applied Physics **30**, 77 (1959).

[157]`http://gwyddion.net`.

[158]`https://riverbankcomputing.com/software/pyqt/intro`.

[159]Y. Chai, T. Salez, J. D. McGraw, M. Benzaquen, K. Dalnoki-Veress, E. Raphaël, and J. A. Forrest, "A Direct Quantitative Measure of Surface Mobility in a Glassy Polymer", Science **343**, 994–999 (2014).

[160]J.-C. Majeste, J.-P. Montfort, A. Allal, and G. Marin, "Viscoelasticity of low molecular weight polymers and the transition to the entangled regime", Rheologica Acta **37**, 486–499 (1998).

[161]M. Ilton, D. Qi, and J. A. Forrest, "Using Nanoparticle Embedding to Probe Surface Rheology and the Length Scale of Surface Mobility in Glassy Polymers", Macromolecules **42**, 6851–6854 (2009).

[162]K. Paeng, S. F. Swallen, and M. D. Ediger, "Direct Measurement of Molecular Motion in Freestanding Polystyrene Thin Films", Journal of the American Chemical Society **133**, 8444–8447 (2011).

[163]C. Zhang, Y. Guo, and R. D. Priestley, "Glass Transition Temperature of Polymer Nanoparticles under Soft and Hard Confinement", Macromolecules **44**, 4001–4006 (2011).

[164]R. M. Hikmet, S. Callister, and A. Keller, "Thermoreversible gelation of atactic polystyrene: phase transformation and morphology", Polymer **29**, 1378–1388 (1988).

[165]G. Xue, J. Zhang, J. Chen, Y. Li, J. Ma, G. Wang, and P. Sun, "Gelation Crystallization of Isotactic Polystyrene in Solvents of Varying Molecular Size", Macromolecules **33**, 2299–2301 (2000).

[166]C. Daniel, A. Menelle, A. Brulet, and J.-M. Guenet, "Thermoreversible gelation of syndiotactic polystyrene in toluene and chloroform", Polymer **38**, 4193–4199 (1997).

[167]H. Tan, A. Moet, A. Hiltner, and E. Baer, "Thermoreversible gelation of atactic polystyrene solutions", Macromolecules **16**, 28–34 (1983).

[168]A. N. Semenov, "Theory of Cluster Formation in Homopolymer Melts", Macromolecules **42**, 6761–6776 (2009).

[169]H. Bodiguel, H. Montes, and C. Fretigny, "Depth sensing and dissipation in tapping mode atomic force microscopy", Review of Scientific Instruments **75**, 2529–2535 (2004).

[170]L. Berthier and M. D. Ediger, "Facets of glass physics", Physics Today **69**, 41–46 (2016).

[171]G. Beaucage, R. Composto, and R. S. Stein, "Ellipsometric study of the glass transition and thermal expansion coefficients of thin polymer films", Journal of Polymer Science Part B: Polymer Physics **31**, 319–326 (1993).

Appendices

Appendix A

Python code for stepped film levelling analysis

A.1 Main Code

This following code is the main part of the step film analysis program. The code can read the pre-levelled AFM text file generated from Gwyddion and fit each individual line into tanh function. Based on fitting parameters, each line is shifted to (0,0) position and the width of each line can be obtained. Finally, the mean profile is generated by averaging over few hundreds of lines.

```
# -*- coding: utf-8 -*-
"""
Created on Tue Apr 24 15:28:46 2012
This program can read data from AFM text file generated from Gwyddion.
Fit each line into tanh function and shift them into 0,0 point.
Then find out the width distribution and mean profile.
author: Yu Chai
"""
import numpy as np
import os
from scipy.optimize import curve_fit
import matplotlib.pyplot as plt
```

```
from scipy.stats import norm, cauchy

def main_code(self, main_file_name,main_number_file, main_n_bins):
    '''
    output mean profile information
    '''
    Mean_profile_output_temp=os.path.split(str(main_file_name))
    Mean_profile_output_path=Mean_profile_output_temp[0]
    Mean_profile_output_name_total=Mean_profile_output_temp[1]
    Mean_profile_output_name_real=os.path.splitext(
    ↪ Mean_profile_output_name_total)[0]
    Mean_profile_output=Mean_profile_output_path+'/'+
    ↪ Mean_profile_output_name_real+'-Mean-profile.dat'
    print Mean_profile_output_path
    print Mean_profile_output_name_real
    #number of file
    n=main_number_file
    #clear all figure
    self.mpl_1.canvas.ax.clear()
    self.mpl_2.canvas.ax.clear()
    self.mpl_3.canvas.ax.clear()
    self.listWidget.clear()
    #figure title str1 all lines str2 mean profile str3 width distribution
    tlt=main_file_name
    '''
    temp=main_temp
    str1='All profile %s.png'%(temp)
    str2='Mean profile %s.pdf'%(temp)
    str3='Width distribution %s.pdf'%(temp)
    '''
    #array initialize
    lmin=9999999
    d=[]
    name=[]
    length=[]
    valmm=[]
    locmm=[]
    c=[]
    xxdict={}
    yyf=[]
    xxf=[]
    t_l=0
    g_l=0
    b_l=0
    #define functions
```

```
    def func(x,a,b,c,d):
        return a*np.tanh((x-b)/c)+d
    def gaussianfit(x,mu,sigma):
        return 1/(sigma * np.sqrt(2 * np.pi)) *np.exp( - (x - mu)**2 / (2 *
    ↪ sigma**2) )
    def cauchyfit(x,x0,gema):
        return 1/np.pi*gema/((x-x0)**2+gema**2)
    '''
    main loop
    '''
    for i in range(n):
        self.listWidget.addItem( 'file loop'+str(i))
        txx=str(tlt)
        name.append(txx)
        #read width and height
        list_s='Reading Data file: '+tlt
        self.listWidget.addItem(list_s)
        f=open(name[i])
        f.readline()
        aw=f.readline()
        ah=f.readline()
        f.closed
        width=float(aw[9:13])*10**-6
        height=float(ah[10:14])*10**-6
        #read data
        rdata=np.loadtxt(name[i])
        data=rdata-np.min(rdata)
        data=data[:,:lmin]
        data=data*10**9
        ly=len(data)
        lx=len(data[0])
        xp=width/(lx-1)
        yp=height/(ly-1)
        x=np.linspace(0,width,lx)*10**6
        xspacing=xp*10**6
        t_l=ly
        for j in range(ly):
            list_s='Doing file ' +str(i)+' line '+str(j)
            self.listWidget.addItem(list_s)
            y=np.array(data[j])
            popt,pcov = curve_fit(func,x,y)
            at=popt[0]
            bt=popt[1]
            ct=popt[2]
            dt=popt[3]
```

```
            #c.append(popt[2])
            reloc=x-bt
            yy=y-dt
            '''
            round the location into nearby bin
            '''
            xx=np.round(reloc/xspacing)*xspacing
            for z in range(len(xx)):
                loc=xx[z]
                vol=yy[z]
                if loc not in xxdict:
                    xxdict[loc]=[vol]
                else:
                    xxdict[loc].append(vol)
            '''
            if this is a bad fit, get rid of this
            and width ia larger than 2
            '''
            fyy=func(x,at,bt,ct,dt)
            fyy=np.array(fyy)-dt
            if np.absolute(fyy[0]-fyy[-1])>1:
                c.append(popt[2])
                locmm.append(xx)
                valmm.append(yy)
                self.mpl_1.canvas.ax.plot(xx,yy,'x')
                self.mpl_1.canvas.ax.plot(xx,fyy)
                g_l=g_l+1
    self.label_23.setText(str(t_l))
    self.label_24.setText(str(g_l))
    self.label_25.setText(str(t_l-g_l))
    self.mpl_1.canvas.draw()
    '''
    mean profile
    '''
    #if the number of file is more than 1, need to consider the height
    ↪ difference.
    summax=0
    for i in sorted(xxdict.keys()):
        if len(xxdict[i])>summax:
            summax=len(xxdict[i])
    # if the number of each location is smaller than summax-10 then drop
    ↪ this one
    for i in sorted(xxdict.keys()):
        if len(xxdict[i])<summax/2.0:
            del xxdict[i]
```

```
        else:
            xxf.append(i)
            yyf.append(np.average(xxdict[i]))
    '''
    reverse array if left high
    '''
    if yyf[0]>yyf[-1]:
        yyf=yyf[::-1]
        popt_2,pcov_2 = curve_fit(func,xxf,yyf)
        at_2=popt_2[0]
        bt_2=popt_2[1]
        ct_2=popt_2[2]
        dt_2=popt_2[3]
        xxf=xxf-bt_2
        yyf=yyf-dt_2

    poptmean,pcovmean = curve_fit(func,xxf,yyf)
    fyyf=func(xxf,poptmean[0],poptmean[1],poptmean[2],poptmean[3])
    self.mpl_2.canvas.ax.plot(xxf,yyf,'x',xxf,fyyf)
    #self.mpl_2.canvas.ax.set_xlabel(r'$X /\mu m$')
    #self.mpl_2.canvas.ax.set_ylabel(r'Height /nm')
    self.label_10.setText(str(poptmean[0]))
    self.label_11.setText(str(poptmean[1]))
    self.label_12.setText(str(poptmean[2]*1000*2))
    self.label_13.setText(str(poptmean[3]))
    self.label_16.setText(str(np.absolute(poptmean[0])*2))
    self.mpl_2.canvas.draw()
    """
    output mean profile
    """
    Mean_profile_x=np.reshape(xxf, (-1,1))
    Mean_profile_y=np.reshape(yyf, (-1,1))
    Mean_profile_line_data=np.append(Mean_profile_x,Mean_profile_y,1)
    print Mean_profile_line_data
    np.savetxt(Mean_profile_output, Mean_profile_line_data)
    '''
    distribution start here
    '''
    #Width
    c=np.array(c)
    c=np.absolute(c)*1000*2
    # the histogram of the data
    if self.checkBox.isChecked():
        n, bins, patches=self.mpl_3.canvas.ax.hist(c,int(main_n_bins),normed
↪   =1)
```

```
    else:
        left_range=int(self.lineEdit_8.text())
        right_range=int(self.lineEdit_7.text())
        n, bins, patches=self.mpl_3.canvas.ax.hist(c,int(main_n_bins),range
    ↪ =(left_range,right_range),normed=1)
    # best fit of data
    if self.checkBox_2.isChecked():
        (mu, sigma) = norm.fit(c)
    else:
        pgt,pge=curve_fit(cauchyfit,bins[:-1],n)
        mu = pgt[0]
        sigma = pgt[1]
        #amp = pgt[2]
        muerr = (pge[0][0])**0.5
        sigmaerr = (pge[1][1])**0.5
    # add a 'best fit' line
    gfd = norm.pdf( bins, mu, sigma)
    self.mpl_3.canvas.ax.plot(bins, gfd, 'r--', linewidth=2)
    #plot
    self.mpl_3.canvas.ax.set_ylabel('Normerized')
    self.mpl_3.canvas.ax.set_xlabel(r'$\mu=%.3f ,\ \sigma=%.3f$' %(mu, sigma
    ↪ ),fontsize=15)
    self.mpl_3.canvas.draw()
    self.label_8.setText(str(sigma))
    self.label_9.setText(str(mu))
```

A.2 GUI code

The following code is the GUI part of the step film analysis program. The GUI framework is QT4.

```
# -*- coding: utf-8 -*-

# Form implementation generated from reading ui file 'mean_profile_form.ui'
#
# Created: Thu Jun 28 10:39:54 2012
#      by: PyQt4 UI code generator 4.9.1
#
# WARNING! All changes made in this file will be lost!

from PyQt4 import QtCore, QtGui
```

```
try:
    _fromUtf8 = QtCore.QString.fromUtf8
except AttributeError:
    _fromUtf8 = lambda s: s

class Ui_MainWindow(object):
    def setupUi(self, MainWindow):
        MainWindow.setObjectName(_fromUtf8("MainWindow"))
        MainWindow.resize(1210, 671)
        self.centralwidget = QtGui.QWidget(MainWindow)
        self.centralwidget.setObjectName(_fromUtf8("centralwidget"))
        self.horizontalLayoutWidget = QtGui.QWidget(self.centralwidget)
        self.horizontalLayoutWidget.setGeometry(QtCore.QRect(10, 50, 1191,
    ↪ 271))
        self.horizontalLayoutWidget.setObjectName(_fromUtf8("
    ↪ horizontalLayoutWidget"))
        self.horizontalLayout = QtGui.QHBoxLayout(self.
    ↪ horizontalLayoutWidget)
        self.horizontalLayout.setMargin(0)
        self.horizontalLayout.setObjectName(_fromUtf8("horizontalLayout"))
        self.groupBox = QtGui.QGroupBox(self.horizontalLayoutWidget)
        self.groupBox.setObjectName(_fromUtf8("groupBox"))
        self.groupBox_4 = QtGui.QGroupBox(self.groupBox)
        self.groupBox_4.setGeometry(QtCore.QRect(10, 120, 331, 141))
        self.groupBox_4.setObjectName(_fromUtf8("groupBox_4"))
        self.checkBox = QtGui.QCheckBox(self.groupBox_4)
        self.checkBox.setGeometry(QtCore.QRect(20, 30, 141, 21))
        self.checkBox.setChecked(True)
        self.checkBox.setTristate(False)
        self.checkBox.setObjectName(_fromUtf8("checkBox"))
        self.label_20 = QtGui.QLabel(self.groupBox_4)
        self.label_20.setGeometry(QtCore.QRect(10, 50, 113, 22))
        self.label_20.setObjectName(_fromUtf8("label_20"))
        self.lineEdit_8 = QtGui.QLineEdit(self.groupBox_4)
        self.lineEdit_8.setGeometry(QtCore.QRect(50, 50, 131, 22))
        self.lineEdit_8.setObjectName(_fromUtf8("lineEdit_8"))
        self.label_19 = QtGui.QLabel(self.groupBox_4)
        self.label_19.setGeometry(QtCore.QRect(10, 80, 113, 22))
        self.label_19.setObjectName(_fromUtf8("label_19"))
        self.lineEdit_7 = QtGui.QLineEdit(self.groupBox_4)
        self.lineEdit_7.setGeometry(QtCore.QRect(50, 80, 131, 22))
        self.lineEdit_7.setObjectName(_fromUtf8("lineEdit_7"))
        self.label_18 = QtGui.QLabel(self.groupBox_4)
        self.label_18.setGeometry(QtCore.QRect(10, 110, 135, 22))
```

```
        self.label_18.setObjectName(_fromUtf8("label_18"))
        self.lineEdit_6 = QtGui.QLineEdit(self.groupBox_4)
        self.lineEdit_6.setGeometry(QtCore.QRect(50, 110, 131, 22))
        self.lineEdit_6.setObjectName(_fromUtf8("lineEdit_6"))
        self.checkBox_2 = QtGui.QCheckBox(self.groupBox_4)
        self.checkBox_2.setGeometry(QtCore.QRect(150, 30, 171, 20))
        self.checkBox_2.setChecked(True)
        self.checkBox_2.setTristate(False)
        self.checkBox_2.setObjectName(_fromUtf8("checkBox_2"))
        self.groupBox_5 = QtGui.QGroupBox(self.groupBox)
        self.groupBox_5.setGeometry(QtCore.QRect(10, 20, 171, 71))
        self.groupBox_5.setObjectName(_fromUtf8("groupBox_5"))
        self.label_14 = QtGui.QLabel(self.groupBox_5)
        self.label_14.setGeometry(QtCore.QRect(10, 30, 71, 21))
        self.label_14.setObjectName(_fromUtf8("label_14"))
        self.lineEdit_2 = QtGui.QLineEdit(self.groupBox_5)
        self.lineEdit_2.setGeometry(QtCore.QRect(70, 30, 71, 22))
        self.lineEdit_2.setObjectName(_fromUtf8("lineEdit_2"))
        self.calendarWidget = QtGui.QCalendarWidget(self.groupBox)
        self.calendarWidget.setGeometry(QtCore.QRect(190, 30, 151, 91))
        self.calendarWidget.setObjectName(_fromUtf8("calendarWidget"))
        self.horizontalLayout.addWidget(self.groupBox)
        self.groupBox_3 = QtGui.QGroupBox(self.horizontalLayoutWidget)
        self.groupBox_3.setObjectName(_fromUtf8("groupBox_3"))
        self.layoutWidget = QtGui.QWidget(self.groupBox_3)
        self.layoutWidget.setGeometry(QtCore.QRect(11, 31, 341, 231))
        self.layoutWidget.setObjectName(_fromUtf8("layoutWidget"))
        self.verticalLayout = QtGui.QVBoxLayout(self.layoutWidget)
        self.verticalLayout.setMargin(0)
        self.verticalLayout.setObjectName(_fromUtf8("verticalLayout"))
        self.listWidget = QtGui.QListWidget(self.layoutWidget)
        self.listWidget.setObjectName(_fromUtf8("listWidget"))
        self.verticalLayout.addWidget(self.listWidget)
        self.formLayout = QtGui.QFormLayout()
        self.formLayout.setObjectName(_fromUtf8("formLayout"))
        self.label_17 = QtGui.QLabel(self.layoutWidget)
        self.label_17.setObjectName(_fromUtf8("label_17"))
        self.formLayout.setWidget(0, QtGui.QFormLayout.LabelRole, self.
↪ label_17)
        self.label_23 = QtGui.QLabel(self.layoutWidget)
        self.label_23.setObjectName(_fromUtf8("label_23"))
        self.formLayout.setWidget(0, QtGui.QFormLayout.FieldRole, self.
↪ label_23)
        self.label_21 = QtGui.QLabel(self.layoutWidget)
        self.label_21.setObjectName(_fromUtf8("label_21"))
```

```
        self.formLayout.setWidget(1, QtGui.QFormLayout.LabelRole, self.
    ↪ label_21)
        self.label_24 = QtGui.QLabel(self.layoutWidget)
        self.label_24.setObjectName(_fromUtf8("label_24"))
        self.formLayout.setWidget(1, QtGui.QFormLayout.FieldRole, self.
    ↪ label_24)
        self.label_22 = QtGui.QLabel(self.layoutWidget)
        self.label_22.setObjectName(_fromUtf8("label_22"))
        self.formLayout.setWidget(2, QtGui.QFormLayout.LabelRole, self.
    ↪ label_22)
        self.label_25 = QtGui.QLabel(self.layoutWidget)
        self.label_25.setObjectName(_fromUtf8("label_25"))
        self.formLayout.setWidget(2, QtGui.QFormLayout.FieldRole, self.
    ↪ label_25)
        self.verticalLayout.addLayout(self.formLayout)
        self.horizontalLayout.addWidget(self.groupBox_3)
        self.groupBox_2 = QtGui.QGroupBox(self.horizontalLayoutWidget)
        self.groupBox_2.setObjectName(_fromUtf8("groupBox_2"))
        self.gridLayoutWidget_3 = QtGui.QWidget(self.groupBox_2)
        self.gridLayoutWidget_3.setGeometry(QtCore.QRect(10, 30, 341, 231))
        self.gridLayoutWidget_3.setObjectName(_fromUtf8("gridLayoutWidget_3"
    ↪ ))
        self.gridLayout_3 = QtGui.QGridLayout(self.gridLayoutWidget_3)
        self.gridLayout_3.setMargin(0)
        self.gridLayout_3.setObjectName(_fromUtf8("gridLayout_3"))
        self.label_2 = QtGui.QLabel(self.gridLayoutWidget_3)
        self.label_2.setObjectName(_fromUtf8("label_2"))
        self.gridLayout_3.addWidget(self.label_2, 3, 0, 1, 1)
        self.label_3 = QtGui.QLabel(self.gridLayoutWidget_3)
        self.label_3.setObjectName(_fromUtf8("label_3"))
        self.gridLayout_3.addWidget(self.label_3, 4, 0, 1, 1)
        self.label_4 = QtGui.QLabel(self.gridLayoutWidget_3)
        self.label_4.setObjectName(_fromUtf8("label_4"))
        self.gridLayout_3.addWidget(self.label_4, 5, 0, 1, 1)
        self.label_5 = QtGui.QLabel(self.gridLayoutWidget_3)
        self.label_5.setObjectName(_fromUtf8("label_5"))
        self.gridLayout_3.addWidget(self.label_5, 7, 0, 1, 1)
        self.label_6 = QtGui.QLabel(self.gridLayoutWidget_3)
        self.label_6.setObjectName(_fromUtf8("label_6"))
        self.gridLayout_3.addWidget(self.label_6, 8, 0, 1, 1)
        self.label_7 = QtGui.QLabel(self.gridLayoutWidget_3)
        self.label_7.setObjectName(_fromUtf8("label_7"))
        self.gridLayout_3.addWidget(self.label_7, 9, 0, 1, 1)
        self.label_8 = QtGui.QLabel(self.gridLayoutWidget_3)
        font = QtGui.QFont()
```

```
        font.setPointSize(15)
        font.setBold(True)
        font.setWeight(75)
        self.label_8.setFont(font)
        self.label_8.setText(_fromUtf8(""))
        self.label_8.setObjectName(_fromUtf8("label_8"))
        self.gridLayout_3.addWidget(self.label_8, 3, 1, 1, 1)
        self.label_9 = QtGui.QLabel(self.gridLayoutWidget_3)
        font = QtGui.QFont()
        font.setPointSize(15)
        font.setBold(True)
        font.setWeight(75)
        self.label_9.setFont(font)
        self.label_9.setMouseTracking(False)
        self.label_9.setText(_fromUtf8(""))
        self.label_9.setObjectName(_fromUtf8("label_9"))
        self.gridLayout_3.addWidget(self.label_9, 4, 1, 1, 1)
        self.label_10 = QtGui.QLabel(self.gridLayoutWidget_3)
        self.label_10.setText(_fromUtf8(""))
        self.label_10.setObjectName(_fromUtf8("label_10"))
        self.gridLayout_3.addWidget(self.label_10, 5, 1, 1, 1)
        self.label_11 = QtGui.QLabel(self.gridLayoutWidget_3)
        self.label_11.setText(_fromUtf8(""))
        self.label_11.setObjectName(_fromUtf8("label_11"))
        self.gridLayout_3.addWidget(self.label_11, 7, 1, 1, 1)
        self.label_12 = QtGui.QLabel(self.gridLayoutWidget_3)
        font = QtGui.QFont()
        font.setPointSize(15)
        font.setBold(True)
        font.setWeight(75)
        self.label_12.setFont(font)
        self.label_12.setText(_fromUtf8(""))
        self.label_12.setObjectName(_fromUtf8("label_12"))
        self.gridLayout_3.addWidget(self.label_12, 8, 1, 1, 1)
        self.label_13 = QtGui.QLabel(self.gridLayoutWidget_3)
        self.label_13.setText(_fromUtf8(""))
        self.label_13.setObjectName(_fromUtf8("label_13"))
        self.gridLayout_3.addWidget(self.label_13, 9, 1, 1, 1)
        self.label_15 = QtGui.QLabel(self.gridLayoutWidget_3)
        self.label_15.setObjectName(_fromUtf8("label_15"))
        self.gridLayout_3.addWidget(self.label_15, 6, 0, 1, 1)
        self.label_16 = QtGui.QLabel(self.gridLayoutWidget_3)
        font = QtGui.QFont()
        font.setPointSize(15)
        font.setBold(True)
```

```
        font.setWeight(75)
        self.label_16.setFont(font)
        self.label_16.setText(_fromUtf8(""))
        self.label_16.setObjectName(_fromUtf8("label_16"))
        self.gridLayout_3.addWidget(self.label_16, 6, 1, 1, 1)
        self.horizontalLayout.addWidget(self.groupBox_2)
        self.horizontalLayoutWidget_2 = QtGui.QWidget(self.centralwidget)
        self.horizontalLayoutWidget_2.setGeometry(QtCore.QRect(10, 0, 1191,
    ↪ 41))
        self.horizontalLayoutWidget_2.setObjectName(_fromUtf8("
    ↪ horizontalLayoutWidget_2"))
        self.horizontalLayout_2 = QtGui.QHBoxLayout(self.
    ↪ horizontalLayoutWidget_2)
        self.horizontalLayout_2.setMargin(0)
        self.horizontalLayout_2.setObjectName(_fromUtf8("horizontalLayout_2"
    ↪ ))
        self.label = QtGui.QLabel(self.horizontalLayoutWidget_2)
        self.label.setObjectName(_fromUtf8("label"))
        self.horizontalLayout_2.addWidget(self.label)
        self.lineEdit = QtGui.QLineEdit(self.horizontalLayoutWidget_2)
        self.lineEdit.setObjectName(_fromUtf8("lineEdit"))
        self.horizontalLayout_2.addWidget(self.lineEdit)
        self.toolButton = QtGui.QToolButton(self.horizontalLayoutWidget_2)
        self.toolButton.setObjectName(_fromUtf8("toolButton"))
        self.horizontalLayout_2.addWidget(self.toolButton)
        self.pushButton = QtGui.QPushButton(self.horizontalLayoutWidget_2)
        self.pushButton.setObjectName(_fromUtf8("pushButton"))
        self.horizontalLayout_2.addWidget(self.pushButton)
        self.horizontalLayoutWidget_3 = QtGui.QWidget(self.centralwidget)
        self.horizontalLayoutWidget_3.setGeometry(QtCore.QRect(10, 330,
    ↪ 1191, 311))
        self.horizontalLayoutWidget_3.setObjectName(_fromUtf8("
    ↪ horizontalLayoutWidget_3"))
        self.horizontalLayout_3 = QtGui.QHBoxLayout(self.
    ↪ horizontalLayoutWidget_3)
        self.horizontalLayout_3.setMargin(0)
        self.horizontalLayout_3.setObjectName(_fromUtf8("horizontalLayout_3"
    ↪ ))
        self.mpl_1 = MplWidget(self.horizontalLayoutWidget_3)
        self.mpl_1.setObjectName(_fromUtf8("mpl_1"))
        self.horizontalLayout_3.addWidget(self.mpl_1)
        self.mpl_2 = MplWidget(self.horizontalLayoutWidget_3)
        self.mpl_2.setObjectName(_fromUtf8("mpl_2"))
        self.horizontalLayout_3.addWidget(self.mpl_2)
        self.mpl_3 = MplWidget(self.horizontalLayoutWidget_3)
```

```
        self.mpl_3.setMouseTracking(True)
        self.mpl_3.setObjectName(_fromUtf8("mpl_3"))
        self.horizontalLayout_3.addWidget(self.mpl_3)
        MainWindow.setCentralWidget(self.centralwidget)
        self.menubar = QtGui.QMenuBar(MainWindow)
        self.menubar.setGeometry(QtCore.QRect(0, 0, 1210, 22))
        self.menubar.setObjectName(_fromUtf8("menubar"))
        self.menuAbout = QtGui.QMenu(self.menubar)
        self.menuAbout.setObjectName(_fromUtf8("menuAbout"))
        MainWindow.setMenuBar(self.menubar)
        self.actionAbout_me = QtGui.QAction(MainWindow)
        self.actionAbout_me.setObjectName(_fromUtf8("actionAbout_me"))
        self.menuAbout.addAction(self.actionAbout_me)
        self.menubar.addAction(self.menuAbout.menuAction())

        self.retranslateUi(MainWindow)
        QtCore.QObject.connect(self.checkBox, QtCore.SIGNAL(_fromUtf8("
↪ toggled(bool)")), self.lineEdit_7.setDisabled)
        QtCore.QObject.connect(self.checkBox, QtCore.SIGNAL(_fromUtf8("
↪ toggled(bool)")), self.lineEdit_8.setDisabled)
        QtCore.QMetaObject.connectSlotsByName(MainWindow)

    def retranslateUi(self, MainWindow):
        MainWindow.setWindowTitle(QtGui.QApplication.translate("MainWindow",
↪  "Step Analysis Program", None, QtGui.QApplication.UnicodeUTF8))
        self.groupBox.setTitle(QtGui.QApplication.translate("MainWindow", "
↪ Options", None, QtGui.QApplication.UnicodeUTF8))
        self.groupBox_4.setTitle(QtGui.QApplication.translate("MainWindow",
↪ "Distribution", None, QtGui.QApplication.UnicodeUTF8))
        self.checkBox.setText(QtGui.QApplication.translate("MainWindow", "
↪ Auto set range", None, QtGui.QApplication.UnicodeUTF8))
        self.label_20.setText(QtGui.QApplication.translate("MainWindow", "
↪ Left", None, QtGui.QApplication.UnicodeUTF8))
        self.label_19.setText(QtGui.QApplication.translate("MainWindow", "
↪ Right", None, QtGui.QApplication.UnicodeUTF8))
        self.label_18.setText(QtGui.QApplication.translate("MainWindow", "N
↪ bins", None, QtGui.QApplication.UnicodeUTF8))
        self.lineEdit_6.setText(QtGui.QApplication.translate("MainWindow", "
↪ 100", None, QtGui.QApplication.UnicodeUTF8))
        self.checkBox_2.setText(QtGui.QApplication.translate("MainWindow", "
↪ Built in Distribution fit", None, QtGui.QApplication.UnicodeUTF8))
        self.groupBox_5.setTitle(QtGui.QApplication.translate("MainWindow",
↪ "Files", None, QtGui.QApplication.UnicodeUTF8))
        self.label_14.setText(QtGui.QApplication.translate("MainWindow", "N
↪ of files", None, QtGui.QApplication.UnicodeUTF8))
```

```
        self.lineEdit_2.setText(QtGui.QApplication.translate("MainWindow", "
    ↪ 1", None, QtGui.QApplication.UnicodeUTF8))
        self.groupBox_3.setTitle(QtGui.QApplication.translate("MainWindow",
    ↪ "State", None, QtGui.QApplication.UnicodeUTF8))
        self.label_17.setText(QtGui.QApplication.translate("MainWindow", "
    ↪ Total lines", None, QtGui.QApplication.UnicodeUTF8))
        self.label_23.setText(QtGui.QApplication.translate("MainWindow", "0"
    ↪ , None, QtGui.QApplication.UnicodeUTF8))
        self.label_21.setText(QtGui.QApplication.translate("MainWindow", "
    ↪ Good lines", None, QtGui.QApplication.UnicodeUTF8))
        self.label_24.setText(QtGui.QApplication.translate("MainWindow", "0"
    ↪ , None, QtGui.QApplication.UnicodeUTF8))
        self.label_22.setText(QtGui.QApplication.translate("MainWindow", "
    ↪ Ignored", None, QtGui.QApplication.UnicodeUTF8))
        self.label_25.setText(QtGui.QApplication.translate("MainWindow", "0"
    ↪ , None, QtGui.QApplication.UnicodeUTF8))
        self.groupBox_2.setTitle(QtGui.QApplication.translate("MainWindow",
    ↪ "Results", None, QtGui.QApplication.UnicodeUTF8))
        self.label_2.setText(QtGui.QApplication.translate("MainWindow", "
    ↪ Sigma", None, QtGui.QApplication.UnicodeUTF8))
        self.label_3.setText(QtGui.QApplication.translate("MainWindow", "mu
    ↪ *1000*2 (nm)", None, QtGui.QApplication.UnicodeUTF8))
        self.label_4.setText(QtGui.QApplication.translate("MainWindow", "Fit
    ↪  a", None, QtGui.QApplication.UnicodeUTF8))
        self.label_5.setText(QtGui.QApplication.translate("MainWindow", "Fit
    ↪  b", None, QtGui.QApplication.UnicodeUTF8))
        self.label_6.setText(QtGui.QApplication.translate("MainWindow", "Fit
    ↪  c*1000*2 (nm)", None, QtGui.QApplication.UnicodeUTF8))
        self.label_7.setText(QtGui.QApplication.translate("MainWindow", "Fit
    ↪  d", None, QtGui.QApplication.UnicodeUTF8))
        self.label_15.setText(QtGui.QApplication.translate("MainWindow", "
    ↪ Height (nm),i.e.abs(a*2)", None, QtGui.QApplication.UnicodeUTF8))
        self.label.setText(QtGui.QApplication.translate("MainWindow", "File
    ↪ Name:", None, QtGui.QApplication.UnicodeUTF8))
        self.lineEdit.setText(QtGui.QApplication.translate("MainWindow", "
    ↪ Input file path", None, QtGui.QApplication.UnicodeUTF8))
        self.toolButton.setText(QtGui.QApplication.translate("MainWindow", "
    ↪ ...", None, QtGui.QApplication.UnicodeUTF8))
        self.pushButton.setText(QtGui.QApplication.translate("MainWindow", "
    ↪ Read File", None, QtGui.QApplication.UnicodeUTF8))
        self.menuAbout.setTitle(QtGui.QApplication.translate("MainWindow", "
    ↪ About", None, QtGui.QApplication.UnicodeUTF8))
        self.actionAbout_me.setText(QtGui.QApplication.translate("MainWindow
    ↪ ", "About me", None, QtGui.QApplication.UnicodeUTF8))
from mplwidget import MplWidget
```

A.3 Application wrap code

The following code is the application wrap of the step film analysis program.

```
import sys

from PyQt4 import QtCore, QtGui
from PyQt4.QtGui import QMainWindow, QPushButton, QApplication
from mean_profile_form import Ui_MainWindow
from main_code import main_code

class MainWindow(QMainWindow, Ui_MainWindow):
    def __init__(self, parent=None):
        super(MainWindow, self).__init__(parent)
        self.setupUi(self)
        self.toolButton.clicked.connect(self.select_file)
        self.pushButton.clicked.connect(self.run_main_code)
        self.actionAbout_me.triggered.connect(self.about_show)

    def select_file(self):
        """opens a file select dialog"""
        # open the dialog and get the selected file
        file = QtGui.QFileDialog.getOpenFileName()
        # if a file is selected
        if file:
        # update the lineEdit text with the selected filename
            self.lineEdit.setText(file)
            self.lineEdit_9.setText(file)

    def about_show(self):
        '''Popup a box with about message.'''
        QtGui.QMessageBox.about(self, "About",\
                "This step analysis software was made by Yu Chai at
    ↪ 2012.05.03")

    def run_main_code(self):
        main_code(self,main_file_name=self.lineEdit.text(),\
                  main_number_file=int(self.lineEdit_2.text()),\
                  main_n_bins=self.lineEdit_6.text())

if __name__ == '__main__':
    app = QApplication(sys.argv)
    frame = MainWindow()
    frame.show()
```

```
    app.exec_()
```

Appendix B

Random walk simulation (C++)

The following C++ code is used to determine the polymer chain distribution in the liquid-like layer.

```
//
//  main.cpp
//  Random Walk Surface Distribution
//  Created by Yu Chai on 2013-10-08.
//

#include <fstream>
#include <iostream>
#include <stdio.h>
#include <time.h>
#include <math.h>
using namespace std;

double start_walk(int walk_nodes,int surface_depth)
{
    /* initialize random seed: */
    srand (time(NULL));
    int total_loops = 10000;
    int total_depth = walk_nodes+10;
    float RR_dist_one = 0;
    ofstream fout;
    fout.open("Random Walk.txt");
    fout <<"Inital z"<<"\t"<<"total_num"<<"\t"<<"total_num_in_surface"<<"\t"
   ↪ <<"total_num_all_in_surface"<<"\t"<<"total_fraction_in_surface"<<"\n";
```

```
double all_free_total =0 , part_free_total=0,fraction_total=0;

/* loop for different initial z locations */
for (int zloo = 0; zloo < total_depth; zloo++) {

    int total_num_all_in_surface = 0;
    int total_num_in_surface = 0;
    int total_num = 0;
    double total_fraction_in_surface = 0;
    float RR_dist = 0;
    float RR_dist_avg = 0;

    /* loop for a lot of random walks with the same initial z location
↪ */
    for (int i = 0; i < total_loops; i++) {

        int x = 0 , y = 0, z = -zloo, zold=0;
        int walkx[walk_nodes], walky[walk_nodes], walkz[walk_nodes];
        int num_node_in_surface = 0;

        for (int j = 0; j < walk_nodes; j++) {
            zold = z;
            int temp = rand() % 6;
            if (temp == 0) {
                x += 1;
            }
            else if (temp == 1){
                y += 1;
            }
            else if (temp == 2){
                if (z >= 0) {
                    z += -1;
                }
                else z += 1;
            }
            else if (temp == 3){
                x += -1;
            }
            else if (temp == 4){
                y += -1;
            }
            else if (temp == 5){
                z += -1;
            }
```

```
                if (z >= surface_depth and zold >= surface_depth) {
                    num_node_in_surface += 1;
                }
            }
            RR_dist_one = pow(x, 2.0)+pow(y, 2.0)+pow(z+zloo, 2.0);
            RR_dist += RR_dist_one;

            if (num_node_in_surface == walk_nodes) {
                total_num_all_in_surface += 1;
            }
            if (num_node_in_surface > 0) {
                total_num_in_surface += 1;
                total_fraction_in_surface += (double)num_node_in_surface/
    ↪ walk_nodes;
            }
        }
        RR_dist_avg = sqrt(RR_dist/total_loops);
        cout <<"Inital z"<<"\t"<<"total_num"<<"\t"<<"total_num_in_surface"<<
    ↪ "\t"<<"total_num_all_in_surface"<<"\t"<<"total_fraction_in_surface"<<"
    ↪ \t"<<"End-end distrance"<<"\n";
        cout <<-zloo<<"\t"<<total_loops<<"\t"<<total_num_in_surface<<"\t"<<
    ↪ total_num_all_in_surface<<"\t"<<total_fraction_in_surface<<"\t"<<
    ↪ RR_dist_avg<<endl;
        fout <<-zloo<<"\t"<<total_loops<<"\t"<<total_num_in_surface<<"\t"<<
    ↪ total_num_all_in_surface<<"\t"<<total_fraction_in_surface<<"\t"<<
    ↪ RR_dist_avg<<"\n";

        all_free_total += total_num_all_in_surface;
        part_free_total += total_fraction_in_surface;
    }
    fraction_total = all_free_total/part_free_total;
    cout<<"*********************************"<<endl;
    cout<<"all_free_total\t"<<"part_free_total\t"<<"fraction_total"<<endl;
    cout<<all_free_total<<"\t"<<part_free_total<<"\t"<<fraction_total<<endl;

    fout<<"*********************************"<<endl;
    fout<<"all_free_total\t"<<"part_free_total\t"<<"fraction_total"<<endl;
    fout<<all_free_total<<"\t"<<part_free_total<<"\t"<<fraction_total<<endl;

    fout.close();
    return fraction_total;
}

int main(int argc, const char * argv[])
{
```

```
    int max_step_size = 100;
    int surface_depth = -3;
    ofstream fout_total;
    fout_total.open("Total_fraction_sum.txt");
    fout_total<<"Step_size\t"<<"Fraction"<<endl;
    for (int step_size=1; step_size < max_step_size; step_size++) {
        double fraction_each = start_walk(step_size,surface_depth);
        fout_total<<step_size<<"\t"<<fraction_each<<endl;
    }
    fout_total.close();
    return 0;
}
```

Appendix C

Thin film expansivity calculation (Matlab)

C.1 Simulation based on the simple model

The following Matlab code is used to determine the simulation expansivity profiles of polymer thin films based on the simple mode discussed in Chapter 5.

```
function [Temp_spline, a_h_spline, T_g_x] = expansivity(h, E_s, a_1)
    a_h = [];
    i = 0;
    Temp = [];
    for T = 200:1:400
        i = i+1;
        % Define parameters
        a_m = 1*10^-3;
        a_g = 2*10^-4;
        w = 5;
        T_0 = 327;
        a_0 = 4;
        T_g = 372;
        B = 1878;
        % Define R_s and epsilon
        R_s = T_0+B*T/E_s;
        epsilon = a_0+a_1*(T_g-T);
        % Define the expansivity at location z at temperature T
```

```
        a_z = @(x) 0.5*((a_m+a_g)+(a_m-a_g)*tanh((T+(R_s-T)*exp(-x*h/epsilon
    ↪ )-T_g)/w));
        % Total expansivity at temperature T
        a_T = integral(a_z,0,1);
        % Output values
        a_h(i) = a_T;
        Temp(i) = T;
    end
    % linear spline
    Temp_spline = linspace(200,400,10000);
    a_h_spline = interp1 (Temp, a_h, Temp_spline);
    [m,n] = min(abs(a_h_spline-0.5*(a_m+a_g)));
    T_g_x = Temp_spline(n);
end
```

C.2 Determine experimental thermal expansivity profiles

Here is the Matlab code to covert the T(Temperature)-P(Polarizer)-A(Analyzer) profile to thermal expansivity profile.

C.2.1 Determine thickness and refractive index

```
%import file
clear all
%import ellip file
[FileName,PathName] = uigetfile({'*.*', 'All Files (*.*)'},'Open Ellip file
    ↪ ');
[Temp,P,A] = importfile([PathName,FileName]);
%% input incident angle
prompt = {'Enter incident angle:'};
dlg_title = 'Input';
num_lines = 1;
defaultans = {'60'};
ind_ang = inputdlg(prompt,dlg_title,num_lines,defaultans);
ind_ang = str2num(ind_ang{1});
%find the thickness at room temperature
location = knnsearch(Temp,20);
```

```
thickness_at_room_temp = find_table_initial(P(location),A(location),ind_ang)
    ↪ ;
%% find thickness
[Thickness,n_ref] = find_table(P,A,thickness_at_room_temp,Temp,ind_ang);
%% output
if ~exist([PathName,'output'], 'dir')
  mkdir([PathName,'output']);
end
%save data
save([PathName,'output/Temp_data'], 'Temp', 'P', 'A', 'Thickness','n_ref','
    ↪ PathName','FileName');
save('Temp_data', 'Temp', 'P', 'A', 'Thickness','n_ref','PathName','FileName
    ↪ ');
%%
run expansivity_run.m
```

C.2.2 Determine expansivity profile

```
%expansivity run
clear all;
close all;
load Temp_data.mat
step = 20;
%% determine the thickness at room temperature
location = knnsearch(Temp,20);
thickness_at_room_temp = Thickness(location);
%% smooth curve by averaging every $step$ data points
Temp_s = arrayfun(@(i) mean(Temp(i:i+step-1)),1:step:length(Temp)-step+1)';
Thickness_s = arrayfun(@(i) mean(Thickness(i:i+step-1)),1:step:length(
    ↪ Thickness)-step+1)';
%% determine expansivity profile
df_Temp_Thickness = diff(Thickness_s)./diff(Temp_s);
Expansivity = 1./Thickness_s(1:end-1).*diff(Thickness_s)./diff(Temp_s);
d_Temp = Temp_s(1:end-1);
```

C.2.3 Generate P and A dataset

```
function data=generate_ellipsometry_table( g_t,a_range,N ,n2,ind_ang)
d=linspace(g_t-a_range,g_t+a_range,N);%Thickness of PS(A)
h2=20;%Thickness of SiOx(A)
phi1=ind_ang/180*pi;%Incidence angle
lambda=6328;%Wavelength
n1=1;n3=1.42;n4=3.875-0.023j;%Index of refraction
%initial value
```

```
a=[];p=[];thickness=[];
cos2=sqrt((n2^2-n1^2*sin(phi1)^2)/n2^2);
cos3=sqrt((n3^2-n1^2*sin(phi1)^2)/n3^2);
cos4=sqrt((n4^2-n1^2*sin(phi1)^2)/n4^2);
r1p=(n2*cos(phi1)-n1*cos2)/(n2*cos(phi1)+n1*cos2);
r1s=(n1*cos(phi1)-n2*cos2)/(n1*cos(phi1)+n2*cos2);
r2p=(n3*cos2-n2*cos3)/(n3*cos2+n2*cos3);
r2s=(n2*cos2-n3*cos3)/(n2*cos2+n3*cos3);
r3p=(n4*cos3-n3*cos4)/(n4*cos3+n3*cos4);
r3s=(n3*cos3-n4*cos4)/(n3*cos3+n4*cos4);
%Using for loop to calculate psi&delta
for h=d
    delta2=2*pi*h2*n3*cos3/lambda;
    R23p=(r2p+r3p*exp(-2*1i*delta2))/(1+r2p*r3p*exp(-2*1i*delta2));
    R23s=(r2s+r3s*exp(-2*1i*delta2))/(1+r2s*r3s*exp(-2*1i*delta2));
    delta1=2*pi*h*n2*cos2/lambda;
    Rp=(r1p+R23p*exp(-2*1i*delta1))/(1+r1p*R23p*exp(-2*1i*delta1));
    Rs=(r1s+R23s*exp(-2*1i*delta1))/(1+r1s*R23s*exp(-2*1i*delta1));
    ratio=Rp/Rs;
    temp=abs(Rp)/abs(Rs);
    psi=atan(temp)*180/pi;
    delta=imag(log(ratio/temp))*180/pi;
    if delta<0|delta==0
        delta=(delta+360);
    end
    y=90-(3*180/4-delta/2);
    a(end+1)=psi;
    p(end+1)=y;
    thickness(end+1)=h;
end
data=[a;p;thickness];
end
```

C.2.4 Determine thickness with recursively updated refractive index

```
function [Thickness_all,n_all] = find_table(exp_p,exp_a,
    ↪ thickness_at_room_Temp,Temp,ind_ang)

    thickness=[];
    n = [];
    last_thickness = thickness_at_room_Temp*10;
    new_n = 1.583;
    n_room = new_n;
```

```
    ind_h = find(Temp>20);
    ind_h_r = flipud(ind_h);
    ind_l = find(Temp<20 | Temp ==20);

    %% loop above 20c data
    for j=1:length(ind_h_r);
        i = ind_h_r(j);
        %generate table based on target thickness
        data=generate_ellipsometry_table(last_thickness,25,500,new_n,ind_ang
↪ );
        %read a,p, thickness
        a=data(1,:)';
        p=data(2,:)';
        h=data(3,:)';
        tp=exp_p(i);
        ta=exp_a(i);
        %find mim distance
        dp=abs(p-tp);
        da=abs(a-ta);
        [dist,ind]=min(sqrt(dp.*dp+da.*da));
        %find new refractive index
        TT_A = (n_room^2-1)/(n_room^2+2);
        TT_B = h(ind)/thickness_at_room_Temp/10;
        TT_C = TT_A/TT_B;
        new_n = sqrt((2*TT_C+1)/(1-TT_C));
        %update last_thickness
        last_thickness = h(ind);
        %add new thickness to array
        thickness(i)=h(ind)/10;
        n(i) = new_n;
    end
    %% loop below 20c data
    new_n = 1.583;
    last_thickness = thickness_at_room_Temp*10;
    for j=1:length(ind_l);
        i = ind_l(j);
        %generate table based on target thickness
        data=generate_ellipsometry_table(last_thickness,25,500,new_n,ind_ang
↪ );
        %read a,p, thickness
        a=data(1,:)';
        p=data(2,:)';
        h=data(3,:)';
        tp=exp_p(i);
        ta=exp_a(i);
```

```
        %find mim distance
        dp=abs(p-tp);
        da=abs(a-ta);
        [dist,ind]=min(sqrt(dp.*dp+da.*da));
        %find new refractive index
        TT_A = (n_room^2-1)/(n_room^2+2);
        TT_B = h(ind)/thickness_at_room_Temp/10;
        TT_C = TT_A/TT_B;
        new_n = sqrt((2*TT_C+1)/(1-TT_C));
        %update last_thickness
        last_thickness = h(ind);
        %add new thickness to array
        thickness(i)=h(ind)/10;
        n(i) = new_n;
    end
    %% output
    thickness=thickness';
    n = n';
    Thickness_all = thickness;
    n_all = n;
end
```

Appendix D

List of publications

[1]Y. Chai, T. Salez, J. D. McGraw, M. Benzaquen, K. Dalnoki-Veress, E. Raphaël, and J. A. Forrest, "A Direct Quantitative Measure of Surface Mobility in a Glassy Polymer", Science **343**, 994–999 (2014).

[2]D. Qi, C. R. Daley, Y. Chai, and J. A. Forrest, "Molecular weight dependence of near surface dynamical mechanical properties of polymers", Soft Matter **9**, 8958 (2013).

[3]Y. Chai and J. A. Forrest, "Molecular weight dependent surface flow near the bulk glass transition temperature", (To be submitted).

[4]Y. Chai and J. A. Forrest, "Crystallization of low molecular weight atactic polystyrene", (To be submitted).

[5]Y. Chai and J. A. Forrest, "Thermal expansion study of polymer thin films", (To be submitted).